Second Kind Single Trace Boundary Element Methods

Master Thesis

written by
Elke Spindler

supervised by
Prof. Dr. R. Hiptmair
Seminar for Applied Mathematics
ETH Zürich

Spring Semester 2012

Contents

0 Introduction

One year ago, X. Claeys published a paper [4] in which a new second kind boundary element formulation for Helmholtz transmission problems was presented. The new method promises to be very well-conditioned in the sense that the condition number of the Galerkin matrices is independent of the mesh size h. Prior to this, the spectral condition number depended for first kind single trace formulations on the mesh size as $\mathcal{O}(h^{-2})$ in the best case and one had to use preconditioners to get acceptable convergence of iterative solvers.

In the same paper it was also mentioned that there is a bounded linear operator $\mathcal{A}_{\kappa_0}$ vanishing on the trial space used for the formulation of the Helmholtz transmission problem.
In our thesis we are going to adopt this fact and modify Claeys' method, taking advantage of the regularizing effect of the trivial operator $\mathcal{A}_{\kappa_0}$. It turns out that the regularized formulation can be defined on a slightly different trial space which makes it possible to discretize the problem using only piecewise constant boundary elements. This in turn makes implementation easier and has an advantage when the boundary data is not well behaving, for example at discontinuities in acute corners of the domain. In these cases, the convergence of the Neumann data is improved.

First, we give a brief introduction of boundary element methods for Helmholtz transmission problems in two dimensions and fixes some notation (Chapter 1, Sections 1.1 - 1.6). At the end of Chapter 1, different kinds of boundary element formulations are stated. The first approach written down in Section 1.7 concerns the classical method for transmission problems while the second approach in Section 1.8 is based on the formulation developed by Claeys in Ref. [4]. We implemented both methods in MATLAB. The first approach is used to have a comparison with the results of the new method and is based on a boundary element framework developed by Patrick Meury during his PhD at ETH Zürich [10]. We dedicate the whole Chapter 2 to the implementation of our new method.

The numerical experiments in Chapter 3 and their discussion conclude this thesis.

1 Theory and Notation

1.1 Sobolev Spaces and Traces

First of all let us introduce the spaces which we are going to work on and some basic operators and functions we are going to use quite often. The definitions and theorems stated in this section can be found in most books concerning boundary element methods, such as [12], [14] or [9].

Definition 1 (Lipschitz hypograph) *An open set Ω is said to be a* Lipschitz hypograph *if $\exists \gamma : \mathbb{R} \to \mathbb{R}$:*

- $|\gamma(x) - \gamma(y)| \leq L|x - y| \; \forall x, y \in \mathbb{R}$
- $\Omega = \{\mathbf{x} = (x_1, x_2)^T \in \mathbb{R}^2 | \, x_2 < \gamma(y) \, \forall y \in \mathbb{R}\}$

Definition 2 (Lipschitz domain) *An open set $\Omega \subset \mathbb{R}^2$ is a* Lipschitz domain *if $\partial\Omega$ is compact and*

- *has a finite open covering $\mathcal{W}$, i.e. $\forall W \in \mathcal{W} : W \subset \mathbb{R}^2$ is open and $\partial\Omega \subset \bigcup_{W \in \mathcal{W}} W$.*
- *$\exists$ a finite family of sets $\mathcal{U}$ s.t. $\forall W \in \mathcal{W} \; \exists U \in \mathcal{U}$: $W \cap U = W \cap \Omega$*
- *$\forall U \in \mathcal{U}$: U can be transformed to a Lipschitz hypograph by rotations and translations.*

Informally speaking, the definition ensures that Ω is locally situated on only one side of its boundary $\partial\Omega$.

Now let us introduce the functional spaces we are going to work on.

Definition 3 ($L^2(\Omega)$) *For $d \in \mathbb{N}$ and an open set $\Omega \subset \mathbb{R}^d$ define the Hilbert space $L^2(\Omega)$ to be the set of all measurable functions $v : \Omega \mapsto \mathbb{C}$ s.t. :*

$$\|v\|^2_{L^2(\Omega)} := \langle v, v \rangle_{L^2(\Omega)} = \int_\Omega |v|^2 \, d\mathbf{x} < \infty.$$

On the boundary $\partial\Omega = \Gamma$ of a Lipschitz domain Ω we can define the space $L^2(\Gamma)$ in the following way

Definition 4 ($L^2(\Gamma)$) *Let Ω be a Lipschitz domain. With the aid of Def. 2 and Def. 1 we have that there is a finite open covering $\mathcal{W}$ of Γ s.t. for all $W \in \mathcal{W}$ there is a local parametrization*

$$\xi_W : (0, 1) \to W \cap \Gamma.$$

Based on this fact we can define the space

$$L^2(\Gamma) := \left\{ \phi : \Gamma \to \mathbb{C} \, \middle| \, \phi \circ \xi_W \in L^2((0, 1)) \, \forall W \in \mathcal{W} \right\}.$$

It is a Hilbert space endowed with the inner product

$$\langle \phi, \psi \rangle_{L^2(\Gamma)} := \int_\Gamma \phi(\mathbf{x}) \overline{\psi(\mathbf{x})}\, dS(\mathbf{x}), \quad \textit{where } \phi, \psi \in L^2(\Gamma).$$

Other important spaces are the Sobolev spaces $H(\Omega)$, $H(\mathrm{div}, \Omega)$, $H^1(\Delta, \Omega)$, $H^{\frac{1}{2}}(\Gamma)$ and its dual $H^{-\frac{1}{2}}(\Gamma)$:

Definition 5 (Commonly used spaces)

$$\begin{aligned}
H^1(\Omega) &:= \left\{ v \in L^2(\Omega) \,\middle|\, \|v\|^2_{H^1(\Omega)} := \int_\Omega |v|^2 + \|\nabla v\|_2^2 d\mathbf{x} < \infty \right\}, \\
H(\mathrm{div}, \Omega) &:= \left\{ \mathbf{q} \in \left(L^2(\Omega)\right)^2 \,\middle|\, \|\mathbf{q}\|^2_{H(\mathrm{div},\Omega)} := \int_\Omega \|\mathbf{q}\|_2^2 + |\operatorname{div} \mathbf{q}|^2 d\mathbf{x} < \infty \right\}, \\
H^1(\Delta, \Omega) &:= \left\{ v \in H^1(\Omega) \,\middle|\, \nabla v \in H(\mathrm{div}, \Omega) \right\}, \\
C^\infty_{comp}(\Omega) &:= \left\{ v|_\Omega \,\middle|\, v \in C^\infty_0(\mathbb{R}) \right\}, \\
H^1_{loc}(\Delta, \Omega) &:= \left\{ v \in \left(C^\infty_{comp}(\Omega)\right)^* \,\middle|\, \phi v \in H^1(\Delta, \Omega)\ \forall \phi \in C^\infty_{comp}(\Omega) \right\}, \\
H^{\frac{1}{2}}(\Gamma) &:= \left\{ v \in L^2(\Gamma) \,\middle|\, \|v\|^2_{H^{\frac{1}{2}}(\Gamma)} := \int_\Gamma |v(\mathbf{x})|^2\, dS(\mathbf{x}) + \int_\Gamma \int_\Gamma \frac{|v(\mathbf{x}) - v(\mathbf{y})|^2}{\|\mathbf{x} - \mathbf{y}\|_2^2} d\mathbf{x}\, d\mathbf{y} < \infty \right\}, \\
H^{-\frac{1}{2}}(\Gamma) &:= \left(H^{\frac{1}{2}}(\Gamma) \right)^* \quad \textit{(topological dual).}
\end{aligned}$$

$H^{-\frac{1}{2}}(\Gamma)$ is equipped with the corresponding dual norm of $H^{\frac{1}{2}}(\Gamma)$:

$$\|w\|_{H^{-\frac{1}{2}}(\Gamma)} := \sup_{v \in H^{\frac{1}{2}}(\Gamma) \setminus \{0\}} \frac{1}{\|v\|_{H^{\frac{1}{2}}(\Gamma)}} \left| \int_\Gamma v(\mathbf{x}) \overline{w(\mathbf{x})}\, dS(\mathbf{x}) \right|.$$

An important concept we need to introduce are linear functionals taking the (interior) boundary restriction, *the trace* of a function $v \in H^1(\Omega)$. For continuous functions $f \in C^0(\overline{\Omega})$, the definition might be intuitively clear:

$$\gamma_D^\Omega f(\mathbf{x}) := \lim_{\substack{\tilde{\mathbf{x}} \in \Omega: \\ \tilde{\mathbf{x}} \to \mathbf{x} \in \partial\Omega}} f(\tilde{\mathbf{x}}), \quad \mathbf{x} \in \partial\Omega.$$

It turns out that for Lipschitz domains Ω, one can extend the trace operator γ_D^Ω continuously to the space $H^1(\Omega)$:

Theorem 1 (Trace theorem) *For a Lipschitz domain Ω, the trace operator γ_D^Ω is a continuous surjective linear operator from $H^1(\Omega)$ to $H^{\frac{1}{2}}(\partial\Omega)$. It holds the desired property that $\forall v \in C^\infty(\overline{\Omega}) \subset H^1(\Omega)$:*

$$\gamma_D^\Omega v(\mathbf{x}) = v|_{\partial\Omega}(\mathbf{x}) \textit{ for a.e. } \mathbf{x} \in \partial\Omega.$$

Consult [9, Theorem 3.37] for a proof.

Analogously we define another kind of trace operator, *the conormal trace operator* γ_N^Ω. But to do so, we first need to introduce the notion of the *normal field* of the boundary $\partial\Omega$.

Definition 6 (Normal field) *Let Ω be a bounded and connected Lipschitz domain with the local parametrization γ from Def. 2 and Def. 1 s.t. $\gamma \in C^1$. Then the* normal field $\mathbf{n} : \partial\Omega \to \mathcal{S}_1 \subset \mathbb{R}^2$ *($\mathcal{S}_1$ is the 1-dim. sphere of radius 1) is given by the vector field assigning to every point $\mathbf{x} \in \partial\Omega$ the vector*

$$\mathbf{n}(\mathbf{x}) := \frac{1}{\|\dot{\gamma}(\mathbf{x}\|}(\dot{\gamma}_2(\mathbf{x}), -\dot{\gamma}_1(\mathbf{x}))^T$$

perpendicular to the derivative of the local parametrization

$$\gamma = (\gamma_1, \gamma_2)^T : [0, 1] \to \mathbb{R}^2$$

of the boundary. Moreover, we assume that γ is chosen in such a way that $\mathbf{n}$ is always directed outside of the domain.

The Theorem below states that we do not need to assume additional properties of Ω but bounded and connected Lipschitz to get the existence of a normal field:

Theorem 2 (Rademacher) *Let Ω be a bounded Lipschitz domain with boundary $\partial\Omega$. Then there exists an outer normal vector $\mathbf{n}$ almost everywhere on $\partial\Omega$ which satisfies $\mathbf{n} \in L^\infty(\partial\Omega)$.*

Now we are ready to define the conormal trace, also called *Neumann trace*, of a function $v \in H^1_{\text{loc}}(\Delta, \overline{\Omega})$. We start again with the intuitive definition for $f \in C^\infty(\overline{\Omega})$:

$$\gamma_N^\Omega f(\mathbf{x}) := \lim_{\substack{\tilde{\mathbf{x}} \in \Omega: \\ \tilde{\mathbf{x}} \to \mathbf{x} \in \partial\Omega}} \mathbf{n}(\mathbf{x}) \cdot \nabla_{\tilde{\mathbf{x}}} f(\tilde{\mathbf{x}}), \quad \mathbf{x} \in \partial\Omega,$$

where $\mathbf{n}$ is the normal field of Ω. Again we are able to extend the conormal trace operator γ_N^Ω from $C^\infty(\overline{\Omega})$ to $H^1_{\text{loc}}(\Delta, \overline{\Omega})$:

Theorem 3 (Conormal trace theorem) *The* conormal trace *operator $\gamma_N^\Omega : H^1_{loc}(\Delta, \overline{\Omega}) \to H^{-\frac{1}{2}}(\partial\Omega)$ is a continuous linear operator. It holds the desired property that $\forall v \in C^\infty(\overline{\Omega}) \subset H^1_{loc}(\Delta, \overline{\Omega})$:*

$$\gamma_N^\Omega v(\mathbf{x}) = \mathbf{n}(\mathbf{x}) \cdot \nabla v|_{\partial\Omega}(\mathbf{x}) \text{ for a.e. } \mathbf{x} \in \partial\Omega.$$

Moreover we have that the mapping below is surjective:

$$(\gamma_D^{\Omega_i},\ \gamma_N^{\Omega_i}) : H^1(\Omega) \times H^1_{loc}(\Delta, \overline{\Omega}_i) \to H^{\frac{1}{2}}(\partial\Omega_i) \times H^{-\frac{1}{2}}(\partial\Omega_i).$$

Cf. [12, Theorem 2.8.3, Lemma 2.8.4] for a proof (the surjectivity follows then by density of $(\gamma_D^{\Omega_i},\ \gamma_N^{\Omega_i})(C_0^\infty(\overline{\Omega}_i) \times C_0^\infty(\overline{\Omega}_i))$ in $H^{\frac{1}{2}}(\partial\Omega_i) \times H^{-\frac{1}{2}}(\partial\Omega_i))$.

1.2 Formulation of the Problem

In this section we introduce the model problem we are going to consider. We want to describe the behaviour of an incident wave hitting a penetrable or scattering obstacle.

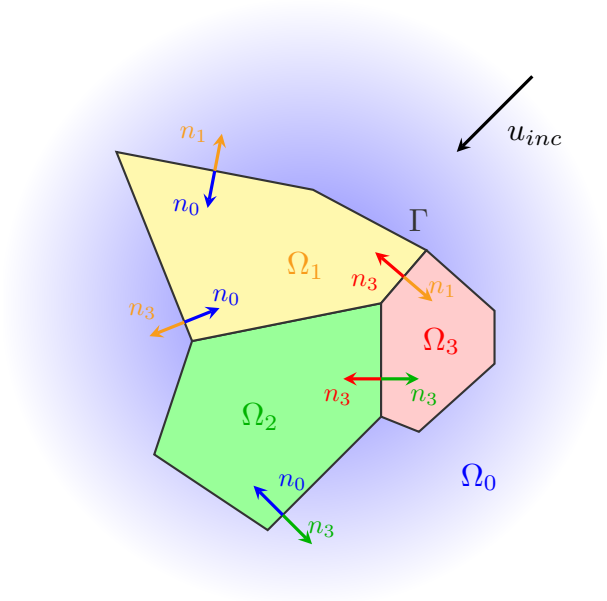

Figure 1.1: Model problem

We assume that the obstacle can be divided into several domains on which the incoming wave has constant wavelength:

Let $\Omega_i \subset \mathbb{R}^2,\ i \in \{0, 1, ..., n\}$ with $\mathbb{R}^2 = \bigcup_{i=0}^{n} \Omega_i$ be a given domain complex. Assume that the domains are numbered in such a way that Ω_0 is the only unbounded domain, the outer space. To ensure that everything is well defined, we assume the domains Ω_i to be connected and Lipschitz. We define the union of all boundaries $\Gamma := \bigcup_{i=0}^{n} \partial\Omega_i$ to be the *skeleton*.

To handle the problem mathematically, we split the solution u of the problem into two parts, $u = u_{inc} + u_{sc}$, where u_{sc} is the *scattered* part of the solution and u_{inc} the incoming wave.

Given the above defined geometry together with a vector $\kappa = (\kappa_0, \kappa_1, ..., \kappa_n) \in \mathbb{R}^{n+1}$ storing the wave numbers κ_i for every domain Ω_i, we consider the following *Helmholtz transmission problem:*

Find $u \in H^1_{\text{loc}}(\Delta, \mathbb{R}^2)$ s.t.

$$-\Delta u_{sc}(\mathbf{x}) - \kappa_i^2 u_{sc}(\mathbf{x}) = 0 \quad \mathbf{x} \in \Omega_i,\ \forall i \in \{0, 1, ..., n\},\ \text{with} \tag{1.1}$$

$$\lim_{|\mathbf{x}|\to\infty} \int_{\partial B_{|\mathbf{x}|}} |\partial_{|\mathbf{x}|} u_{sc}(\mathbf{x}) - \mathrm{i}\kappa_0 u_{sc}(\mathbf{x})|^2 d\sigma(|\mathbf{x}|) = 0. \tag{1.2}$$

where $B_{|\mathbf{x}|} := \left\{ \mathbf{y} \in \mathbb{R}^2 \middle| |\mathbf{y}| < |\mathbf{x}| \right\}$ and (1.2) is called the *Sommerfeld radiation condition* which guarantees the solution to be unique by enforcing a decaying outgoing wave.

In this thesis, u_{inc} is assumed to be a *plane wave*, propagating in direction $\mathbf{d} \in B_1$, i.e.

$$u_{\text{inc}}(\mathbf{x}) := \exp\left(\mathrm{i}\kappa_0 \mathbf{d} \cdot \mathbf{x}\right), \quad \mathbf{x} \in \mathbb{R}^2.$$

In the next steps, we reformulate the *Helmholtz transmission problem* using that $u \in H^1_{\text{loc}}(\Delta, \mathbb{R}^2)$ means by definition that $u \in H^1_{\text{loc}}(\mathbb{R}^2),\ \nabla u \in H^1_{\text{loc}}(\text{div}, \mathbb{R}^2)$. Thus, we have no Dirichlet jumps at the boundaries of Ω_i, $i \in \{0, 1, ..., n\}$ and only a sign flip in the Neumann data coming from the change of the outer normal field. These conditions are called the *transmission conditions*. We get a *localized* version of the problem:

Find u s.t. for all $i \in \{0, 1, ..., n\}$ we have $u|_{\Omega_i} \in H^1_{\text{loc}}(\Delta, \overline{\Omega}_i)$ and

$$\begin{aligned}
-\Delta u_{sc}(\mathbf{x}) - \kappa_i^2 u_{sc}(\mathbf{x}) &= 0 \quad \mathbf{x} \in \Omega_i, \\
\gamma_D^{(\Omega_i)^c} u(\mathbf{x}) - \gamma_D^{\Omega_i} u(\mathbf{x}) &= 0 \quad \mathbf{x} \in \partial\Omega_i, \\
\gamma_N^{(\Omega_i)^c} u(\mathbf{x}) + \gamma_N^{\Omega_i} u(\mathbf{x}) &= 0 \quad \mathbf{x} \in \partial\Omega_i,\ \text{with} \\
\lim_{|\mathbf{x}|\to\infty} \int_{\partial B_{|\mathbf{x}|}} |\partial_{|\mathbf{x}|} u_{sc}(\mathbf{x}) - \mathrm{i}\kappa_0 u_{sc}(\mathbf{x})|^2 d\sigma(|\mathbf{x}|) &= 0.
\end{aligned} \tag{1.3}$$

1.3 Spaces of BEM

For boundary element methods, it is useful to introduce some special spaces. First, the *multi trace space* $\mathbb{H}(\Gamma)$ defined as

$$\mathbb{H}(\Gamma) := \prod_{i=0}^{n} \left(H^{\frac{1}{2}}(\partial\Omega_i) \times H^{-\frac{1}{2}}(\partial\Omega_i) \right).$$

It is a Hilbert space equipped with the inner product (by identifying the dual space of $\mathbb{H}(\Gamma)$ with the space $\mathbb{H}(\Gamma)$ itself)

$$B(U, V) := \sum_{i=0}^{n} \int_{\partial\Omega_i} u_i \overline{q_i}\, dS - \int_{\partial\Omega_i} p_i \overline{v_i}\, dS. \tag{1.4}$$

Second, we denote the *single trace space* $\mathbb{X}(\Gamma)$, a subspace of $\mathbb{H}(\Gamma)$ defined using the spaces $\mathbb{X}^{\frac{1}{2}}(\Gamma)$ and $\mathbb{X}^{-\frac{1}{2}}(\Gamma)$:

$$\mathbb{X}^{\frac{1}{2}}(\Gamma) := \Bigg\{ (v_0,\, v_1,\, ...,\, v_n) \in \prod_{i=0}^{n} H^{\frac{1}{2}}(\partial\Omega_i) \,\Big|\, \exists v \in H^1(\mathbb{R}^2) \text{ s.t. } \gamma_D^{\Omega_i} v = v_i,\ \forall i \in \{0,1,...,n\} \Bigg\},$$

$$\mathbb{X}^{-\frac{1}{2}}(\Gamma) := \Bigg\{ (q_0,\, q_1,\, ...,\, q_n) \in \prod_{i=0}^{n} H^{-\frac{1}{2}}(\partial\Omega_i) \,\Big|\, \exists \mathbf{q} \in H(\mathrm{div}, \mathbb{R}^2) \text{ s.t. } \mathbf{n}_i \cdot (\gamma_D^{\Omega_i}, \gamma_D^{\Omega_i})\mathbf{q} = q_i,\ \forall i \in \{0,1,...,n\} \Bigg\},$$

where $\mathbf{n}_i$ is the normal field of Ω_i:

$$\mathbb{X}(\Gamma) := \Big\{ (v_i, q_i)_{0\le i\le n} \in \mathbb{H}(\Gamma) \,\Big|\, (v_0, v_1, ..., v_n) \in \mathbb{X}^{\frac{1}{2}}(\Gamma),\ (q_1, q_2, ..., q_n) \in \mathbb{X}^{-\frac{1}{2}}(\Gamma) \Big\}$$

An important characterization of $\mathbb{X}(\Gamma)$ in $\mathbb{H}(\Gamma)$ is given by the following statement:
For any $U \in \mathbb{H}(\Gamma)$ it holds

$$U \in \mathbb{X}(\Gamma) \Leftrightarrow B(U, V) = 0 \quad \forall V \in \mathbb{X}(\Gamma). \tag{1.5}$$

See [4, Prop. 2.1] for a proof.
Finally we define $\mathbb{Y}(\Gamma)$ to be a complement of $\mathbb{X}(\Gamma) \subset \mathbb{H}(\Gamma)$.

Now we are ready to again reformulate the *Helmholtz transmission problem* using the above introduced spaces:

Find u s.t. for all $i \in \{0,1,...,n\}$, we have $u|_{\Omega_i} \in H^1_{loc}(\Delta, \overline{\Omega}_i)$ and furthermore it holds:

$$\begin{aligned} -\Delta u_{sc}(\mathbf{x}) - \kappa_i^2 u_{sc}(\mathbf{x}) &= 0 \quad \text{for } \mathbf{x} \in \Omega_i, \\ (\gamma_D^{\Omega_i} u, \gamma_N^{\Omega_i} u)_{0\le i\le n} &\in \mathbb{X}(\Gamma) \text{ and} \\ \lim_{|\mathbf{x}|\to\infty} \int_{\partial B_{|\mathbf{x}|}} |\partial_{|\mathbf{x}|} u_{sc}(\mathbf{x}) - \mathrm{i}\kappa_0 u_{sc}(\mathbf{x})|^2 dS(|\mathbf{x}|) &= 0. \end{aligned} \tag{1.6}$$

1.4 Potentials and Boundary Integral Operators

Now we are ready to introduce the notion of the *fundamental solution* $\mathcal{G}_\kappa$ which is going to be very important later on.

Definition 7 *The solution $\mathcal{G}_\kappa$ to the Helmholtz equation with the Dirac distribution in zero as the right hand side:*

$$\begin{aligned} -\Delta\mathcal{G}_\kappa(\mathbf{x},\mathbf{y}) - \kappa^2\mathcal{G}_\kappa(\mathbf{x},\mathbf{y}) &= \delta_0(\mathbf{x}-\mathbf{y}), \quad \mathbf{x},\,\mathbf{y}\in\mathbb{R}^2, \text{ with} \\ \lim_{\|\mathbf{x}-\mathbf{y}\|\to\infty}\int_{\partial B_{\|\mathbf{x}-\mathbf{y}\|}} |\partial_{\|\mathbf{x}-\mathbf{y}\|}\mathcal{G}_\kappa(\mathbf{x},\mathbf{y}) - i\kappa\mathcal{G}_\kappa(\mathbf{x},\mathbf{y})|^2 d\sigma(\|\mathbf{x}-\mathbf{y}\|) &= 0, \end{aligned} \tag{1.7}$$

is called fundamental solution *of the Helmholtz operator. The equation (1.7) is meant in distributional sense.*

It can be given analytically to be

$$\mathcal{G}_\kappa(\mathbf{x},\mathbf{y}) = \frac{\mathrm{i}}{4}H_0^{(1)}(\kappa\|\mathbf{x}-\mathbf{y}\|), \quad \kappa\in\mathbb{R}_+, \tag{1.8}$$

where $H_0^{(1)}$ is the Hankel function of the first kind, also known as the Bessel function of the third kind (see Appendix A for more information) .

To give a motivation, we show in the following what idea the boundary integral equations are based on. We start with the *Green's formulas* and derive a representation of the solution u of the Helmholtz problem (1.3) only involving the traces $\gamma_D^{\Omega_i}u$, $\gamma_N^{\Omega_i}u$, $i\in\{0,1,...,n\}$.

First we use *Green's first formula*, also known as *integration by parts*, applied to the Helmholtz operator (weak form):

$$-\int_\Omega \left(\Delta+\kappa^2\right)u(\mathbf{y})v(\mathbf{y})\,d\mathbf{y} + \int_\Gamma \gamma_N^\Omega u(\mathbf{y})\gamma_D^\Omega v(\mathbf{y})\,dS(\mathbf{y}) = \int_\Omega \nabla u(\mathbf{y})\cdot\nabla v(\mathbf{y})\,d\mathbf{y}. \tag{1.9}$$

Utilizing the symmetry in u and v of the equation above we get *Green's second formula* applied to the *Helmholtz operator*:

$$\begin{aligned} -\int_\Omega (\Delta+\kappa^2)u(\mathbf{y})v(\mathbf{y})\,d\mathbf{y} + \int_\Gamma \gamma_N^\Omega u(\mathbf{y})\gamma_D^\Omega v(\mathbf{y})\,dS(\mathbf{y}) \\ = -\int_\Omega (\Delta+\kappa^2)v(\mathbf{y})u(\mathbf{y})\,d\mathbf{y} + \int_\Gamma \gamma_N^\Omega v(\mathbf{y})\gamma_D^\Omega u(\mathbf{y})\,dS(\mathbf{y}) \end{aligned} \tag{1.10}$$

and finally by plugging in the first Green's identity for the function u into (1.3), we obtain for all $v\in C_0^\infty(\mathbb{R}^2)$ and $i\in\{0,1,...,n\}$ that

$$\begin{aligned} \int_{\Omega_i} (-\Delta-\kappa_i^2)v(\mathbf{y})u(\mathbf{y})\,d\mathbf{y} \\ = \int_{\partial\Omega_i} \gamma_N^{\Omega_i}u(\mathbf{y})\gamma_D^{\Omega_i}v(\mathbf{y})\,dS(\mathbf{y}) - \int_{\partial\Omega_i}\gamma_N^{\Omega_i}v(\mathbf{y})\gamma_D^{\Omega_i}u(\mathbf{y})\,dS(\mathbf{y}). \end{aligned} \tag{1.11}$$

Setting now $v(\mathbf{y}) = \mathcal{G}_{\kappa_i}(\mathbf{x},\mathbf{y})$, $\mathbf{x}\in\mathbb{R}^2\backslash\Gamma$ fixed, $i\in\{0,1,...,n\}$ we get by rewriting (1.11), the following identity:

$$\begin{aligned} u(\mathbf{x})\chi_{\Omega_i}(\mathbf{x}) = \int_{\partial\Omega_i}\gamma_N^{\Omega_i}u(\mathbf{y})\gamma_{D,\mathbf{y}}^{\Omega_i}\mathcal{G}_{\kappa_i}(\mathbf{x},\mathbf{y})\,dS(\mathbf{y}) \\ - \int_{\partial\Omega_i}\gamma_{N,\mathbf{y}}^{\Omega_i}\mathcal{G}_{\kappa_i}(\mathbf{x},\mathbf{y})\gamma_D^{\Omega_i}u(\mathbf{y})\,dS(\mathbf{y}), \end{aligned} \tag{1.12}$$

where χ_{Ω_i} is the characteristic function of the set Ω_i.
Now, summing over all $i \in \{0, 1, ..., n\}$, we arrive at

$$u(\mathbf{x}) = \sum_{i=0}^{n} \left\{ \int_{\partial\Omega_i} \gamma_N^{\Omega_i} u(\mathbf{y}) \gamma_{D,\mathbf{y}}^{\Omega_i} \mathcal{G}_{\kappa_i}(\mathbf{x}, \mathbf{y})\, dS(\mathbf{y}) \right. \\ \left. - \int_{\partial\Omega_i} \gamma_{N,\mathbf{y}}^{\Omega_i} \mathcal{G}_{\kappa_i}(\mathbf{x}, \mathbf{y}) \gamma_D^{\Omega_i} u(\mathbf{y})\, dS(\mathbf{y}) \right\}. \tag{1.13}$$

This equation is the starting point for boundary element formulations. The idea is to find $\gamma_D^{\Omega_i} u(\mathbf{y})$, $\gamma_N^{\Omega_i} u(\mathbf{y})$ for all $\mathbf{y} \in \Gamma$, $i \in \{0, 1, ...n\}$, satisfying the *transmission conditions* in (1.3) and then plugging them into (1.13) to get the solution of the Helmholtz transmission problem on the whole space $\mathbb{R}^2$.

Before we continue developing the boundary element equations, we have to introduce some established notions concerning equation (1.13):

Definition 8 (Global, double layer and single layer potential) *Taking the right hand side of equation (1.13) and interpreting it as a continuous operator taking functions from* $\mathbb{X}(\Gamma)$ *to* $\prod_{j=0}^{n} H^1_{loc}(\Delta, \overline{\Omega}_j)$ *(for details c.f. [12, p. 112 ff.]), we define the* global potential

$$\Phi_\kappa\{U\}(\mathbf{x}) := \sum_{i=0}^{n} \left\{ \mathcal{SL}^i_{\kappa_i}\{p_i\}(\mathbf{x}) + \mathcal{DL}^i_{\kappa_i}\{u_i\}(\mathbf{x}) \right\}, \quad \mathbf{x} \in \mathbb{R}^2 \backslash \Gamma, \tag{1.14}$$

where $U := (u_i, p_i)_{0 \le i \le n} \in \mathbb{X}(\Gamma)$ *and*

$$\mathcal{DL}^i_{\kappa_i} : H^{\frac{1}{2}}(\partial\Omega_i) \to \prod_{j=0}^{n} H^1_{loc}(\Delta, \overline{\Omega}_j),$$
$$\mathcal{DL}^i_{\kappa_i}\{v\}(\mathbf{x}) := -\int_{\partial\Omega_i} \mathbf{n}_i(\mathbf{y}) \cdot \nabla \mathcal{G}_{\kappa_i}(\mathbf{x}, \mathbf{y})\, v(\mathbf{y}) dS(\mathbf{y}), \quad v \in H^{\frac{1}{2}}(\partial\Omega_i), \tag{1.15}$$

denotes the continuous double layer potential*, where on the other hand*

$$\mathcal{SL}^i_{\kappa_i} : H^{-\frac{1}{2}}(\partial\Omega_i) \to \prod_{j=0}^{n} H^1_{loc}(\Delta, \overline{\Omega}_j),$$
$$\mathcal{SL}^i_{\kappa_i}\{q\}(\mathbf{x}) = \int_{\partial\Omega_i} \mathcal{G}_{\kappa_i}(\mathbf{x}, \mathbf{y})\, q(\mathbf{y}) dS(\mathbf{y}), \quad q \in H^{-\frac{1}{2}}(\partial\Omega_i), \tag{1.16}$$

represents the single layer potential *which is a continuous mapping between the two spaces above.*

The next step is to find the equations to solve for the traces $\gamma_D^{\Omega_i} u$, $\gamma_N^{\Omega_i} u$. Since the global potential has its image in $\prod_{j=0}^{n} H^1_{loc}(\Delta, \overline{\Omega}_j)$, taking traces of it is well defined by Theorem 1 and 3. So we obtain the equations by simply taking the traces of equation (1.13) on both sides for all $i \in \{0, 1, ..., n\}$, $x \in \partial\Omega_i$:

$$\begin{aligned} \gamma_D^{\Omega_i} u(\mathbf{x}) &= \gamma_D^{\Omega_i} \Phi_\kappa \left((\gamma_D^{\Omega_i} u(\mathbf{x}), \gamma_N^{\Omega_i} u(\mathbf{x}))_{0 \le i \le n} \right), \\ \gamma_N^{\Omega_i} u(\mathbf{x}) &= \gamma_N^{\Omega_i} \Phi_\kappa \left((\gamma_D^{\Omega_i} u(\mathbf{x}), \gamma_N^{\Omega_i} u(\mathbf{x}))_{0 \le i \le n} \right). \end{aligned} \tag{1.17}$$

By equation (1.12) we have that for the trace on $\partial\Omega_i$ only the potentials indexed by i have a contribution:

$$\begin{aligned}\gamma_D^{\Omega_i} u(\mathbf{x}) &= \gamma_D^{\Omega_i}\mathcal{DL}^i_{\kappa_i}\{\gamma_D^{\Omega_i}u\}(\mathbf{x}) + \gamma_D^{\Omega_i}\mathcal{SL}^i_{\kappa_i}\{\gamma_N^{\Omega_i}u\}(\mathbf{x}),\\ \gamma_D^{\Omega_i} u(\mathbf{x}) &= \gamma_D^{\Omega_i}\mathcal{DL}^i_{\kappa_i}\{\gamma_D^{\Omega_i}u\}(\mathbf{x}) + \gamma_D^{\Omega_i}\mathcal{SL}^i_{\kappa_i}\{\gamma_N^{\Omega_i}u\}(\mathbf{x}).\end{aligned} \tag{1.18}$$

Admissible boundary data of the Helmholtz solution is given by the set of *Cauchy data*:

Definition 9 (Cauchy data) *Let $i \in \{0,1,...,n\}$ and $(v,q) \in H^{\frac{1}{2}}(\partial\Omega_i) \times H^{-\frac{1}{2}}(\partial\Omega_i)$. We say that (v,q) is a* Cauchy datum *of the domain Ω_i if there is a $u \in H_{loc}(\Delta, \overline{\Omega}_i)$ such that equation (1.1) holds in Ω_i and (1.2) holds additionally if $i = 0$. Moreover we demand that $\gamma_D^{\Omega_i} u = v$ and $\gamma_N^{\Omega_i} u = q$.*
The space of Cauchy data of $\partial\Omega_i$ *is defined by $\mathcal{C}(\partial\Omega_i)$. The* global Cauchy data space *is denoted by $\mathcal{C}(\Gamma) := \prod_{i=0}^n \mathcal{C}(\partial\Omega_i)$.*

Additionally, there is another equivalent characterization of the Cauchy data $\mathcal{C}(\partial\Omega_i)$. One direction of the equivalence we obtain directly using identity (1.18). For more details consult [9, Section 6.3].

Theorem 4 *For all $i \in \{0,1,...,n\}$ and any $(v,q) \in H^{\frac{1}{2}}(\partial\Omega_i) \times H^{-\frac{1}{2}}(\partial\Omega_i)$ we have that*

$$(v,q) \in \mathcal{C}(\partial\Omega_i) \Leftrightarrow \begin{cases}\gamma_D^{\Omega_i}\mathcal{DL}^i_{\kappa_i}\{v\} + \gamma_D^{\Omega_i}\mathcal{SL}^i_{\kappa_i}\{q\} = v\\ \gamma_N^{\Omega_i}\mathcal{DL}^i_{\kappa_i}\{v\} + \gamma_N^{\Omega_i}\mathcal{SL}^i_{\kappa_i}\{q\} = q\end{cases} \tag{1.19}$$

or globally, by summing over all $i \in \{0,1,...n\}$, we get for $U \in \mathbb{H}(\Gamma)$:

$$\begin{gathered} U = (v_j, q_j)_{0\le j\le n} \in \mathcal{C}(\Gamma)\\ \Updownarrow \\ \left(\gamma_D^{\Omega_i}\mathcal{DL}^i_{\kappa_i}\{v_j\} + \gamma_D^{\Omega_i}\mathcal{SL}^i_{\kappa_i}\{q_j\}, \gamma_N^{\Omega_i}\mathcal{DL}^i_{\kappa_i}\{v_j\} + \gamma_N^{\Omega_i}\mathcal{SL}^i_{\kappa_i}\{q_j\}\right)_{0\le i\le n} = U\end{gathered} \tag{1.20}$$

Now, with the intention to get in the end an explicit representation of $\gamma_D^{\Omega_i^c}\mathcal{SL}^j_{\kappa_j}$, $\gamma_N^{\Omega_i^c}\mathcal{SL}^j_{\kappa_j}$, $\gamma_D^{\Omega_i^c}\mathcal{DL}^j_{\kappa_j}$ and $\gamma_N^{\Omega_i^c}\mathcal{DL}^j_{\kappa_j}$ for $i,j \in \{0,1,...,n\}$, we introduce the *boundary integral operators*:

Definition 10 (Boundary integral operators) *Let $i,j \in \{0,1,...,n\}$.*
The weakly singular operator $\mathcal{V}^i_{\kappa_j,j}$ *denotes the continuous mapping*

$$\mathcal{V}^i_{j,\kappa_j} := \gamma_D^{\Omega_i}\mathcal{SL}^j_{\kappa_j} : H^{-\frac{1}{2}}(\partial\Omega_j) \to H^{\frac{1}{2}}(\partial\Omega_i).$$

The double layer potential $\mathcal{K}^i_{\kappa_j}$ *denotes the continuous mapping*

$$\mathcal{K}^i_{j,\kappa_j} := -\frac{1}{2}\left(\gamma_D^{\Omega_i}\mathcal{DL}^j_{\kappa_j} + \gamma_D^{\Omega_i^c}\mathcal{DL}^j_{\kappa_j}\right) : H^{\frac{1}{2}}(\partial\Omega_j) \to H^{\frac{1}{2}}(\partial\Omega_i)$$

and the adjoint double layer potential $\mathcal{K}'^i_{j,\kappa_j}$, *the adjoint of $\mathcal{K}^i_{j,\kappa_j}$, is given by the continuous operator*

$$\mathcal{K}'^i_{j,\kappa_j} := \frac{1}{2}\left(\gamma_N^{\Omega_i}\mathcal{SL}^j_{\kappa_j} + \gamma_N^{\Omega_i^c}\mathcal{SL}^j_{\kappa_j}\right) : H^{-\frac{1}{2}}(\partial\Omega_j) \to H^{-\frac{1}{2}}(\partial\Omega_i).$$

Finally, we have the continuous hypersingular operator $\mathcal{W}^i_{\kappa_j}$

$$\mathcal{W}^i_{j,\,\kappa_j} := \gamma_N^{\Omega_i} \mathcal{D}\mathcal{L}^j_{\kappa_j} : H^{\frac{1}{2}}(\partial\Omega_j) \to H^{-\frac{1}{2}}(\partial\Omega_i).$$

For a proof of continuity consult [12, Theorem 3.1.16]. We have to keep in mind that the definitions of the double layer potential $\mathcal{D}\mathcal{L}^i_{\kappa_i}$ in [12] differ by a minus sign.

If we assume additionally that the surface Γ lies in C^2_{pw}, the class of piecewise two times continuously differentiable functions, it is possible to show (using the *jump relations* stated directly below) that the identities of Theorem 6 below hold (c.f. for example [12, Theorem 3.3.14 and 3.3.15]).

Theorem 5 (Jump relations) *Let Ω_i be a bounded Lipschitz domain. The single and double layer potentials satisfy for all $(v, q) \in H^{\frac{1}{2}}(\partial\Omega_i) \times H^{-\frac{1}{2}}(\partial\Omega_i)$ the* jump relations

$$\begin{aligned}
\gamma_D^{\Omega_i^c} \mathcal{S}\mathcal{L}^i_{\kappa_i}\{q\} - \gamma_D^{\Omega_i} \mathcal{S}\mathcal{L}^i_{\kappa_i}\{q\} &= 0 && \text{in } H^{\frac{1}{2}}(\partial\Omega_i)\\
\gamma_D^{\Omega_i^c} \mathcal{D}\mathcal{L}^i_{\kappa_i}\{v\} - \gamma_D^{\Omega_i} \mathcal{D}\mathcal{L}^i_{\kappa_i}\{v\} &= -v && \text{in } H^{\frac{1}{2}}(\partial\Omega_i)\\
\gamma_N^{\Omega_i^c} \mathcal{S}\mathcal{L}^i_{\kappa_i}\{q\} - \gamma_N^{\Omega_i} \mathcal{S}\mathcal{L}^i_{\kappa_i}\{q\} &= -q && \text{in } H^{-\frac{1}{2}}(\partial\Omega_i)\\
\gamma_N^{\Omega_i^c} \mathcal{D}\mathcal{L}^i_{\kappa_i}\{v\} - \gamma_N^{\Omega_i} \mathcal{D}\mathcal{L}^i_{\kappa_i}\{v\} &= 0 && \text{in } H^{-\frac{1}{2}}(\partial\Omega_i)
\end{aligned}$$

for a proof consult again [12, Theorem 3.3.1]. Attention has to be paid to the definition of $\mathcal{D}\mathcal{L}^i_{\kappa_i}$, differing by a minus sign.

Theorem 6 (Identities for boundary integral operators)
For $v,\, q \in C^1_{pw}(\Gamma)$ it holds for all $i \in \{0, 1, ..., n\}$:

$$\begin{aligned}
\gamma_D^{\Omega_i} \mathcal{D}\mathcal{L}^i_{\kappa_i}\{v\} &= \frac{1}{2} v - \mathcal{K}^i_{i,\,\kappa_i}\{v\} && \text{in } L^2(\partial\Omega_i),\\
\gamma_D^{(\Omega_i)^c} \mathcal{D}\mathcal{L}^i_{\kappa_i}\{v\} &= -\frac{1}{2} v - \mathcal{K}^i_{i,\,\kappa_i}\{v\} && \text{in } L^2(\partial\Omega_i),\\
\gamma_N^{\Omega_i} \mathcal{S}\mathcal{L}^i_{\kappa_i}\{q\} &= -\left(-\frac{1}{2} q + \mathcal{K}'^i_{i,\,\kappa_i}\{q\} \right) && \text{a.e. on } \partial\Omega_i,\\
\gamma_N^{(\Omega_i)^c} \mathcal{S}\mathcal{L}^i_{\kappa_i}\{q\} &= -\left(\frac{1}{2} q + \mathcal{K}'^i_{i,\,\kappa_i}\{q\} \right) && \text{a.e. on } \partial\Omega_i.
\end{aligned}$$

Now, combining Theorem 6 with Theorem 4, we reformulate the *Helmholtz transmission problem* (1.6) again only involving traces and the boundary potential operators. To do so, we introduce another operator, called *Calderon operator*:

Definition 11 (Calderon operator) *The* Calderon operator $\mathcal{C}_\kappa$ *is a continuous operator from $\mathbb{H}(\Gamma)$ to itself, defined as*

$$\mathcal{C}_\kappa := \operatorname{diag}\left(\mathcal{C}^i_{\kappa_i}\right)_{0 \le i \le n},$$

where

$$\mathcal{C}^i_\kappa := \begin{bmatrix} -\mathcal{K}^i_{i,\,\kappa} & \mathcal{V}^i_{i,\,\kappa} \\ \mathcal{W}^i_{i,\,\kappa} & \mathcal{K}'^i_{i,\,\kappa} \end{bmatrix}.$$

Moreover we have that $\frac{Id}{2} + \mathcal{C}_\kappa$ *is a projector, i.e.* $\left(\frac{Id}{2} + \mathcal{C}_\kappa\right)\big|_{\mathrm{Im}\left(\frac{Id}{2}+\mathcal{C}_\kappa\right)} \equiv Id$. *It is clear by definition (see (1.20)) that* $\mathrm{Im}\left(\frac{Id}{2} + \mathcal{C}_\kappa\right) = \mathcal{C}(\Gamma)$.

We get because of the projection property of $\frac{Id}{2} + \mathcal{C}_\kappa$ that the following formulation is equivalent to (1.6):

Find $U := U_{sc} + U_{inc} \in \mathbb{X}(\Gamma)$,
with $U_{inc} := (\gamma_D^{\Omega_0} u_{inc},\, \gamma_N^{\Omega_0} u_{inc},\, 0,\, ...,\, 0)^T$ such that

$$U_{sc} - \left(\frac{Id}{2} + \mathcal{C}_\kappa\right) U_{sc} = 0, \tag{1.21}$$

where we interpret U_{sc} as a column vector.

To do numerical computations, it is absolutely necessary to have concrete representations of the boundary integral operators. Unfortunately, the integrals involved in the intuitive representation do not exist in the usual manner. The operators $\mathcal{V}^i_{j,\,\kappa_j}$, $\mathcal{K}^i_{j,\,\kappa_j}$, $\mathcal{K}'^i_{j,\,\kappa_j}$ can in general only be defined as improper integrals and $\mathcal{W}^i_{j,\,\kappa_j}$ even only as a Cauchy principal value.

Definition 12 (Cauchy principal value) *For a kernel function* k *one says that the* Cauchy principal value *exists if for all functions* $f \in L^\infty(\Gamma)$, *with* f *Hölder-continuous with exponent* $\lambda > 0$ *(consult [12, p.48] for a definition):*

$$\lim_{\epsilon \to 0} \int_{\Gamma \setminus B_\epsilon(\mathbf{x})} k(\mathbf{x}, \mathbf{y}) f(\mathbf{y})\, dS(\mathbf{y}) \tag{1.22}$$

exists in a local neighbourhood of $\mathbf{x} \in \Gamma$.

Theorem 7 (Integral representations of boundary integral operators) *For* $i, j \in \{0, 1, ..., n\}$, $\phi \in L^\infty(\partial\Omega_j)$ *and* $\mathbf{x} \in \partial\Omega_i$, *we have the following integral representations of the boundary integral operators:*

$$\begin{aligned}
\mathcal{V}^i_{j,\,\kappa}\{\phi\}(\mathbf{x}) &= \int_{\partial\Omega_j} \mathcal{G}_\kappa(\mathbf{x}, \mathbf{y}) \phi(\mathbf{y})\, dS(\mathbf{y}) \\
\mathcal{K}^i_{j,\,\kappa}\{\phi\}(\mathbf{x}) &= \int_{\partial\Omega_j} \mathbf{n}_j(\mathbf{y}) \cdot \nabla_{\mathbf{y}} \mathcal{G}_\kappa(\mathbf{x}, \mathbf{y}) \phi(\mathbf{y})\, dS(\mathbf{y}) \\
\mathcal{K}'^i_{j,\,\kappa}\{\phi\}(\mathbf{x}) &= \int_{\partial\Omega_j} \mathbf{n}_i(\mathbf{x}) \cdot \nabla_{\mathbf{x}} \mathcal{G}_\kappa(\mathbf{x}, \mathbf{y}) \phi(\mathbf{y})\, dS(\mathbf{y}) \\
\mathcal{W}^i_{j,\,\kappa}\{\phi\}(\mathbf{x}) &= -\mathbf{n}_i(\mathbf{x}) \cdot \nabla_{\mathbf{x}} \int_{\partial\Omega_j} \mathbf{n}_j(\mathbf{y}) \cdot \nabla_{\mathbf{y}} \mathcal{G}_\kappa(\mathbf{x}, \mathbf{y}) \phi(\mathbf{y})\, dS(\mathbf{y})
\end{aligned}$$

For a detailed derivation, see [12, Subsections 3.3.2, 3.3.3 and 3.3.4].

1.5 Boundary Element Spaces and Approximation Properties

Until now, we have defined the machinery which is needed to formulate boundary element methods. To be able to approximate the unknown Dirichlet and

Neumann data, we need finite dimensional subspaces of the spaces defined in Section 1.3. To do so, we first of all we have to substitute the skeleton Γ by a piecewise linear approximation Γ_{disc}. The skeleton Γ_{disc} then can be decomposed into finitely many, relatively open, linear *panels* or *segments* S, which build together a regular *(boundary) mesh* $\mathcal{T}$ of Γ_{disc} and satisfy the following conditions:

1. $\mathcal{T}$ is a covering of Γ_{disc}, i.e.
$$\Gamma_{\text{disc}} = \overline{\bigcup_{S\in\mathcal{T}} S}.$$
2. Every segment $S \in \mathcal{T}$ can be described by the *affine mapping*
$$\xi_S : [0,1] \to S, \quad \xi_S(t) = (P_{2S} - P_{1S})t + P_{1S},$$
where P_{1S}, P_{2S} are the two vertices of the segment S.
3. $\mathcal{T}$ is *regular*, i.e. for two different segments S, $S' \in \mathcal{T}$ there holds:
$$\overline{S} \cap \overline{S}' = \emptyset \text{ or } \{P\}, \text{where } P \text{ is the common vertex.}$$

We also introduce the *mesh width* $h_{\mathcal{T}}$ and the *quasi-uniformity* $q_{\mathcal{T}}$ of a surface mesh $\mathcal{T}$:

$$h_{\mathcal{T}} := \max_{S\in\mathcal{T}} |P_{2S} - P_{1S}|,$$
$$q_{\mathcal{T}} := \frac{h_{\mathcal{T}}}{\min_{S\in\mathcal{T}} |P_{2S} - P_{1S}|}$$

To study the convergence of boundary element methods, we are going to use sequences of boundary meshes $(\mathcal{T}_l)_{l\in\mathbb{N}}$ with $\mathcal{T}_{l+1} \subset \mathcal{T}_l$ for $l \in \mathbb{N}$ and $h_{\mathcal{T}_l} \to 0$ for $l \to \infty$. To obtain convergence of the approximation it is essential to have *quasi-uniformity* of our mesh sequence $(\mathcal{T}_l)_{l\in\mathbb{N}}$:

$$\sup_{l\in\mathbb{N}} q_{\mathcal{T}_l} \leq q < \infty.$$

1.5.1 Discontinuous Piecewise Constant Boundary Elements

Let Γ_{disc} be piecewise linear and let $\mathcal{T}$ be a boundary mesh on Γ_{disc}. Then $\mathcal{S}^0_{\mathcal{T}}(\Gamma_{\text{disc}})$ denotes the set of all piecewise constant functions on the mesh $\mathcal{T}$:

$$\mathcal{S}^0_{\mathcal{T}}(\Gamma_{\text{disc}}) := \left\{\psi \in L^\infty(\Gamma_{\text{disc}}) \,\middle|\, \forall S \in \mathcal{T} : \psi|_S \text{ is constant}\right\}.$$

Every function $\psi \in \mathcal{S}^0_{\mathcal{T}}(\Gamma_{\text{disc}})$ is defined by its constant values ψ_S on the segments $S \in \mathcal{T}$ and can be written as

$$\psi(\mathbf{x}) = \sum_{S\in\mathcal{T}} \psi_S \chi_S(\mathbf{x}),$$

where

$$\chi_S : \Gamma_{\text{disc}} \to \mathbb{R}, \quad \chi_S(\mathbf{x}) := \begin{cases} 1 & \mathbf{x} \in S, \\ 0 & \text{elsewhere} \end{cases}$$

denotes the characteristic function of the segment $S \in \mathcal{T}$.
This shows that $\mathcal{S}^0_{\mathcal{T}}(\Gamma_{\text{disc}})$ is a vector space of dimension $N = \#\{S \,|\, S \in \mathcal{T}\}$ with basis $\{\chi_S \,|\, S \in \mathcal{T}\}$.

The theorem below gives us an estimate of the approximation error. A proof is found in [14, Theorem 10.4]:

Theorem 8 *Let Γ_{disc} be a piecewise linear skeleton and $\sigma \in [-1, 0]$. Furthermore let $u \in H^s(\Gamma_{disc})$ be given for some $s \in [\sigma, 1]$. There holds the approximation property of $\mathcal{S}^0_{\mathcal{T}}(\Gamma_{disc})$*

$$\inf_{v \in \mathcal{S}^0_{\mathcal{T}}(\Gamma_{disc})} \|u - v\|_{H^\sigma(\Gamma_{disc})} \leq C h_{\mathcal{T}}^{s-\sigma} |u|_{H^s(\Gamma_{disc})} \tag{1.23}$$

1.5.2 Continuous Piecewise Linear Boundary Elements

The discontinuous boundary element functions introduced in the section before are not contained in $H^{\frac{1}{2}}(\Gamma_{\text{disc}})$. In order to obtain discrete subspaces of the classical space of Dirichlet data $H^{\frac{1}{2}}(\Gamma_{\text{disc}})$, we introduce the continuous piecewise linear boundary element space $\mathcal{S}^1_{\mathcal{T}}(\Gamma_{\text{disc}})$.

Let Γ_{disc} be again a piecewise linear approximation of the skeleton Γ and let $\mathcal{T}$ be a boundary mesh on Γ_{disc}. Then $\mathcal{S}^1_{\mathcal{T}}(\Gamma_{\text{disc}})$ denotes the set of all piecewise linear and globally continuous functions on the mesh $\mathcal{T}$:

$$\mathcal{S}^1_{\mathcal{T}}(\Gamma_{\text{disc}}) := \left\{\psi \in C^0(\Gamma_{\text{disc}}) \,\middle|\, \forall S \in \mathcal{T} : \psi|_S \in \mathbb{P}_1(S), \text{the set of lin. polyn. on } S\right\}.$$

Every function $\psi \in \mathcal{S}^1_{\mathcal{T}}(\Gamma_{\text{disc}})$ is defined by its nodal values ψ_τ on the vertices P, the edge points of the segments $S \in \mathcal{T}$. The set of all vertices is denoted by

$$\mathcal{V}(\mathcal{T}) := \{P \in \Gamma_{\text{disc}} \,|\, \exists S,\, S' \in \mathcal{T} \text{ s.t. } \{P\} = \overline{S} \cap \overline{S}'\}.$$

Using this notation we can express all $\psi \in \mathcal{S}^1_{\mathcal{T}}(\Gamma_{\text{disc}})$ in the following way:

$$\psi(\mathbf{x}) = \sum_{P \in \mathcal{V}(\mathcal{T})} \psi_P \phi_P(\mathbf{x}),$$

where

$$\phi_P : \Gamma_{\text{disc}} \to \mathbb{R}, \quad \phi_P(\mathbf{x}) := \begin{cases} 1 & \mathbf{x} = P, \\ 0 & \mathbf{x} \in \mathcal{V}(\mathcal{T}) \backslash \{P\}, \\ \text{linear} & \text{elsewhere} \end{cases},$$

denotes the hat function associated to the vertex $P \in \mathcal{V}(\mathcal{T})$.
This shows that $\mathcal{S}^1_{\mathcal{T}}(\Gamma_{\text{disc}})$ is a vector space of dimension $N = \#\{P \,|\, P \in \mathcal{V}(\mathcal{T})\}$ with basis $\{\phi_P \,|\, P \in \mathcal{V}(\mathcal{T})\}$.

The Theorem below gives us an estimate for the approximation error. A proof is found in [14, Theorem 10.9]:

Theorem 9 *Let Γ_{disc} be a piecewise linear skeleton, and $\sigma \in [0, 1]$. Furthermore let $u \in H^s(\Gamma_{disc})$ be given for some $s \in [\sigma, 2]$. Then there holds the approximation property of $\mathcal{S}^1_{\mathcal{T}}(\Gamma_{disc})$*

$$\inf_{v \in \mathcal{S}^1_{\mathcal{T}}(\Gamma_{disc})} \|u - v\|_{H^\sigma(\Gamma_{disc})} \leq C h_{\mathcal{T}}^{s-\sigma} |u|_{H^s(\Gamma_{disc})} \tag{1.24}$$

1.6 Important Results from Functional Analysis

Let H be a Hilbert space. Let $T : H \to H^*$ be a compact operator with $t : H \times H \to \mathbb{C}$, defined to be its associated sesquilinear form ${}_{H^*}\langle T\cdot, \cdot\rangle_H$. Moreover, let $F \in H^*$ and $a(\cdot,\cdot) : H \times H \to \mathbb{C}$ be a sesquilinear form. We consider the following abstract variational formulation:

Find $u \in H$ such that

$$a(u,v) + t(u,v) = F(v) \quad \forall v \in H. \tag{1.25}$$

The discretization of (1.25) can be obtained substituting the Hilbert space H for a finite-dimensional subspace S:

Find $u_N \in S$ such that

$$a(u_N,v) + t(u_N,v) = F(v) \quad \forall v \in S. \tag{1.26}$$

Next, we introduce the notion of *H-ellipticity*:

Definition 13 (H-ellipticity) *A sesquilinear form $a(\cdot,\cdot)$ is called* H-elliptic *if there is a constant $\gamma > 0$ such that*

$$\forall u \in H : \quad |a(u,u)| \geq \gamma \|u\|_H^2 \tag{1.27}$$

Then we have the following important result which gives us existence and uniqueness of the solution and convergence of the discrete approximations u_l of u in H for $l \to \infty$. Moreover, we have quasi-optimality for the approximation errors:

Theorem 10 *Let H be a Hilbert space and $(S_l)_l$ a dense sequence of finite-dimensional subspaces in H. We assume that for the sesquilinear forms $a(\cdot,\cdot)$ and $t(\cdot,\cdot)$ of the variational problem (1.25) it holds:*

1. *$a(\cdot,\cdot)$ satisfies the ellipticity condition (1.27).*
2. *The operator T associated with the sesquilinear form t is compact.*
3. *We assume that, for F=0, (1.25) only has the trivial solution:*

$$\forall v \in H\backslash\{0\} : \quad a(u,v) + t(u,v) = 0 \Rightarrow u = 0. \tag{1.28}$$

Then the variational problem (1.25) has a unique solution $u \in H$ for every $F \in H^*$.
Moreover there exists a constant $l_0 > 0$ such that for all $l \geq l_0$ the Galerkin equations (1.26) (taking S_l instead of S for every $l \in \mathbb{N}$) have a unique solution

$u_l \in S_l$. The sequence $(u_l)_l$ of the Galerkin solutions converges to u and, for $l \geq l_0$, satisfies the quasi-optimal error estimate

$$\|u - u_l\|_H \leq C \min_{v_l \in S_l} \|u - v_l\|_H \tag{1.29}$$

with a constant C which is independent of l.

For a proof consult [12, Theorem 4.2.9].

1.7 First Kind BEM Formulation

In this section we introduce the classical single trace formulation of the boundary integral equations, first analyzed by Von-Petersdorff in [15] and written down in the above introduced functional setting in [4].

We get the formulation directly from (1.21), building a variational formulation out of it using the sesquilinear form $B(\cdot,\cdot)$ and taking test functions $V \in \mathbb{X}(\Gamma)$:

Find $U \in \mathbb{X}(\Gamma)$ such that

$$B\left(\left(\frac{Id}{2} - \mathcal{C}_\kappa\right)U, V\right) = B\left(\left(\frac{Id}{2} - \mathcal{C}_\kappa\right)U_{inc}, V\right) \quad \forall V \in \mathbb{X}(\Gamma). \tag{1.30}$$

Making use of the single trace space's characterization (1.5), we arrive at the equivalent *first kind single trace formulation*

Find $U \in \mathbb{X}(\Gamma)$ such that

$$B\big(-\mathcal{C}_\kappa U, V\big) = B\left(\left(\frac{Id}{2} - \mathcal{C}_\kappa\right)U_{inc}, V\right) \quad \forall V \in \mathbb{X}(\Gamma). \tag{1.31}$$

If one is interested in a proof of equivalence to (1.21) or a proof of existence and uniqueness of the solution we refer to [4, Proposition 4.1] .

We are going to use this classical approach to compare our results with. The code is based on a BEM framework for acoustic scattering developed by P. Meury during his PhD at ETH Zurich (for details consult his thesis [10]).

1.8 Second Kind BEM Formulation

In the following we are going to write down statements concerning the method recently developed by Xavier Claeys [4]. Afterwards we modify the statements to our needs. The intention is to derive a formulation so that we can use piecewise constants to approximate both, Dirichlet and Neumann trace of our solution to the transmission problem discussed in section 1.2. To do so, we first of all make

some definitions and state some theorems and lemmas from [4]. For detailed information and proofs we refer to [4].

Definition 14 (boundary integral operator $\mathcal{A}_\kappa$) *The operator $\mathcal{A}_\kappa$ is a continuous linear operator based on the global potential defined in Definition 8:*

$$\begin{aligned} &\mathcal{A}_\kappa : \mathbb{H}(\Gamma) \to \mathbb{H}(\Gamma), \\ &\mathcal{A}_\kappa(U) := \left(\gamma_D^{\Omega_i}\Phi_\kappa(U),\, \gamma_N^{\Omega_i}\Phi_\kappa(U)\right)_{0\le i\le n}. \end{aligned} \tag{1.32}$$

Lemma 1 *Assume that $\kappa_i = \kappa_0\ \forall i \in \{1,2,...,n\}$. Then*

$$\Phi(U)(\mathbf{x}) \equiv 0 \quad \forall \mathbf{x} \in \mathbb{R}^2,\ \forall U \in \mathbb{X}(\Gamma).$$

The lemma directly implies:

Corollary 1 *Assume that $\kappa_i = \kappa_0\ \forall i \in \{1,2,...,n\}$. Then*

$$\mathcal{A}_\kappa(U)(\mathbf{x}) \equiv 0 \quad \forall \mathbf{x} \in \Gamma,\ \forall U \in \mathbb{X}(\Gamma).$$

One of the central statements of the paper [4] is given by Theorem 11:

Theorem 11 *Let $\delta > 0$ be small enough such that $\max_{j\in\{1,2,...,n\}} |\kappa_j - \kappa_0| < \delta$ and $(Id - \mathcal{A}_\kappa)|_{\mathbb{X}(\Gamma)}$ is an isomorphism (small contrast assumption). Then $u \in H^1_{loc}(\mathbb{R}^2)$ is the solution to the problem (1.1), (1.2) if and only if*

$$U = \left(\gamma_D^{\Omega_i} u, \gamma_N^{\Omega_i} u\right)_{0\le i\le n} \in \mathbb{X}(\Gamma) \tag{1.33}$$

and

$$(Id - \mathcal{A}_\kappa)\, U = (Id - \mathcal{A}_\kappa)\, U_{inc}, \tag{1.34}$$

where $U_{inc} := (\gamma_D^{\Omega_i} u_{inc},\, \gamma_N^{\Omega_i} u_{inc})_{0\le i\le n}$.

So, combining the statements of the theorems above, we can reformulate the transmission problem in the following way:

Find $U \in \mathbb{X}(\Gamma)$ such that

$$(Id - (\mathcal{A}_\kappa - \mathcal{A}_{\kappa_0}))\, U = (Id - \mathcal{A}_\kappa)\, U_{inc}, \tag{1.35}$$

where $U_{inc} := (\gamma_D^{\Omega_i} u_{inc},\, \gamma_N^{\Omega_i} u_{inc})_{0\le i\le n}$ and $\mathcal{A}_{\kappa_0}$ denotes the operator defined in (1.32) with $\kappa_i = \kappa_0\ \forall i \in \{1,2,...,n\}$.

In what follows next, we are going to see that we can modify the function spaces we are working on, because taking the difference $\mathcal{A}_\kappa - \mathcal{A}_{\kappa_0}$ instead of $\mathcal{A}_\kappa$ has a regularizing effect on the operator.

We introduce the spaces $\widetilde{\mathbb{H}}(\Gamma)$, $\widetilde{\mathbb{X}}(\Gamma)$ and $\widetilde{\mathbb{Y}}(\Gamma)$, slightly modified versions of the multi trace space $\mathbb{H}(\Gamma)$, the single trace space $\mathbb{X}(\Gamma)$ and its complement in $\mathbb{H}(\Gamma)$, $\mathbb{Y}(\Gamma)$. We obtain their definitions by just substituting $H^{\frac{1}{2}}(\partial\Omega_i) \times H^{-\frac{1}{2}}(\partial\Omega_i)$ everywhere for $L^2(\partial\Omega_i) \times L^2(\partial\Omega_i)$ (see Section 1.3).

The next theorem gives us not only the well-definedness of the considered operator on $\widetilde{\mathbb{H}}(\Gamma) = \prod_{j=0}^{n} L^2(\partial\Omega_j) \times L^2(\partial\Omega_j)$, but also implies existence and uniqueness of the solution of (1.35) on the extended space $\widetilde{\mathbb{X}}(\Gamma)$. So we obtain that it is indeed possible to extend the space of Dirichlet data to $L^2(\partial\Omega_i)$, $i \in \{0, 1, ...n\}$. This is crucial for us, since our aim is to approximate both, the Dirichlet and the Neumann data of the solution u by piecewise constants.

Theorem 12 *The operator $\mathcal{A}_\kappa - \mathcal{A}_{\kappa_0}$ is a compact operator from $\widetilde{\mathbb{H}}(\Gamma)$ to itself.*

Proof of Theorem 12: To proof our aim, we are following closely [12, Remark 3.1.3]. First of all we need another representation of the single and double layer potentials (Definition 8). We take any i, $j \in \{0, 1, ..., n\}$. Following [12, Section 3.1.1], one derives that they can be expressed using the *Newton potential*

$$\mathcal{N}^i_{\kappa_j}\phi(\mathbf{x}) := \int_{\Omega_i} \mathcal{G}_{\kappa_j}(\mathbf{x}, \mathbf{y})\phi(\mathbf{y})\, dS(\mathbf{y}).$$

Namely, $\mathcal{SL}^i_{\kappa_j}\{\phi\} = \mathcal{N}^i_{\kappa_j}\gamma_D^{\Omega_i\prime}$, $\mathcal{DL}^i_{\kappa_j}\{\phi\} = -\mathcal{N}^i_{\kappa_j}\gamma_N^{\Omega_i\prime}$, where $\gamma_D^{\Omega_i\prime}$, $\gamma_N^{\Omega_i\prime}$ denote the adjoint trace operators of $\gamma_D^{\Omega_i}$, resp. $\gamma_N^{\Omega_i}$. We have that

$$\begin{aligned}
\mathcal{V}^i_{j,\kappa_j} - \mathcal{V}^i_{j,\kappa_0} &= \gamma_D^{\Omega_i}(\mathcal{N}^j_{\kappa_j} - \mathcal{N}^j_{\kappa_0})\gamma_D^{\Omega_j\prime},\\
\mathcal{K}^i_{j,\kappa_j} - \mathcal{K}^i_{j,\kappa_0} &= \frac{1}{2}(\gamma_D^{\Omega_i} + \gamma_D^{\Omega_i^c})(\mathcal{N}^j_{\kappa_j} - \mathcal{N}^j_{\kappa_0})\gamma_N^{\Omega_j\prime},\\
\mathcal{K}'^i_{j,\kappa_j} - \mathcal{K}'^i_{j,\kappa_0} &= \frac{1}{2}(\gamma_N^{\Omega_i} + \gamma_N^{\Omega_i^c})(\mathcal{N}^j_{\kappa_j} - \mathcal{N}^j_{\kappa_0})\gamma_D^{\Omega_j\prime},\\
\mathcal{W}^i_{j,\kappa_j} - \mathcal{W}^i_{j,\kappa_0} &= -\gamma_N^{\Omega_i}(\mathcal{N}^j_{\kappa_j} - \mathcal{N}^j_{\kappa_0})\gamma_N^{\Omega_j\prime}.
\end{aligned} \tag{1.36}$$

Furthermore, we need a more general result for the trace mappings. [9, Thm. 3.37 and Thm. 3.38] lead to the following statement for Lipschitz domains:

For $s \in \left(\frac{1}{2}, \frac{3}{2}\right)$, the mapping

$$\gamma_D^{\Omega_i} : H^s_{loc}(\Omega_i) \to H^{s-\frac{1}{2}}(\partial\Omega_i) \tag{1.37}$$

is continuous.
This implies that the Neumann trace is compact from $H^{\frac{3}{2}+\epsilon}(\Omega_i)$ to $L^2(\partial\Omega_i)$ for any $\frac{1}{2} > \epsilon > 0$ using the following decomposition together with the Rellich Theorem [12, Theorem 2.5.5] for the compact embedding in the end:

$$\begin{aligned}
\gamma_N^{\Omega_i} : H^{\frac{3}{2}+\epsilon}_{\mathrm{loc}}(\Delta, \overline{\Omega}_i) \xrightarrow{\nabla} H^{\frac{1}{2}+\epsilon}_{\mathrm{loc}}(\mathrm{div}, \Omega_i) \subset (H^{\frac{1}{2}+\epsilon}_{\mathrm{loc}}(\Omega_i))^2 \xrightarrow{(\gamma_D^{\Omega_i}, \gamma_D^{\Omega_i}),\, s=\frac{1}{2}+\epsilon} (H^\epsilon(\partial\Omega_i))^2\\
\xrightarrow{\cdot\mathbf{n}_i} H^\epsilon(\partial\Omega_i) \subset\subset L^2(\Omega).
\end{aligned} \tag{1.38}$$

Writing out the operator, it turns out that we can represent $\mathcal{A}_\kappa - \mathcal{A}_{\kappa_0}$ using the integral operators defined above in (1.36) together with the identity operator Id on $L^2(\partial\Omega_i)$.
It is well-known that adding a multiple of the identity Id and taking the product of continuous operators is a continuous operation. Also we have that the composition of compact and continuous operators is again compact. Thus, we can reduce our claim to the following claim:

Claim 1: *The operators written down in (1.36) are compact on the following spaces:*

$$\begin{aligned}
\mathcal{V}^i_{j,\kappa_j} - \mathcal{V}^i_{j,\kappa_0} &: L^2(\partial\Omega_j) \to L^2(\partial\Omega_i),\\
\mathcal{K}^i_{j,\kappa_j} - \mathcal{K}^i_{j,\kappa_0} &: L^2(\partial\Omega_j) \to L^2(\partial\Omega_i),\\
\mathcal{K}'^i_{j,\kappa_j} - \mathcal{K}'^i_{j,\kappa_0} &: L^2(\partial\Omega_j) \to L^2(\partial\Omega_i),\\
\mathcal{W}^i_{j,\kappa_j} - \mathcal{W}^i_{j,\kappa_0} &: L^2(\partial\Omega_j) \to L^2(\partial\Omega_i).
\end{aligned} \tag{1.39}$$

When we expand the kernel $\left(\mathcal{G}_{\kappa_j} - \mathcal{G}_{\kappa_0}\right)$ of the Newton potential $\left(\mathcal{N}^j_{\kappa_j} - \mathcal{N}^j_{\kappa_0}\right)$ into series, we obtain that it has the form (c.f. Equation (2.6)):

$$p(\|\mathbf{x}-\mathbf{y}\|) + \log(\|\mathbf{x}-\mathbf{y}\|)q(\|\mathbf{x}-\mathbf{y}\|) + C, \tag{1.40}$$

where p, q are analytic in $\|\mathbf{x}-\mathbf{y}\|$ and of homogeneous degree 2. C is a term independent of $\mathbf{x}$ and $\mathbf{y}$.
So we have by [8, Definition 7.1.1 and Equation (7.1.2)] that $\mathcal{G}_{\kappa_j} - \mathcal{G}_{\kappa_0}$ has a pseudohomogeneous expansion of degree 2. Therefore, using [8, Theorem 7.1.1], we get that

$$\mathcal{N}^j_{\kappa_j} - \mathcal{N}^j_{\kappa_0} \in \mathcal{L}^{-4}_{cl}(\Omega_i),$$

where by $\mathcal{L}^{-4}_{cl}(\Omega_i)$ we denote the set of all classical pseudodifferential operators of order (-4) (cf. [8, Definition 6.1.6, p.310 (def. "pseudohomogeneous/classical symbol")] for detailed information).
Thus, by [8, Theorem 6.1.12], the below mapping is continuous for all $s \in \mathbb{R}$:

$$\mathcal{N}^j_{\kappa_j} - \mathcal{N}^j_{\kappa_0} : H^s_{comp}(\Omega_i) \to H^{s+4}_{loc}(\Omega_i). \tag{1.41}$$

Now, combining (1.41) with (1.38), (1.37), (1.36) and the fact (cf. [9, p. 77, 78]) that $H^s_{loc}(\Omega_i)^* = H^{-s}_{comp}(\Omega_i)$, $H^s(\Omega_i)^* = H^{-s}(\Omega_i)$, and

$$H^{\frac{3}{2}+\epsilon}_{loc}(\Delta, \overline{\Omega}_i)^* \subset H^2_{comp}(\Omega_i)^* = H^{-2}(\overline{\Omega}_i) = H^{-2}_{comp}(\Omega_i)$$

for $\frac{1}{2} > \epsilon > 0$, we obtain:

$$L^2(\partial\Omega_i) \xrightarrow{\gamma_N^{\Omega_i\prime},\ \text{from (1.37)}} H^{-2}_{comp}(\Omega_i) \xrightarrow{\mathcal{N}^j_{\kappa_j} - \mathcal{N}^j_{\kappa_0},\ s=-2} H^2_{loc}(\Omega_i) \subset H^{\frac{3}{2}+\epsilon}_{loc}(\Delta, \overline{\Omega}_i) \xrightarrow[\text{compact}]{\gamma_N^{\Omega_i},\ \text{from (1.37)}} L^2(\partial\Omega_i),$$

$$L^2(\partial\Omega_i) \xrightarrow{\gamma_N^{\Omega_i\prime},\ \text{from (1.37)}} H^{-2}_{comp}(\Omega_i) \xrightarrow{\mathcal{N}^j_{\kappa_j} - \mathcal{N}^j_{\kappa_0},\ s=-2} H^2_{loc}(\Omega_i) \subset H^1_{loc}(\Omega_i) \xrightarrow{\gamma_D^{\Omega_i},\ s=1} H^{\frac{1}{2}}(\partial\Omega_i) \subset\subset L^2(\partial\Omega_i),$$

$$L^2(\partial\Omega_i) \subset H^{-\frac{1}{2}}(\partial\Omega_i) \xrightarrow{\gamma_D^{\Omega_i\prime},\ s=1} H^{-1}_{comp}(\Omega_i) \xrightarrow{\mathcal{N}^j_{\kappa_j} - \mathcal{N}^j_{\kappa_0},\ s=-1} H^3_{loc}(\Omega_i) \subset H^{\frac{3}{2}+\epsilon}_{loc}(\Delta, \overline{\Omega}_i) \xrightarrow[\text{compact}]{\gamma_N^{\Omega_i},\ \text{from (1.37)}} L^1(\partial\Omega_i),$$

$$L^2(\partial\Omega_i) \subset H^{-\frac{1}{2}}(\partial\Omega_i) \xrightarrow{\gamma_D^{\Omega_i\prime},\ s=1} H^{-1}_{comp}(\Omega_i) \xrightarrow{\mathcal{N}^j_{\kappa_j} - \mathcal{N}^j_{\kappa_0},\ s=-1} H^3_{loc}(\Omega_i) \subset H^1_{loc}(\Omega_i) \xrightarrow{\gamma_D^{\Omega_i},\ s=1} H^{\frac{1}{2}}(\partial\Omega_i) \subset\subset L^2(\partial\Omega_i),$$

where the compact embeddings are obtained using Rellich Theorem [12, Theorem 2.5.5].

So we have shown Claim 1. This directly implies by the above that $\left(\mathcal{A}_\kappa - \mathcal{A}_{\kappa_0}\right)$ is a compact operator on $\widetilde{\mathbb{H}}(\Gamma)$. This closes our proof.

□

Indeed, we have found a second kind formulation of Fredholm type, since in equation (1.35) we have the identity operator plus a compact one. Moreover, it holds:

Theorem 13 *Let $\delta > 0$ be small enough such that $\max_{j\in\{1,2,\dots,n\}} |\kappa_j - \kappa_0| < \delta$ and $(Id - (\mathcal{A}_\kappa - \mathcal{A}_{\kappa_0}))|_{\widetilde{\mathbb{X}}(\Gamma)}$ is an isomorphism (small contrast assumption). Moreover, for all $i \in \{0, 1, ..., n\}$, let Ω_i be $C^{1,1}$ domains (cf. [9, p. 90]). Then $u \in H^1_{loc}(\mathbb{R}^2)$ is the solution to the problem (1.1), (1.2) if and only if*

$$U = \left(\gamma_D^{\Omega_i} u, \gamma_N^{\Omega_i} u\right)_{0\le i\le n} \in \widetilde{\mathbb{X}}(\Gamma) \tag{1.42}$$

and

$$(Id - (\mathcal{A}_\kappa - \mathcal{A}_{\kappa_0}))\, U = (Id - \mathcal{A}_\kappa)\, U_{inc}, \tag{1.43}$$

where $U_{inc} := (\gamma_D^{\Omega_i} u_{inc}, \gamma_N^{\Omega_i} u_{inc})_{0\le i\le n}$.

Proof of Theorem 13 Using the statement of Theorem 10 and Theorem 12, it only remains to show that $Id - (\mathcal{A}_\kappa - \mathcal{A}_{\kappa_0})$ is an injection on $\widetilde{\mathbb{X}}$ to proof the existence and uniqueness of the solution to (1.42), (1.43).

Claim 1: *$Id - (\mathcal{A}_\kappa - \mathcal{A}_{\kappa_0})$ is an injection on $\widetilde{\mathbb{X}}$.*

In the case of $\kappa_i = \kappa_0$, $\forall i \in \{1, ..., n\}$, we have that $\mathcal{A}_\kappa - \mathcal{A}_{\kappa_0} \equiv 0$ and thus $Id - (\mathcal{A}_\kappa - \mathcal{A}_{\kappa_0}) \equiv Id$, what implies injectivity for the case $\kappa_i = \kappa_0$, $\forall i \in \{1, ..., n\}$. The extension to problems satisfying the small contrast assumption we get from [4, Theorem 5.1]: The Theorem implies that the operator is injective on $\mathbb{X}(\Gamma) \cap \widetilde{\mathbb{H}}(\Gamma)$, which lies densely in $\widetilde{\mathbb{X}}(\Gamma)$. This gives us, using continuity of $Id - (\mathcal{A}_\kappa - \mathcal{A}_{\kappa_0})$, injectivity of the operator on the whole space $\widetilde{\mathbb{X}}(\Gamma)$.

To proof equivalence of the formulation (1.42), (1.43) to the problem (1.1), (1.2), we only need to show its equivalence to (1.35) (using Theorem 11).

Claim 2: *The solutions of the two formulations (1.35) and (1.42), (1.43) agree with each other.*

For strongly elliptic partial differential equations with incident plane wave, we know the Dirichlet resp. Neumann data of the solution $\gamma_D^{\Omega_i}$ resp. $\gamma_N^{\Omega_i} u$ to be in $L^2(\partial\Omega_i)$ (combine [9, Theorem 4.20] for $r = 0$ together with (1.38)). Thus, we have for the unique Helmholtz transmission solution u of (1.35) that $(\gamma_D^{\Omega_i} u, \gamma_N^{\Omega_i} u) \in \mathbb{X}(\Gamma) \cap \widetilde{\mathbb{H}}(\Gamma) \subset \widetilde{\mathbb{X}}(\Gamma)$. Since the equations in (1.35), (1.43) coincide, we have that their unique solutions have to be the same.
This closes the proof of Theorem 13.

□

We obtain the variational formulation of (1.42), (1.43) by plugging the equation into the sesquilinear form B defined in (1.4). The sesquilinear form is clearly valid for our modified space: The terms in the definition of B are just the standard $L^2(\partial\Omega_i)$ inner products. Thus, well definedness is clear and non-degeneracy follows directly.
So by non-degeneracy of B, we get the weak formulation of (1.42), (1.43), taking test functions out of $\widetilde{\mathbb{H}}(\Gamma)$:

Find $U \in \widetilde{\mathbb{X}}(\Gamma)$ such that

$$B((Id - (\mathcal{A}_\kappa - \mathcal{A}_{\kappa_0}))\, U, V) = B((Id - \mathcal{A}_\kappa)\, U_{inc}, V) \quad \forall V \in \widetilde{\mathbb{H}}(\Gamma), \quad (1.44)$$

where $U_{inc} := (\gamma_D^{\Omega_i} u_{inc}, \gamma_N^{\Omega_i} u_{inc})_{0 \le i \le n}$ and $\mathcal{A}_{\kappa_0}$ denotes the operator defined in (1.32) with $\kappa_i = \kappa_0 \; \forall i \in \{1, 2, ..., n\}$.

Since Claeys showed that for the weak form of (1.35), it suffices to take test functions out of $\mathbb{Y}(\Gamma)$, our aim is to do the same for the modified formulation (1.42), (1.43).

We remark that we can adopt the important property stated in [4, Prop. 2.1] of the single trace space $\mathbb{X}(\Gamma)$ to our space $\widetilde{\mathbb{X}}(\Gamma)$ (just replace $H^{\frac{1}{2}}(\partial\Omega_i)$ resp. $H^{-\frac{1}{2}}(\partial\Omega_i)$ by $L^2(\partial\Omega_i)$ in the proof there). It implies directly that $\widetilde{\mathbb{X}}(\Gamma)$ is closed and

$$B(U, V) = 0 \quad \forall V \in \widetilde{\mathbb{X}}(\Gamma) \quad \Leftrightarrow \quad U \in \widetilde{\mathbb{X}}(\Gamma). \quad (1.45)$$

Closedness of $\widetilde{\mathbb{X}}(\Gamma)$ together with Theorem 12 and density of $\mathbb{X}(\Gamma) \cap \widetilde{\mathbb{H}}(\Gamma)$ in $\widetilde{\mathbb{X}}(\Gamma)$ allows us to adopt the statement of [4, Corollary 5.1] to our modified space:

Theorem 14 $\left(\mathcal{A}_\kappa - \mathcal{A}_{\kappa_0}\right)$ *maps* $\widetilde{\mathbb{X}}(\Gamma)$ *into itself.*

Combined with (1.45), one obtains for all $U, V \in \widetilde{\mathbb{X}}(\Gamma)$:

$$B((Id - (\mathcal{A}_\kappa - \mathcal{A}_{\kappa_0}))U, V) = B(U, V) - B((\mathcal{A}_\kappa - \mathcal{A}_{\kappa_0})U, V) = 0. \quad (1.46)$$

Thus, we can restrict from $\widetilde{\mathbb{H}}(\Gamma)$ to $\widetilde{\mathbb{Y}}(\Gamma)$. More precisely, we have that

$$B((Id-(\mathcal{A}_\kappa-\mathcal{A}_{\kappa_0}))U, V) = 0,\ \forall V \in \widetilde{\mathbb{Y}}(\Gamma) \ \Rightarrow\ B((Id-(\mathcal{A}_\kappa-\mathcal{A}_{\kappa_0}))U, V) = 0,\ \forall V \in \widetilde{\mathbb{H}}(\Gamma).$$

And so we get, using non-degeneracy of B, the following final reformulation of the problem (1.44) resp. of the original problem (1.1), (1.2):

Find $U \in \widetilde{\mathbb{X}}(\Gamma)$ such that

$$B((Id - (\mathcal{A}_\kappa - \mathcal{A}_{\kappa_0}))\, U, V) = B((Id - \mathcal{A}_\kappa)\, U_{inc}, V) \quad \forall V \in \widetilde{\mathbb{Y}}(\Gamma), \quad (1.47)$$

where $U_{inc} := (\gamma_D^{\Omega_i} u_{inc}, \gamma_N^{\Omega_i} u_{inc})_{0 \le i \le n}$ and $\mathcal{A}_{\kappa_0}$ denotes the operator defined in (1.32) with $\kappa_i = \kappa_0 \; \forall i \in \{1, 2, ..., n\}$.

2 Implementation and Coding

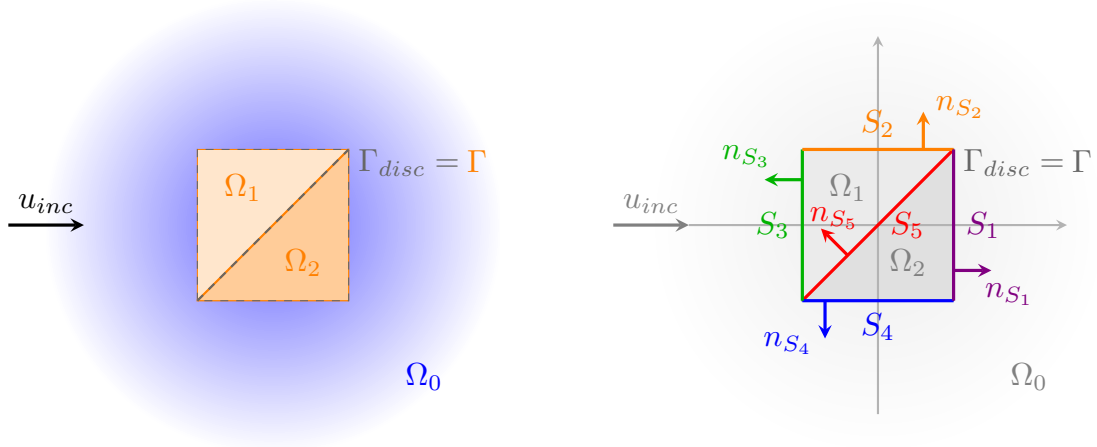

geometry **corresponding mesh**

Figure 2.1: Example problem

In this Chapter we are going to explain our implementation with the help of a simple three domain Helmholtz problem having the geometry of two triangles forming a square, as shown in Figure 2.1. The incident wave u_{inc} has the direction of propagation $\mathbf{d} = (d_1, d_2)^T$ and the wave numbers for each domain are stored in $\kappa = (\kappa_0, \kappa_1, \kappa_2)^T$.

2.1 Skeleton Discretization

We discretize our skeleton Γ using linear segments. It is stored using a class called *skeleton* having the following member variables characterizing the mesh:

- `number_of_segments` : stores the total number of segments, in the following always denoted by N_{seg}.
- `p1` : $2 \times N_{\text{seg}}$-matrix, storing the coordinates of the first edgepoint P_{1i} of the i^{th} segment S_i in `p1(:,i)`.
- `p2` : $2 \times N_{\text{seg}}$-matrix, storing the coordinates of the second edgepoint P_{2i} of the i^{th} segment S_i in `p2(:,i)`.

- `normal` : $2 \times N_{seg}$-matrix, storing the normal vector $\mathbf{n}_{S_i}$ of the i^{th} segment S_i in `normal(:,i)`.
- `size` : $1 \times N_{\text{seg}}$-matrix, storing the size of the i^{th} segment S_i in `size(1,i)`.
- `adjacent` : $2 \times N_{\text{seg}}$-matrix, storing the domains lying adjacent to the i^{th} segment S_i in such a way that the outward pointing normal $\mathbf{n}_{i_1}$ of the domain numbered by `adjacent(1,i)` $=: i_1$ points in the same direction as $\mathbf{n}_{S_i}$, while the outward pointing normal $\mathbf{n}_{i_2}$ of the domain numbered by `adjacent(2,i)` $=: i_2$ points into the opposite direction of $\mathbf{n}_{S_i}$.

Let us construct the class for our example. For simplicity we discretize the boundary using as few segments as possible (see Figure 2.1). Thus, we have for the skeleton `skel` representing the mesh of our example:

- `skel.number_of_segments = 5`,
- `skel.p1` $= \begin{pmatrix} 0.5 & 0.5 & -0.5 & -0.5 & -0.5 \\ -0.5 & 0.5 & 0.5 & -0.5 & -0.5 \end{pmatrix}$,
- `skel.p2` $= \begin{pmatrix} 0.5 & -0.5 & -0.5 & 0.5 & 0.5 \\ 0.5 & 0.5 & -0.5 & -0.5 & 0.5 \end{pmatrix}$,
- `skel.normal` $= \begin{pmatrix} 1 & 0 & -1 & 0 & \frac{-\sqrt{2}}{2} \\ 0 & 1 & 0 & -1 & \frac{\sqrt{2}}{2} \end{pmatrix}$,
- `skel.size` $= \begin{pmatrix} 1 & 1 & 1 & 1 & \sqrt{2} \end{pmatrix}$,
- `skel.adjacent` $= \begin{pmatrix} 2 & 1 & 1 & 2 & 2 \\ 0 & 0 & 0 & 0 & 1 \end{pmatrix}$.

One should remark that the choices are not unique. For example the choice for the first and second edgepoint can be interchanged or one could swap the orientation, i.e. the sign before the normal vector, for each segment.

2.2 Assembly of Operator Matrices

In this section we are going to derive a matrix representation of our operator $(\mathcal{A}_\kappa - \mathcal{A}_{\kappa_0})$. Since we are going to take segmentwise constant ansatz and test functions it makes sense to partition the operator into its segmentwise restrictions.

Segmentwise notation of $U \in \widetilde{\mathbb{X}}(\Gamma_{\text{disc}})$: We first of all have to introduce a new segmentwise notation of the elements $U = (v_j, q_j)_{0 \le j \le n} \in \widetilde{\mathbb{X}}(\Gamma_{\text{disc}})$. We focus on an arbitrary segment S_i for $i \in \{1, ..., N_{\text{seg}}\}$. Using the property stored in `adjacent`, here shortened to $(i_1, i_2)^T :=$ `adjacent(:,i)`, we have by definition that there is a $u \in H^1(\mathbb{R}^2)$ and a $\mathbf{q} \in H^1(\text{div}, \mathbb{R}^2)$ such that for the Dirichlet data we obtain

$$v_{i_1}|_{S_i} = \gamma_D^{\Omega_{i_1}}|_{S_i} u = \gamma_D^{\Omega_{i_2}}|_{S_i} u = v_{i_2}|_{S_i},$$

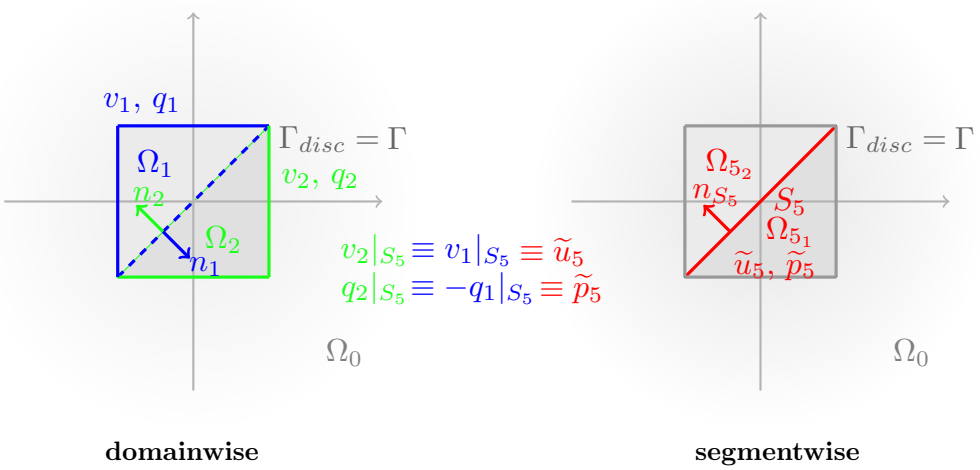

Figure 2.2: Representation of $U \in \widetilde{\mathbb{X}}(\Gamma_{\text{disc}})$, example for segment S_5

and for the Neumann data

$$\begin{aligned} q_{i_1}|_{S_i} &= \mathbf{n}_{S_i} \cdot (\gamma_D^{\Omega_{i_1}}, \gamma_D^{\Omega_{i_1}})|_{S_i}\mathbf{q} \\ &= \mathbf{n}_{i_1} \cdot (\gamma_D^{\Omega_{i_1}}, \gamma_D^{\Omega_{i_1}})|_{S_i}\mathbf{q} \\ &= -\mathbf{n}_{i_2} \cdot (\gamma_D^{\Omega_{i_2}}, \gamma_D^{\Omega_{i_2}})|_{S_i}\mathbf{q} = q_{i_2}|_{S_i}, \end{aligned}$$

using the jump conditions for $\mathbf{q}$ resp. u from Theorem 5. Thus, we can represent $U \in \widetilde{\mathbb{X}}(\Gamma_{\text{disc}})$ as

$$U = (v_{i_1}|_{S_i}, q_{i_1}|_{S_i}, v_{i_1}|_{S_i}, -q_{i_1}|_{S_i})_{1\le i\le N_{\text{seg}}}^T =: (\widetilde{u}_i, \widetilde{p}_i, \widetilde{u}_i, -\widetilde{p}_i)_{1\le i\le N_{\text{seg}}}^T.$$

Finally, projecting into the piecewise constant boundary element space $\mathcal{S}^0_{\mathcal{T}}(\Gamma_{\text{disc}})$, we can write $U \in \widetilde{\mathbb{X}}(\Gamma_{\text{disc}}) \cap \mathcal{S}^0_{\mathcal{T}}(\Gamma_{\text{disc}})$ as

$$\widetilde{\mathbf{U}} = \left((u_i, p_i) \begin{pmatrix} 1 & 0 & 1 & 0 \\ 0 & 1 & 0 & -1 \end{pmatrix} \right)_{1\le i\le N_{\text{seg}}}^T \in \mathbb{C}^{4N_{\text{seg}}}, \tag{2.1}$$

which represents the coefficient vector relative to the ansatz functions χ_{S_i}, for $i \in \{1, ..., N_{seg}\}$.

$$\chi_{S_i}(\mathbf{x}) := \begin{cases} 1 & \mathbf{x} \in S_i \\ 0 & \text{else} \end{cases}$$

is the characteristic function of the i^{th} segment S_i. Define also

$$\mathbf{U} := (u_i, p_i)_{1\le i\le N_{\text{seg}}} \in \mathbb{C}^{2N_{\text{seg}}}$$

to be the *segmentwise Dirichlet resp. Neumann data.*

In Figure 2.2 one can find an example explaining the segmentwise representation: Focusing on segment S_5, the adjacent domains of the segment are Ω_1 and Ω_2. Ω_2 has the same orientation as S_5, while Ω_1 is oriented contrariwise. Therefore,

the Dirichlet data v_2 of Ω_2 restricted to the segment S_5 is defined to be the Dirichlet data $\widetilde{u}_5$ of segment S_5 and coincides with the Dirichlet data v_1 of the adjacent domain Ω_1 restricted to S_5. For the Neumann data we have that q_2 of Ω_2 restricted to the segment S_5 is defined to be the Neumann data $\widetilde{p}_5$, while q_1 has the opposite sign of $\widetilde{p}_5$.

Segmentwise notation of $V \in \widetilde{\mathbb{Y}}(\Gamma_{\mathbf{disc}}) \cap \mathcal{S}^0_{\mathcal{T}}(\Gamma_{\mathbf{disc}})$: Our test functions in (1.47) we take from a complement of $\widetilde{\mathbb{X}}(\Gamma_{\text{disc}})$ in $\widetilde{\mathbb{H}}(\Gamma_{\text{disc}})$. Using the segmentwise representation (2.1) for $U \in \widetilde{\mathbb{X}}(\Gamma_{\text{disc}}) \cap \mathcal{S}^0_{\mathcal{T}}(\Gamma_{\text{disc}})$ from the preceding paragraph, an obvious choice for the discrete test space $\widetilde{\mathbb{Y}}(\Gamma_{\text{disc}}) \cap \mathcal{S}^0_{\mathcal{T}}(\Gamma_{\text{disc}})$ is given by

$$\left\{ \left((v_i, q_i) \begin{pmatrix} 1 & 0 & -1 & 0 \\ 0 & 1 & 0 & 1 \end{pmatrix} \right)^T_{1 \leq i \leq N_{\text{seg}}} \in \mathbb{C}^{4N_{\text{seg}}} \,\middle|\, (v_i, q_i)_{1 \leq i \leq N_{\text{seg}}} \in \mathbb{C}^{2N_{\text{seg}}} \right\}. \tag{2.2}$$

Again, the vectors represent the coefficients relative to the ansatz functions χ_{S_i}, for $i \in \{1, ..., N_{seg}\}$.

Segmentwise notation of $\left(\mathcal{A}_\kappa - \mathcal{A}_{\kappa_0}\right)$: In the following steps, we are going to rewrite the operator $\left(\mathcal{A}_\kappa - \mathcal{A}_{\kappa_0}\right)$. We explain the modifications using our example problem sketched in Figure 2.1. Moreover, we only explain the steps for the matrix resp. vector entries which are colored in red, since the reformulations work out analogously for all domains (segments).

We recall the definition of $\left(\mathcal{A}_\kappa - \mathcal{A}_{\kappa_0}\right)$:

$$\left(\mathcal{A}_\kappa - \mathcal{A}_{\kappa_0}\right) U = \begin{pmatrix} \gamma_D^{\Omega_i}(\Phi_\kappa(U) - \Phi_{\kappa_0}(U)) \\ \gamma_N^{\Omega_i}(\Phi_\kappa(U) - \Phi_{\kappa_0}(U)) \end{pmatrix}_{0 \leq i \leq n}.$$

Φ_{κ_0} is the potential we get by setting $\kappa_i = \kappa_0$, $\forall i \in \{1, 2, ..., n\}$. Therefore, for our example we have

$$\left(\mathcal{A}_\kappa - \mathcal{A}_{\kappa_0}\right) U = \begin{pmatrix} \gamma_D^{\Omega_0}(\Phi_\kappa(U) - \Phi_{\kappa_0}(U)) \\ \gamma_N^{\Omega_0}(\Phi_\kappa(U) - \Phi_{\kappa_0}(U)) \\ \gamma_D^{\Omega_1}(\Phi_\kappa(U) - \Phi_{\kappa_0}(U)) \\ \gamma_N^{\Omega_1}(\Phi_\kappa(U) - \Phi_{\kappa_0}(U)) \\ \gamma_D^{\Omega_2}(\Phi_\kappa(U) - \Phi_{\kappa_0}(U)) \\ \gamma_N^{\Omega_2}(\Phi_\kappa(U) - \Phi_{\kappa_0}(U)) \end{pmatrix}. \tag{2.3}$$

First of all it is clear that we can partition the domainwise traces into segmentwise traces. Since it works similar for every domain Ω_i, we only write it down for Ω_1, the part marked red in (2.3). We can partition the boundary as $\partial\Omega_1 = S_2 \cup S_3 \cup S_5$ and therefore obtain for $\begin{pmatrix} \gamma_D^{\Omega_1}(\Phi_\kappa(U) - \Phi_{\kappa_0}(U)) \\ \gamma_N^{\Omega_1}(\Phi_\kappa(U) - \Phi_{\kappa_0}(U)) \end{pmatrix}$:

$$\begin{pmatrix} \gamma_D^{\Omega_1}|_{S_2}(\Phi_\kappa(U) - \Phi_{\kappa_0}(U)) + \gamma_D^{\Omega_1}|_{S_3}(\Phi_\kappa(U) - \Phi_{\kappa_0}(U)) + \gamma_D^{\Omega_1}|_{S_5}(\Phi_\kappa(U) - \Phi_{\kappa_0}(U)) \\ \gamma_N^{\Omega_1}|_{S_2}(\Phi_\kappa(U) - \Phi_{\kappa_0}(U)) + \gamma_N^{\Omega_1}|_{S_3}(\Phi_\kappa(U) - \Phi_{\kappa_0}(U)) + \gamma_N^{\Omega_1}|_{S_5}(\Phi_\kappa(U) - \Phi_{\kappa_0}(U)) \end{pmatrix}.$$

Since we also want the image data of the operator also being stored segmentwise, we rewrite the part of the operator taking the trace from Ω_1 again:

$$\begin{pmatrix} \gamma_D^{\Omega_1}|_{S_2}(\Phi_\kappa(U)-\Phi_{\kappa_0}(U)) \\ \gamma_N^{\Omega_1}|_{S_2}(\Phi_\kappa(U)-\Phi_{\kappa_0}(U)) \\ \gamma_D^{\Omega_1}|_{S_3}(\Phi_\kappa(U)-\Phi_{\kappa_0}(U)) \\ \gamma_N^{\Omega_1}|_{S_3}(\Phi_\kappa(U)-\Phi_{\kappa_0}(U)) \\ \gamma_D^{\Omega_1}|_{S_5}(\Phi_\kappa(U)-\Phi_{\kappa_0}(U)) \\ \gamma_N^{\Omega_1}|_{S_5}(\Phi_\kappa(U)-\Phi_{\kappa_0}(U)) \end{pmatrix}. \tag{2.4}$$

Furthermore, by definition we have

$$\begin{aligned} \Phi_\kappa\{U\}-\Phi_{\kappa_0}\{U\} &= \sum_{j=0}^{n}\Big\{\mathcal{SL}^j_{\kappa_j}(q_j)-\mathcal{SL}^j_{\kappa_0}(q_j)+\mathcal{DL}^j_{\kappa_j}(v_j)-\mathcal{DL}^j_{\kappa_0}(v_j)\Big\} \\ &= \sum_{j=0}^{N_{\text{seg}}}\Big\{\mathcal{SL}^{j_1}_{\kappa_{j_1}}(\widetilde{p}_j)-\mathcal{SL}^{j_1}_{\kappa_0}(\widetilde{p}_j)+\mathcal{DL}^{j_1}_{\kappa_{j_1}}(\widetilde{u}_j)-\mathcal{DL}^{j_1}_{\kappa_0}(\widetilde{u}_j) \\ &\qquad +\mathcal{SL}^{j_2}_{\kappa_{j_2}}(\widetilde{p}_j)-\mathcal{SL}^{j_2}_{\kappa_0}(\widetilde{p}_j)+\mathcal{DL}^{j_2}_{\kappa_{j_2}}(\widetilde{u}_j)-\mathcal{DL}^{j_2}_{\kappa_0}(\widetilde{u}_j)\Big\}. \end{aligned}$$

Thus, for domain Ω_1 and segment 5, i.e. for the part marked red in (2.4), we end up with

$$\begin{pmatrix} \gamma_D^{\Omega_1}|_{S_5}\left(\mathcal{DL}^{j_1}_{\kappa_{j_1}}-\mathcal{DL}^{j_1}_{\kappa_0}\right) & \gamma_D^{\Omega_1}|_{S_5}\left(\mathcal{SL}^{j_1}_{\kappa_{j_1}}-\mathcal{SL}^{j_1}_{\kappa_0}\right) & \gamma_D^{\Omega_1}|_{S_5}\left(\mathcal{DL}^{j_2}_{\kappa_{j_2}}-\mathcal{DL}^{j_2}_{\kappa_0}\right) & \gamma_D^{\Omega_1}|_{S_5}\left(\mathcal{SL}^{j_2}_{\kappa_{j_2}}-\mathcal{SL}^{j_2}_{\kappa_0}\right) \\ \gamma_N^{\Omega_1}|_{S_5}\left(\mathcal{DL}^{j_1}_{\kappa_{j_1}}-\mathcal{DL}^{j_1}_{\kappa_0}\right) & \gamma_N^{\Omega_1}|_{S_5}\left(\mathcal{SL}^{j_1}_{\kappa_{j_1}}-\mathcal{SL}^{j_1}_{\kappa_0}\right) & \gamma_N^{\Omega_1}|_{S_5}\left(\mathcal{DL}^{j_2}_{\kappa_{j_2}}-\mathcal{DL}^{j_2}_{\kappa_0}\right) & \gamma_N^{\Omega_1}|_{S_5}\left(\mathcal{SL}^{j_2}_{\kappa_{j_2}}-\mathcal{SL}^{j_2}_{\kappa_0}\right) \end{pmatrix}_{j=1}^{N_{\text{seg}}} \begin{pmatrix} \widetilde{u}_j \\ \widetilde{p}_j \\ \widetilde{u}_j \\ -\widetilde{p}_j \end{pmatrix}_{j=1}^{N_{\text{seg}}}.$$

Repeating these reformulation steps for all domains and segments one obtains for each segment four rows concerning its trace. We order the rows by the numbering of segments. For each segment, its four rows are ordered in such a way that the first two rows represent the Dirichlet resp. Neumann traces respecting the orientation of the segment, while the the third and fourth row represent the traces with respect to the opposite orientation (the orientation of Ω_{i_2}).

We obtain for the general case

$$\begin{pmatrix} \gamma_D^{\Omega_{i_1}}|_{S_i}\left(\mathcal{DL}^{j_1}_{\kappa_{j_1}}-\mathcal{DL}^{j_1}_{\kappa_0}\right) & \gamma_D^{\Omega_{i_1}}|_{S_i}\left(\mathcal{SL}^{j_1}_{\kappa_{j_1}}-\mathcal{SL}^{j_1}_{\kappa_0}\right) & \gamma_D^{\Omega_{i_1}}|_{S_i}\left(\mathcal{DL}^{j_2}_{\kappa_{j_2}}-\mathcal{DL}^{j_2}_{\kappa_0}\right) & \gamma_D^{\Omega_{i_1}}|_{S_i}\left(\mathcal{SL}^{j_2}_{\kappa_{j_2}}-\mathcal{SL}^{j_2}_{\kappa_0}\right) \\ \gamma_N^{\Omega_{i_1}}|_{S_i}\left(\mathcal{DL}^{j_1}_{\kappa_{j_1}}-\mathcal{DL}^{j_1}_{\kappa_0}\right) & \gamma_N^{\Omega_{i_1}}|_{S_i}\left(\mathcal{SL}^{j_1}_{\kappa_{j_1}}-\mathcal{SL}^{j_1}_{\kappa_0}\right) & \gamma_N^{\Omega_{i_1}}|_{S_i}\left(\mathcal{DL}^{j_2}_{\kappa_{j_2}}-\mathcal{DL}^{j_2}_{\kappa_0}\right) & \gamma_N^{\Omega_{i_1}}|_{S_i}\left(\mathcal{SL}^{j_2}_{\kappa_{j_2}}-\mathcal{SL}^{j_2}_{\kappa_0}\right) \\ \gamma_D^{\Omega_{i_2}}|_{S_i}\left(\mathcal{DL}^{j_1}_{\kappa_{j_1}}-\mathcal{DL}^{j_1}_{\kappa_0}\right) & \gamma_D^{\Omega_{i_2}}|_{S_i}\left(\mathcal{SL}^{j_1}_{\kappa_{j_1}}-\mathcal{SL}^{j_1}_{\kappa_0}\right) & \gamma_D^{\Omega_{i_2}}|_{S_i}\left(\mathcal{DL}^{j_2}_{\kappa_{j_2}}-\mathcal{DL}^{j_2}_{\kappa_0}\right) & \gamma_D^{\Omega_{i_2}}|_{S_i}\left(\mathcal{SL}^{j_2}_{\kappa_{j_2}}-\mathcal{SL}^{j_2}_{\kappa_0}\right) \\ \gamma_N^{\Omega_{i_2}}|_{S_i}\left(\mathcal{DL}^{j_1}_{\kappa_{j_1}}-\mathcal{DL}^{j_1}_{\kappa_0}\right) & \gamma_N^{\Omega_{i_2}}|_{S_i}\left(\mathcal{SL}^{j_1}_{\kappa_{j_1}}-\mathcal{SL}^{j_1}_{\kappa_0}\right) & \gamma_N^{\Omega_{i_2}}|_{S_i}\left(\mathcal{DL}^{j_2}_{\kappa_{j_2}}-\mathcal{DL}^{j_2}_{\kappa_0}\right) & \gamma_N^{\Omega_{i_2}}|_{S_i}\left(\mathcal{SL}^{j_2}_{\kappa_{j_2}}-\mathcal{SL}^{j_2}_{\kappa_0}\right) \end{pmatrix}_{i,j=1}^{N_{\text{seg}}} \begin{pmatrix} \widetilde{u}_j \\ \widetilde{p}_j \\ \widetilde{u}_j \\ -\widetilde{p}_j \end{pmatrix}_{j=1}^{N_{\text{seg}}}.$$

Matrix representation of the left hand side of the variational formulation: The next step is to rewrite the variational formulation (1.47) in matrix-vector form using the above representation of the operator $\left(\mathcal{A}_\kappa-\mathcal{A}_{\kappa_0}\right)$, but additionally including the integral-part of the sesquilinear form B directly into the operator. The same we do for the operator Id. We then use the notations $\widetilde{\mathcal{A}}_\kappa, \widetilde{\mathcal{A}}_{\kappa_0}$ resp. $\widetilde{Id}$ for them and get:

$$\mathbf{V}^T\mathbf{P}_{\mathbb{Y}}^T\mathbf{B}\left(\widetilde{Id}-(\widetilde{\mathcal{A}}_\kappa-\widetilde{\mathcal{A}}_{\kappa_0})\right)\mathbf{P}_{\mathbb{X}}\mathbf{U}=\mathbf{RHS},$$

with

$$\mathbf{P}_{\mathbb{X}} = \mathbf{diag}\left\{\left(\begin{pmatrix}1 & 0\\ 0 & 1\\ 1 & 0\\ 0 & -1\end{pmatrix}\right)_{i=1}^{N_{seg}}\right\},$$

$$\mathbf{P}_{\mathbb{Y}} = \mathbf{diag}\left\{\left(\begin{pmatrix}1 & 0\\ 0 & -1\\ 1 & 0\\ 0 & 1\end{pmatrix}\right)_{i=1}^{N_{seg}}\right\}$$

and finally,

$$\mathbf{B} = \mathbf{diag}\left\{\left(\begin{pmatrix}0 & -1\\ 1 & 0\end{pmatrix}\right)_{i=1}^{2N_{seg}}\right\}.$$

The formulation of the right hand side **RHS** can be found in Subsection 2.3 below.

$\widetilde{Id}$ can be expressed in the following way:

$$\left(\mathbb{1}_{4\times 4}\int_{S_i}\chi_{S_i}(\mathbf{x})\chi_{S_j}(\mathbf{x})\,dS(\mathbf{x})\right)_{i,j=1}^{N_{\text{seg}}},$$

which simplifies to

$$\mathbf{diag}\left\{\left(\begin{pmatrix}|S_i| & 0 & 0 & 0\\ 0 & |S_i| & 0 & 0\\ 0 & 0 & |S_i| & 0\\ 0 & 0 & 0 & |S_i|\end{pmatrix}\right)_{i=1}^{N_{\text{seg}}}\right\}.$$

The just defined operator $\left(\widetilde{\mathcal{A}}_{\kappa}-\widetilde{\mathcal{A}}_{\kappa_0}\right)$ has the form

$$\begin{pmatrix}
\int_{S_i}\gamma_D^{\Omega_{i_1}}\left(\mathcal{DL}^{j_1}_{\kappa_{j_1}}-\mathcal{DL}^{j_1}_{\kappa_0}\right)\{\chi_{S_j}\}(\mathbf{x})\,dS(\mathbf{x}) & \int_{S_i}\gamma_D^{\Omega_{i_1}}\left(\mathcal{SL}^{j_1}_{\kappa_{j_1}}-\mathcal{SL}^{j_1}_{\kappa_0}\right)\{\chi_{S_j}\}(\mathbf{x})\,dS(\mathbf{x})\\
\int_{S_i}\gamma_N^{\Omega_{i_1}}\left(\mathcal{DL}^{j_1}_{\kappa_{j_1}}-\mathcal{DL}^{j_1}_{\kappa_0}\right)\{\chi_{S_j}\}(\mathbf{x})\,dS(\mathbf{x}) & \int_{S_i}\gamma_N^{\Omega_{i_1}}\left(\mathcal{SL}^{j_1}_{\kappa_{j_1}}-\mathcal{SL}^{j_1}_{\kappa_0}\right)\{\chi_{S_j}\}(\mathbf{x})\,dS(\mathbf{x})\\
\int_{S_i}\gamma_D^{\Omega_{i_2}}\left(\mathcal{DL}^{j_1}_{\kappa_{j_1}}-\mathcal{DL}^{j_1}_{\kappa_0}\right)\{\chi_{S_j}\}(\mathbf{x})\,dS(\mathbf{x}) & \int_{S_i}\gamma_D^{\Omega_{i_2}}\left(\mathcal{SL}^{j_1}_{\kappa_{j_1}}-\mathcal{SL}^{j_1}_{\kappa_0}\right)\{\chi_{S_j}\}(\mathbf{x})\,dS(\mathbf{x})\\
\int_{S_i}\gamma_N^{\Omega_{i_2}}\left(\mathcal{DL}^{j_1}_{\kappa_{j_1}}-\mathcal{DL}^{j_1}_{\kappa_0}\right)\{\chi_{S_j}\}(\mathbf{x})\,dS(\mathbf{x}) & \int_{S_i}\gamma_N^{\Omega_{i_2}}\left(\mathcal{SL}^{j_1}_{\kappa_{j_1}}-\mathcal{SL}^{j_1}_{\kappa_0}\right)\{\chi_{S_j}\}(\mathbf{x})\,dS(\mathbf{x})
\end{pmatrix}$$

$$\begin{pmatrix}
\int_{S_i}\gamma_D^{\Omega_{i_1}}\left(\mathcal{DL}^{j_2}_{\kappa_{j_2}}-\mathcal{DL}^{j_2}_{\kappa_0}\right)\{\chi_{S_j}\}(\mathbf{x})\,dS(\mathbf{x}) & \int_{S_i}\gamma_D^{\Omega_{i_1}}\left(\mathcal{SL}^{j_2}_{\kappa_{j_2}}-\mathcal{SL}^{j_2}_{\kappa_0}\right)\{\chi_{S_j}\}(\mathbf{x})\,dS(\mathbf{x})\\
\int_{S_i}\gamma_N^{\Omega_{i_1}}\left(\mathcal{DL}^{j_2}_{\kappa_{j_2}}-\mathcal{DL}^{j_2}_{\kappa_0}\right)\{\chi_{S_j}\}(\mathbf{x})\,dS(\mathbf{x}) & \int_{S_i}\gamma_N^{\Omega_{i_1}}\left(\mathcal{SL}^{j_2}_{\kappa_{j_2}}-\mathcal{SL}^{j_2}_{\kappa_0}\right)\{\chi_{S_j}\}(\mathbf{x})\,dS(\mathbf{x})\\
\int_{S_i}\gamma_D^{\Omega_{i_2}}\left(\mathcal{DL}^{j_2}_{\kappa_{j_2}}-\mathcal{DL}^{j_2}_{\kappa_0}\right)\{\chi_{S_j}\}(\mathbf{x})\,dS(\mathbf{x}) & \int_{S_i}\gamma_D^{\Omega_{i_2}}\left(\mathcal{SL}^{j_2}_{\kappa_{j_2}}-\mathcal{SL}^{j_2}_{\kappa_0}\right)\{\chi_{S_j}\}(\mathbf{x})\,dS(\mathbf{x})\\
\int_{S_i}\gamma_N^{\Omega_{i_2}}\left(\mathcal{DL}^{j_2}_{\kappa_{j_2}}-\mathcal{DL}^{j_2}_{\kappa_0}\right)\{\chi_{S_j}\}(\mathbf{x})\,dS(\mathbf{x}) & \int_{S_i}\gamma_N^{\Omega_{i_2}}\left(\mathcal{SL}^{j_2}_{\kappa_{j_2}}-\mathcal{SL}^{j_2}_{\kappa_0}\right)\{\chi_{S_j}\}(\mathbf{x})\,dS(\mathbf{x})
\end{pmatrix}_{i,\,j=1}^{N_{\text{seg}}}$$

and takes the coefficient vector $\widetilde{\mathbf{U}} = (u_j, p_j, u_j, -p_j)^T_{1\le j\le N_{\text{seg}}} \in \mathbb{C}^{4N_{\text{seg}}}$ from the discretized space $\widetilde{\mathbb{X}}(\Gamma)\cap\mathcal{S}^0_{\mathcal{T}}(\Gamma_{\text{disc}})$ as input. Again i_1, i_2 resp. j_1, j_2 are the indices of the domains lying adjacent to the segment S_i.

As a next step, we replace the traces of the single and double layer potentials by the operators defined in Definition 10 and using Theorem 6:

$$\begin{pmatrix} \int_{S_i} \frac{1}{2}\chi_{S_j}(\mathbf{x}) - \mathcal{K}^{i_1}_{j_1,\kappa_{j_1}}\{\chi_{S_j}\}(\mathbf{x})\,dS(\mathbf{x}) & \int_{S_i} \mathcal{V}^{i_1}_{j_1,\kappa_{j_1}}\{\chi_{S_j}\}(\mathbf{x})\,dS(\mathbf{x}) \\ \int_{S_i} \mathcal{W}^{i_1}_{j_1,\kappa_{j_1}}\{\chi_{S_j}\}(\mathbf{x})\,dS(\mathbf{x}) & \int_{S_i} \frac{1}{2}\chi_{S_j}(\mathbf{x}) + \mathcal{K}'^{\,i_1}_{j_1,\kappa_{j_1}}\{\chi_{S_j}\}(\mathbf{x})\,dS(\mathbf{x}) \\ \int_{S_i} -\frac{1}{2}\chi_{S_j}(\mathbf{x}) - \mathcal{K}^{i_2}_{j_1,\kappa_{j_1}}\{\chi_{S_j}\}(\mathbf{x})\,dS(\mathbf{x}) & \int_{S_i} \mathcal{V}^{i_2}_{j_1,\kappa_{j_1}}\{\chi_{S_j}\}(\mathbf{x})\,dS(\mathbf{x}) \\ \int_{S_i} \mathcal{W}^{i_2}_{j_1,\kappa_{j_1}}\{\chi_{S_j}\}(\mathbf{x})\,dS(\mathbf{x}) & \int_{S_i} \frac{1}{2}\chi_{S_j}(\mathbf{x}) + \mathcal{K}'^{\,i_2}_{j_1,\kappa_{j_1}}\{\chi_{S_j}\}(\mathbf{x})\,dS(\mathbf{x}) \end{pmatrix}$$

$$\begin{pmatrix} \int_{S_i} -\frac{1}{2}\chi_{S_j}(\mathbf{x}) - \mathcal{K}^{i_1}_{j_2,\kappa_{j_2}}\{\chi_{S_j}\}(\mathbf{x})\,dS(\mathbf{x}) & \int_{S_i} \mathcal{V}^{i_1}_{j_2,\kappa_{j_2}}\{\chi_{S_j}\}(\mathbf{x})\,dS(\mathbf{x}) \\ \int_{S_i} \mathcal{W}^{i_1}_{j_2,\kappa_{j_2}}\{\chi_{S_j}\}(\mathbf{x})\,dS(\mathbf{x}) & \int_{S_i} \frac{1}{2}\chi_{S_j}(\mathbf{x}) + \mathcal{K}'^{\,i_1}_{j_2,\kappa_{j_2}}\{\chi_{j}\}(\mathbf{x})\,dS(\mathbf{x}) \\ \int_{S_i} \frac{1}{2}\chi_{S_j}(\mathbf{x}) - \mathcal{K}^{i_2}_{j_2,\kappa_{j_2}}\{\chi_{j}\}(\mathbf{x})\,dS(\mathbf{x}) & \int_{S_i} \mathcal{V}^{i_2}_{j_2,\kappa_{j_2}}\{\chi_{S_j}\}(\mathbf{x})\,dS(\mathbf{x}) \\ \int_{S_i} \mathcal{W}^{i_2}_{j_2,\kappa_{j_2}}\{\chi_{S_j}\}(\mathbf{x})\,dS(\mathbf{x}) & \int_{S_i} \frac{1}{2}\chi_{S_j}(\mathbf{x}) + \mathcal{K}'^{\,i_2}_{j_2,\kappa_{j_2}}\{\chi_{S_j}\}(\mathbf{x})\,dS(\mathbf{x}) \end{pmatrix}_{i,\,j=1}^{N_{\text{seg}}}.$$

With the help of the integral representations of the boundary integral operators $\mathcal{V}^i_{j,\kappa_j}$, $\mathcal{K}^i_{j,\kappa_j}$, $\mathcal{K}'^{\,i}_{j,\kappa_j}$ and $\mathcal{W}^i_{j,\kappa_j}$ from Theorem 7, we define $\widetilde{v}^i_{j,\kappa}$, $\widetilde{k}^i_{j,\kappa}$, $\widetilde{k'}^{\,i}_{j,\kappa}$ and $\widetilde{w}^i_{j,\kappa}$. These expressions build our matrix entries and only depend on the orientation of the segments.

$$\begin{aligned}
\widetilde{v}^i_{j,\kappa} &:= \int_{S_i} \gamma_D^{\Omega_{i_1}} \int_{S_j} \gamma_D^{\Omega_{j_1}} \left(\mathcal{G}_\kappa - \mathcal{G}_{\kappa_0}\right)(\mathbf{x},\mathbf{y})\,\chi_{S_j}(\mathbf{x})\,dS(\mathbf{y})\,dS(\mathbf{x}) \\
&= \int_{S_i}\int_{S_j} \left(\mathcal{G}_\kappa - \mathcal{G}_{\kappa_0}\right)(\mathbf{x},\mathbf{y})\,dS(\mathbf{y})\,dS(\mathbf{x}) \\
\widetilde{k}^i_{j,\kappa} &:= \int_{S_i} \gamma_D^{\Omega_{i_1}} \int_{S_j} \gamma_D^{\Omega_{j_1}} \left(\mathbf{n}_{S_j}(\mathbf{y})\cdot\nabla_{\mathbf{y}}\left(\mathcal{G}_\kappa - \mathcal{G}_{\kappa_0}\right)(\mathbf{x},\mathbf{y})\right)\,\chi_{S_j}(\mathbf{x})\,dS(\mathbf{y})\,dS(\mathbf{x}) \\
&= \int_{S_i}\int_{S_j} \mathbf{n}_{S_j}(\mathbf{y})\cdot\nabla_{\mathbf{y}}\left(\mathcal{G}_\kappa - \mathcal{G}_{\kappa_0}\right)(\mathbf{x},\mathbf{y})\,dS(\mathbf{y})\,dS(\mathbf{x}), \\
\widetilde{k'}^{\,i}_{j,\kappa} &:= \int_{S_i} \gamma_D^{\Omega_{i_1}} \mathbf{n}_{S_i}(\mathbf{x})\cdot\nabla_{\mathbf{x}} \left(\int_{S_j} \gamma_D^{\Omega_{j_1}} \left(\mathcal{G}_\kappa - \mathcal{G}_{\kappa_0}\right)(\mathbf{x},\mathbf{y})\,\chi_{S_j}(\mathbf{x})\,dS(\mathbf{y})\right) dS(\mathbf{x}) \\
&= \int_{S_i} \mathbf{n}_{S_i}(\mathbf{x})\cdot\nabla_{\mathbf{x}} \left(\int_{S_j} \left(\mathcal{G}_\kappa - \mathcal{G}_{\kappa_0}\right)(\mathbf{x},\mathbf{y})\;dS(\mathbf{y})\right) dS(\mathbf{x}) \\
&= \int_{S_i}\int_{S_j} \mathbf{n}_{S_i}(\mathbf{x})\cdot\nabla_{\mathbf{x}}\left(\mathcal{G}_\kappa - \mathcal{G}_{\kappa_0}\right)(\mathbf{x},\mathbf{y})\,dS(\mathbf{y})\,dS(\mathbf{x}),
\end{aligned}$$

and finally,

$$\begin{aligned}
\widetilde{w}^i_{j,\kappa} &:= \int_{S_i} \gamma_D^{\Omega_{i_1}} \mathbf{n}_{S_i}(\mathbf{x})\cdot\nabla_{\mathbf{x}} \left(\int_{S_j} \gamma_D^{\Omega_{j_1}} \mathbf{n}_{S_j}(\mathbf{y})\cdot\nabla_{\mathbf{y}}\left(\mathcal{G}_\kappa - \mathcal{G}_{\kappa_0}\right)(\mathbf{x},\mathbf{y})\,\chi_{S_j}(\mathbf{x})\,dS(\mathbf{y})\right) dS(\mathbf{x}) \\
&= \int_{S_i}\int_{S_j} \mathbf{n}_{i_1}(\mathbf{x})\cdot\nabla_{\mathbf{x}}\left(\mathbf{n}_{j_1}(\mathbf{y})\cdot\nabla_{\mathbf{y}}\left(\mathcal{G}_{\kappa_{j_1}} - \mathcal{G}_{\kappa_0}\right)(\mathbf{x},\mathbf{y})\right)\,dS(\mathbf{y})\,dS(\mathbf{x}).
\end{aligned}$$

The MATLAB functions calculating these values are implemented in `integralV.m`,

`integralK.m`, `integralK_prime.m` and `integralW.m`, which are found in the folder `Library_2nd_kind`.

The matrix for the operator $\left(\widetilde{\mathcal{A}}_\kappa - \widetilde{\mathcal{A}}_{\kappa_0}\right)$ can then be rewritten as:

$$\begin{pmatrix} \frac{1}{2}|S_i|\delta_{i=j} - \widetilde{k}^i_{j,\,\kappa_{j_1}} & \widetilde{v}^i_{j,\,\kappa_{j_1}} & -\frac{1}{2}|S_i|\delta_{i=j} + \widetilde{k}^i_{j,\,\kappa_{j_2}} & \widetilde{v}^i_{j,\,\kappa_{j_2}} \\ \widetilde{w}^i_{j,\,\kappa_{j_1}} & \frac{1}{2}|S_i|\delta_{i=j} + \widetilde{k'}^i_{j,\,\kappa_{j_1}} & -\widetilde{w}^i_{j,\,\kappa_{j_2}} & \frac{1}{2}|S_i|\delta_{i=j} + \widetilde{k'}^i_{j,\,\kappa_{j_2}} \\ -\frac{1}{2}|S_i|\delta_{i=j} - \widetilde{k}^i_{j,\,\kappa_{j_1}} & \widetilde{v}^i_{j,\,\kappa_{j_1}} & \frac{1}{2}|S_i|\delta_{i=j} + \widetilde{k}^i_{j,\,\kappa_{j_2}} & \widetilde{v}^i_{j,\,\kappa_{j_2}} \\ -\widetilde{w}^i_{j,\,\kappa_{j_1}} & \frac{1}{2}|S_i|\delta_{i=j} - \widetilde{k'}^i_{j,\,\kappa_{j_1}} & \widetilde{w}^i_{j,\,\kappa_{j_2}} & \frac{1}{2}|S_i|\delta_{i=j} - \widetilde{k'}^i_{j,\,\kappa_{j_2}} \end{pmatrix}^{N_{\text{seg}}}_{i,\,j=1}. \tag{2.5}$$

One has to take care of the signs. There are signs coming from the orientation of the potential part and others coming from the orientation of the traces taken of the potential. This representation is the one we used to implement the second kind formulation. The MATLAB function assembling the matrix (2.5) is called `operator_A.m` and is found in the folder `Library_2nd_kind`.

As already pointed out in Section 1.8, the integrands of the above defined operators involve $\left(\mathcal{G}_\kappa - \mathcal{G}_{\kappa_0}\right)$. This kernel is more regular than the isolated parts of the difference. To exploit this as good as possible for our numerical experiments, we expand the expressions into series and then cancel as much terms as possible. This is done in the next subsection.

2.2.1 Series Expansions of Kernels

In this subsection we are going to use the properties of the Bessel and Hankel funktions which are written down in Appendix A. First of all we look at the kernel of the modified weakly singular operator $\widetilde{\mathcal{V}}^i_{j,\,\kappa}$, which is the easiest to handle. We have that $\left(\mathcal{G}_\kappa - \mathcal{G}_{\kappa_0}\right)(\mathbf{x}, \mathbf{y})$ is equal to

$$\begin{aligned} &\frac{\mathrm{i}}{4}\left(H_0^{(1)}(\kappa\|\mathbf{x}-\mathbf{y}\|) - H_0^{(1)}(\kappa_0\|\mathbf{x}-\mathbf{y}\|)\right) \\ &\quad\overset{(A.1)}{=} \frac{\mathrm{i}}{4}\left(J_0(\kappa\|\mathbf{x}-\mathbf{y}\|) - J_0(\kappa_0\|\mathbf{x}-\mathbf{y}\|)\right. \\ &\qquad \left. +\mathrm{i}Y_0(\kappa\|\mathbf{x}-\mathbf{y}\|) - \mathrm{i}Y_0(\kappa_0\|\mathbf{x}-\mathbf{y}\|)\right) \\ &\quad\overset{(A.4)}{=} \frac{1}{4}\left[\left(\mathrm{i} + \frac{2\psi(1)}{\pi}\right)\left\{J_0(\kappa\|\mathbf{x}-\mathbf{y}\|) - J_0(\kappa_0\|\mathbf{x}-\mathbf{y}\|)\right\}\right. \\ &\qquad -\frac{2}{\pi}\left\{\log\frac{\kappa}{\kappa_0} + \sum_{k=1}^{\infty}\frac{(-4)^{-k}}{k!^2}\|\mathbf{x}-\mathbf{y}\|^{2k}\left(\log\left(\frac{1}{2}\kappa\|\mathbf{x}-\mathbf{y}\|\right)\kappa^{2k}\right.\right. \\ &\qquad\quad \left.\left.\left. -\log\left(\frac{1}{2}\kappa_0\|\mathbf{x}-\mathbf{y}\|\right)\kappa_0^{2k} - \left(\sum_{\nu=1}^{k}\frac{1}{\nu}\right)\left(\kappa^{2k}-\kappa_0^{2k}\right)\right)\right\}\right]. \end{aligned} \tag{2.6}$$

So in the end we get rid of all singularities, since for $k \geq 1$ we have using *de l'Hôpital's rule*

$$\lim_{r\to 0} r^{2k}\log r = \lim_{r\to 0}\frac{\frac{d}{dr}\log r}{\frac{d}{dr}r^{-2k}} = \lim_{r\to 0} r^{2k} = 0.$$

Analyzing the kernel of the modified double layer potential $\widetilde{\mathcal{K}}^i_{j,\kappa}$, one obtains:

$$\begin{aligned}
&\mathbf{n}_{S_j}\cdot\nabla_{\mathbf{y}}\left(\mathcal{G}_\kappa-\mathcal{G}_{\kappa_0}\right)(\mathbf{x},\mathbf{y})\\
&\quad\overset{(A.6)}{=}\frac{\mathrm{i}}{4}\left(-H_1^{(1)}(\kappa\|\mathbf{x}-\mathbf{y}\|)\kappa+H_1^{(1)}(\kappa_0\|\mathbf{x}-\mathbf{y}\|)\kappa_0\right)\frac{\mathbf{n}_{S_j}\cdot(\mathbf{x}-\mathbf{y})}{\|\mathbf{x}-\mathbf{y}\|}\\
&\quad\overset{(A.3),(A.4)}{=}\left[\left\{\mathrm{i}-\frac{2}{\pi}\log\left(\frac{1}{2}\kappa\|\mathbf{x}-\mathbf{y}\|\right)\right\}\left(\sum_{k=0}^{\infty}\frac{(-4)^k\kappa^{2k+2}}{k!(k+1)!}\|\mathbf{x}-\mathbf{y}\|^{2k}\right)\right.\\
&\qquad-\left\{\mathrm{i}-\frac{2}{\pi}\log\left(\frac{1}{2}\kappa_0\|\mathbf{x}-\mathbf{y}\|\right)\right\}\left(\sum_{k=0}^{\infty}\frac{(-4)^k\kappa_0^{2k+2}}{k!(k+1)!}\|\mathbf{x}-\mathbf{y}\|^{2k}\right)\\
&\qquad\left.+\sum_{k=0}^{\infty}\frac{(-4)^k(\psi(k+1)+\psi(k+2))(\kappa^{2k+2}-\kappa_0^{2k+2})}{\pi k!(k+1)!}\|\mathbf{x}-\mathbf{y}\|^{2k}\right]\frac{\mathbf{n}_{S_j}\cdot(\mathbf{x}-\mathbf{y})}{8}
\end{aligned}\tag{2.7}$$

Here we also got rid of the singularities using the same explanation as above. Remark that we can rewrite the inner product as

$$\mathbf{n}_{S_j}\cdot(\mathbf{x}-\mathbf{y})=\|\mathbf{x}-\mathbf{y}\|\cos(\alpha(\mathbf{n}_{S_j},\,\mathbf{x}-\mathbf{y}))\tag{2.8}$$

For the kernel of the modified adjoint double layer potential $\widetilde{\mathcal{K}'}^i_{j,\kappa}$, we get in a related way an analogous result as for the kernel of the modified double layer potential $\widetilde{\mathcal{K}}^i_{j,\kappa}$:

$$\begin{aligned}
&\mathbf{n}_{S_i}\cdot\nabla_{\mathbf{x}}\left(\mathcal{G}_\kappa-\mathcal{G}_{\kappa_0}\right)(\mathbf{x},\mathbf{y})\\
&\quad=\left[\left\{\mathrm{i}-\frac{2}{\pi}\log\left(\frac{1}{2}\kappa\|\mathbf{x}-\mathbf{y}\|\right)\right\}\left(\sum_{k=0}^{\infty}\frac{(-4)^k\kappa^{2k+2}}{k!(k+1)!}\|\mathbf{x}-\mathbf{y}\|^{2k}\right)\right.\\
&\qquad-\left\{\mathrm{i}-\frac{2}{\pi}\log\left(\frac{1}{2}\kappa_0\|\mathbf{x}-\mathbf{y}\|\right)\right\}\left(\sum_{k=0}^{\infty}\frac{(-4)^k\kappa_0^{2k+2}}{k!(k+1)!}\|\mathbf{x}-\mathbf{y}\|^{2k}\right)\\
&\qquad\left.+\sum_{k=0}^{\infty}\frac{(-4)^k(\psi(k+1)+\psi(k+2))(\kappa^{2k+2}-\kappa_0^{2k+2})}{\pi k!(k+1)!}\|\mathbf{x}-\mathbf{y}\|^{2k}\right]\frac{-\mathbf{n}_{S_i}\cdot(\mathbf{x}-\mathbf{y})}{8}.
\end{aligned}\tag{2.9}$$

The last operator we have to consider is the modified hypersingular operator $\widetilde{\mathcal{W}}^i_{j,\kappa}$. It is the most complicated to analyze. Its kernel

$$\mathbf{n}_{S_i}\cdot\nabla_{\mathbf{x}}\left(\mathbf{n}_{S_j}\cdot\nabla_{\mathbf{y}}\left(\mathcal{G}_\kappa-\mathcal{G}_{\kappa_0}\right)(\mathbf{x},\mathbf{y})\right)$$

can be rewritten as

$$\begin{aligned}
&\frac{\mathrm{i}}{4}\mathbf{n}_{S_i}\cdot\nabla_{\mathbf{x}}\left(-H_1^{(1)}(\kappa\|\mathbf{x}-\mathbf{y}\|)\kappa+H_1^{(1)}(\kappa_0\|\mathbf{x}-\mathbf{y}\|)\kappa_0\right)\frac{\mathbf{n}_{S_j}\cdot(\mathbf{x}-\mathbf{y})}{\|\mathbf{x}-\mathbf{y}\|}\\
&\quad=\frac{\mathrm{i}}{4}\left(H_0^{(1)}(\kappa\|\mathbf{x}-\mathbf{y}\|)\kappa^2-\frac{\kappa}{\|\mathbf{x}-\mathbf{y}\|}H_1^{(1)}(\kappa\|\mathbf{x}-\mathbf{y}\|)\right.\\
&\qquad\left.-H_0^{(1)}(\kappa_0\|\mathbf{x}-\mathbf{y}\|)\kappa_0^2+\frac{\kappa_0}{\|\mathbf{x}-\mathbf{y}\|}H_1^{(1)}(\kappa_0\|\mathbf{x}-\mathbf{y}\|)\right)\frac{\mathbf{n}_{S_i}\cdot(\mathbf{x}-\mathbf{y})\;\mathbf{n}_{S_j}\cdot(\mathbf{x}-\mathbf{y})}{\|\mathbf{x}-\mathbf{y}\|^2}\\
&\qquad+\frac{\mathrm{i}}{4}\left(H_1^{(1)}(\kappa\|\mathbf{x}-\mathbf{y}\|)\kappa-H_1^{(1)}(\kappa_0\|\mathbf{x}-\mathbf{y}\|)\kappa_0\right)\left(\frac{\mathbf{n}_{S_i}\cdot\mathbf{n}_{S_j}}{\|\mathbf{x}-\mathbf{y}\|}-\frac{\mathbf{n}_{S_i}\cdot(\mathbf{x}-\mathbf{y})\;\mathbf{n}_{S_j}\cdot(\mathbf{x}-\mathbf{y})}{\|\mathbf{x}-\mathbf{y}\|^2}\right)
\end{aligned}$$

just by writing out the derivatives using (A.6). Furthermore, using (2.8) with shorthand notation for the angles $\alpha_{S_i} := \alpha(\mathbf{n}_{S_i}, \mathbf{x}-\mathbf{y})$, $\alpha_{S_j} := \alpha(\mathbf{n}_{S_j}, \mathbf{x}-\mathbf{y})$, we can simplify this to

$$
\begin{aligned}
&= \frac{\mathrm{i}}{4}\Big(H_0^{(1)}(\kappa\|\mathbf{x}-\mathbf{y}\|)\kappa^2 - H_0^{(1)}(\kappa_0\|\mathbf{x}-\mathbf{y}\|)\kappa_0^2 \\
&\qquad -2\frac{\kappa}{\|\mathbf{x}-\mathbf{y}\|}H_1^{(1)}(\kappa\|\mathbf{x}-\mathbf{y}\|) + 2\frac{\kappa_0}{\|\mathbf{x}-\mathbf{y}\|}H_1^{(1)}(\kappa_0\|\mathbf{x}-\mathbf{y}\|)\Big)\cos(\alpha_{S_i})\cos(\alpha_{S_j}) \\
&\quad + \frac{\mathrm{i}}{4}\left(H_1^{(1)}(\kappa\|\mathbf{x}-\mathbf{y}\|)\frac{\kappa}{\|\mathbf{x}-\mathbf{y}\|} - H_1^{(1)}(\kappa_0\|\mathbf{x}-\mathbf{y}\|)\frac{\kappa_0}{\|\mathbf{x}-\mathbf{y}\|}\right)\mathbf{n}_{S_i}\cdot\mathbf{n}_{S_j}.
\end{aligned}
$$

At the final form we arrive using (A.1) and the series expansions in (A.3) respectively (A.4):

$$
\begin{aligned}
&= \frac{\cos(\alpha_{S_i})\cos(\alpha_{S_j})}{4}\Bigg\{(\mathrm{i}+\frac{2\psi(1)}{\pi})\left[J_0(\kappa\|\mathbf{x}-\mathbf{y}\|)\kappa^2 - J_0(\kappa_0\|\mathbf{x}-\mathbf{y}\|)\kappa_0^2\right] \\
&\qquad -\frac{2}{\pi}\log(\frac{1}{2}\kappa\|\mathbf{x}-\mathbf{y}\|)\left[\sum_{k=1}^{\infty}\frac{(-4)^{-k}\kappa^{2k+2}}{(k!)^2}\|\mathbf{x}-\mathbf{y}\|^{2k}\right] \\
&\qquad +\frac{2}{\pi}\log(\frac{1}{2}\kappa_0\|\mathbf{x}-\mathbf{y}\|)\left[\sum_{k=1}^{\infty}\frac{(-4)^{-k}\kappa_0^{2k+2}}{(k!)^2}\|\mathbf{x}-\mathbf{y}\|^{2k}\right] \\
&\qquad +\frac{2}{\pi}\sum_{k=1}^{\infty}\frac{(-4)}{(k!)^2}\left(\sum_{\nu=1}^{k}\frac{1}{\nu}\right)(\kappa^{2k+2}-\kappa_0^{2k+2})\|\mathbf{x}-\mathbf{y}\|^{2k}\Bigg\} \\
&\quad + \Bigg\{\sum_{k=1}^{\infty}\Bigg[\left(\mathrm{i}-\frac{2}{\pi}\log\left(\frac{1}{2}\kappa\|\mathbf{x}-\mathbf{y}\|\right)\right)\kappa^{2k+2} - \left(\mathrm{i}-\frac{2}{\pi}\log\left(\frac{1}{2}\kappa_0\|\mathbf{x}-\mathbf{y}\|\right)\right)\kappa_0^{2k+2} \\
&\qquad +\frac{1}{\pi}(\psi(k+1)+\psi(k+2))(\kappa^{2k+2}-\kappa_0^{2k+2})\Bigg]\frac{(-4)^{-k}}{(k!)^2}\|\mathbf{x}-\mathbf{y}\|^{2k} \\
&\qquad + \left(\mathrm{i}+\frac{1}{\pi}(\psi(k+1)+\psi(k+2))\right)(\kappa^2-\kappa_0^2)\Bigg\}\left(\frac{\mathbf{n}_{S_i}\cdot\mathbf{n}_{S_j}}{8} - \frac{\cos(\alpha_{S_i})\cos(\alpha_{S_j})}{4}\right) \\
&\quad + \frac{\mathbf{n}_{S_i}\cdot\mathbf{n}_{S_j}}{8}\left(-\frac{2}{\pi}\log\left(\frac{1}{2}\kappa\right)\kappa^2 + \frac{2}{\pi}\log\left(\frac{1}{2}\kappa_0\right)\kappa_0^2 - \frac{2}{\pi}\log\left(\|\mathbf{x}-\mathbf{y}\|\right)(\kappa^2-\kappa_0^2)\right).
\end{aligned}
\tag{2.10}
$$

Remark that everything is bounded except the last term, which is a weak logarithmic singularity.

For numerical computations, we need to truncate the series. Clearly, the behaviour of the series depends on the wave numbers κ and κ_0. Numerical tests showed that truncation at $N_{\text{series}} = 20$ together with a validity radius $r_{\text{val}} = 0.7$ seems to be a good choice. r_{val} is chosen in such a way that $\|\mathbf{x}-\mathbf{y}\| < r_{\text{val}}$ guarantees the approximation to be accurate enough for values κ, $\kappa_0 \in [1, 10]$. For higher truncation numbers, there is no noticeable improvement of precision or enlargement of the validity radius r_{val} anymore.

Figure 2.3 below shows the convergence of the series for different wave numbers κ, κ_0 and different truncation numbers N_{series}. Remark that we take as the reference solution the difference of the integrands without expansion. This makes

sense for checking the validity radius, but is not well defined around zero, since these integrands have a singularity there.

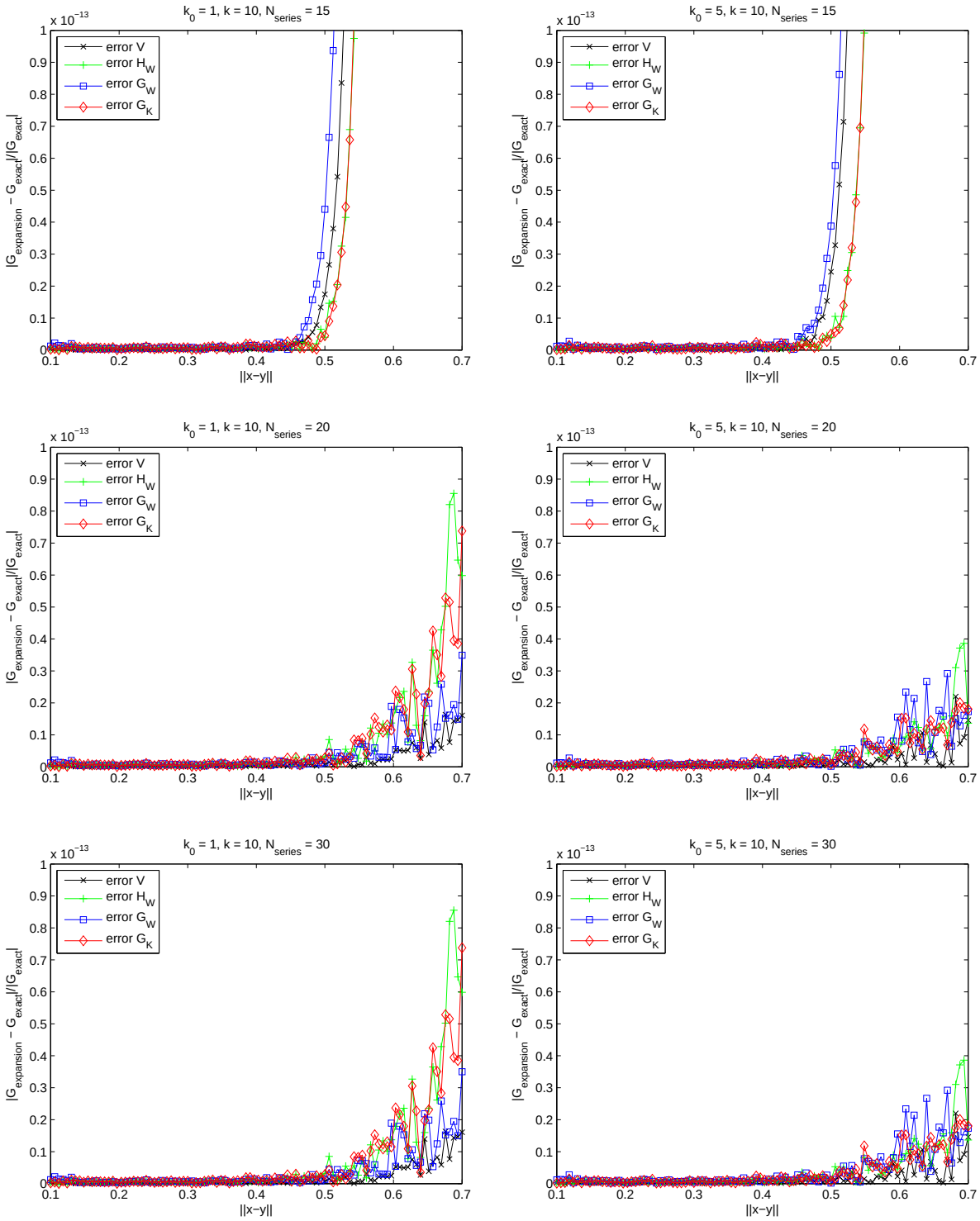

Figure 2.3: Convergence of series expansions:

V : kernel of the weakly singular operator $\mathcal{V}_\kappa$,

H_W : part of the kernel of the operator $\mathcal{W}_\kappa$ which is afterwards multiplied by $\mathbf{n}_{S_i} \cdot \mathbf{n}_{S_j}$,

G_W : part of $\mathcal{W}_\kappa$, which is afterwards multiplied by $\frac{\mathbf{n}_{S_i}\cdot(\mathbf{x}-\mathbf{y})\mathbf{n}_{S_j}\cdot(\mathbf{x}-\mathbf{y})}{\|\mathbf{x}-\mathbf{y}\|^2}$,

G_K : part of the kernel of $\mathcal{K}_\kappa$ ($\mathcal{K}'_\kappa$) which is multiplied by $\frac{(\mathbf{y}-\mathbf{x})\cdot\mathbf{n}_{S_j}}{\|\mathbf{x}-\mathbf{y}\|}$, resp. $\frac{(\mathbf{x}-\mathbf{y})\cdot\mathbf{n}_{S_i}}{\|\mathbf{x}-\mathbf{y}\|}$.

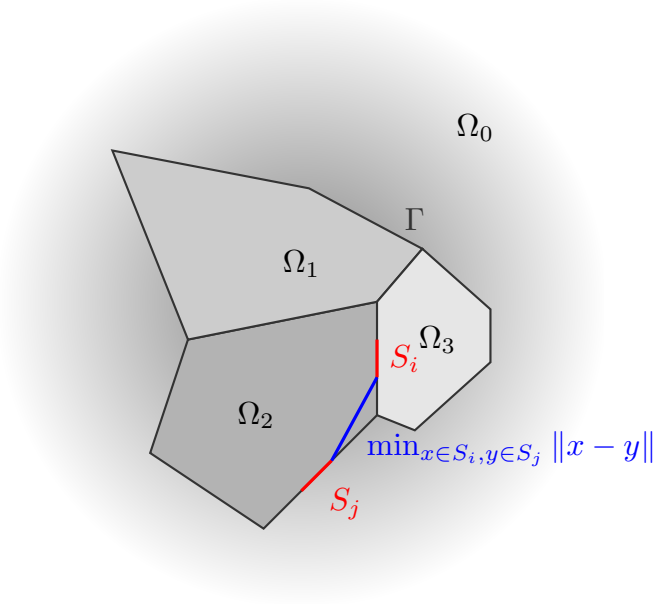

Figure 2.4: Visualization of the criterion which decides if series expansion is done or not.

2.2.2 Integration and Quadratures

To calculate the entries of the operator matrix $\left(\widetilde{\mathcal{A}}_\kappa - \widetilde{\mathcal{A}}_{\kappa_0}\right)$ numerically, we need to deal with integrands having a weak singularity at zero. In this section, we partition our problem into different cases of matrix entries which we will discuss individually. We distinguish between

- S_i and S_j are close to each other, i.e.

$$\min_{\mathbf{x}\in S_i,\, \mathbf{y}\in S_j} \|\mathbf{x}-\mathbf{y}\| < 0.4. \tag{2.11}$$

  Note that in general it makes sense to introduce a scaling number behaving like $h_\mathcal{T}$ or $\operatorname{diam}(\Gamma)$. But in our case of normalized domain sizes, the condition above is sufficient.
  We have again three cases which we examine separately:

  I. $S_i = S_j$,

  II. S_i and S_j are direct neighbours,

  III. neither $i = j$ nor S_i and S_j are neighbours.

- S_i and S_j are far away from each other, i.e.

$$\min_{\mathbf{x}\in S_i,\, \mathbf{y}\in S_j} \|\mathbf{x}-\mathbf{y}\| \geq 0.4. \tag{2.12}$$

First case:

The first case deals with $i, j \in \{1, ..., N_{\text{seg}}\}$ such that $\min_{\mathbf{x}\in S_i,\, \mathbf{y}\in S_j} \|\mathbf{x}-\mathbf{y}\| < 0.4$. The segments S_i and S_j lie close to each other and so we are close to the singularity. To avoid cancellation due to the big values of the isolated parts of the difference in the kernels, we make use of the series expansions derived in Subsection 2.2.1. Assuming additionally the mesh to be fine enough such that

$$\max_{\mathbf{x}\in S_i,\, \mathbf{y}\in S_j} \|\mathbf{x}-\mathbf{y}\| < 0.7,$$

we ensure that the truncated series expansions are accurate enough.

I. Identical segments: If the segments are identical, i.e. $\mathbf{i} = \mathbf{j}$, we are able to integrate analytically over the truncated series. First of all we point out that the double layer potential $\mathcal{K}_\kappa$ and its adjoint $\mathcal{K}'_\kappa$ are identically equal to zero because

$$\mathbf{n}_{S_i} \cdot (\mathbf{x}-\mathbf{y}) \equiv 0 \text{ for all } \mathbf{x},\, \mathbf{y} \in S_i.$$

The same holds for the part of the hypersingular operator $\mathcal{W}_\kappa$ involving the inner product above. So the only contribution is due to the part multiplied by $\mathbf{n}_{S_i} \cdot \mathbf{n}_{S_j} = 1$. Using linearity of integration, one obtains analyzing (2.6) and (2.10) that it suffices to find the antiderivative of the following expression for $k \in \mathbb{N}_0$:

$$\int_{S_i}\int_{S_j} \|\mathbf{x}-\mathbf{y}\|^{2k} \log(\|\mathbf{x}-\mathbf{y}\|)\, dS(\mathbf{y})\, dS(\mathbf{x}).$$

Parametrizing the segment $S_i = S_j$ with vertices P_{i1}, P_{i2} using

$$\xi_i : [0,1] \to S_i, \quad s \mapsto (P_{2i} - P_{1i})s + P_{1i},$$

we obtain

$$\int_0^1\int_0^1 \|(P_{2i} - P_{1i})(s-t)\|^{2k} \log(|(s-t)|)|S_i|^2\, dt\, ds.$$

Furthermore, using multiplicativity of the 2-norm and logarithm rules, we arrive at

$$|S_i|^{2k+2}\int_0^1\int_0^1 |s-t|^{2k}\log(|s-t|)\, dt\, ds + \log(|S_i|)|S_i|^{2k+2}\int_0^1\int_0^1 |s-t|^{2k}\, dt\, ds.$$

These integrals can be calculated analytically:

$$\int_0^1\int_0^1 |s-t|^{2k}\log(|s-t|)\, dt\, ds = \frac{2}{(2+2k)^2} - \frac{2}{(1+2k)^2}$$

and

$$\int_0^1\int_0^1 |s-t|^{2k}\, dt\, ds = \frac{2}{(2k+1)(2k+2)},$$

respectively. This closes the discussion for the case of identical segments.

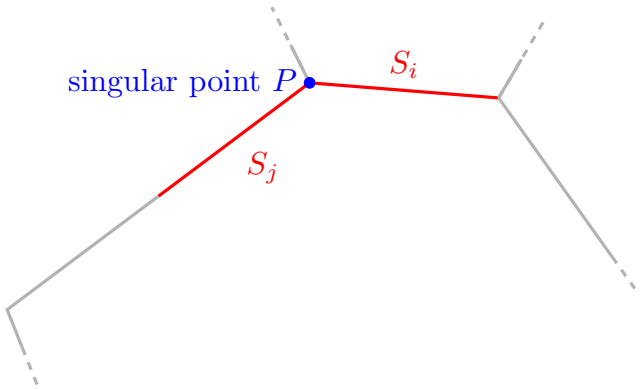

Figure 2.5: Two neighbouring segments.

II. Neighbouring segments: For neighbouring segments it is not clear how to integrate everything analytically. Thus, we have to find an appropriate quadrature rule. But first of all we are going to derive the concrete form of the integral for the case of neighbouring segments.

The singularity sits at the common edge point P of the neighbouring segments. We parametrize in such a way that the common edge point P is evaluated in zero:

$$\xi_i : [0,1] \to S_i,\ \xi_j : [0,1] \to S_j,$$

such that

$$\xi_i(0) = \xi_j(0) = P.$$

This implies that the singularity lies on the boundary of our interval of integration and that the constant part of the two linear parametrizations drops out of the integrand after taking their differences. For our calculations we assume w.l.o.g. that $P_{1i} = P_{2j} = P$:

$$\int_0^1 \int_0^1 \|(P_{2i} - P_{1i})s - (P_{1j} - P_{2j})t\|^{2k} \log(\|(P_{2i} - P_{1i})s - (P_{1j} - P_{2j})t\|)|S_i||S_j| dt\, ds. \tag{2.13}$$

To solve this particular integral, four different approaches were tested:

II.a) Inner integration analytical, outer integration using a quadrature rule,

II.b) Duffy's trick,

II.c) Log-weighted Gauss-Legendre quadrature rule,

II.d) Geometric composite Gauss-Legendre quadrature rule,

which we will now review in detail:

II.a) Inner integration analytical, outer integration using a quadrature rule: The inner integral can be solved analytically, interpreting

$$\|(P_{1j} - P_{2j})s - (P_{2i} - P_{1i})t\|^2$$

as a quadratic polynomial in t: $at^2 + b(s)t + c(s)$. But there seems to be no expression available for the antiderivative with variable $k \in \mathbb{N}$. Tests for $k = 0$ show that the accuracy is only slightly better than for the straightforward approach which approximates both integrals using Gauss-Legendre or any other of the below discussed quadrature rules (see Figure 2.8). So we decided that it is not worth the huge effort of implementing the antiderivative for every $k \in \{0, 1, ..., N_{\text{series}}\}$ independently.

II.b) Duffy's trick: Another idea was to apply *Duffy's trick*, a special substitution of variables, which is commonly used in three dimensions to weaken the singularity of the integrand (see e.g. [5]). We do not have exactly the form for which the integrals are shown to be regularized, since we can not describe the domain of integration of the inner integral by $\{t \in (0, s) | s \in [0, 1]\}$. Nevertheless, we try the substitution. We obtain, substituting $t = su$, that

$$\left(\int_0^1 \int_0^{\frac{1}{s}} \|(P_{1j} - P_{2j})u - (P_{2i} - P_{1i})\|^{2k} \log(\|(P_{1j} - P_{2j})u - (P_{2i} - P_{1i})\|) du\, s^{2k+1}\, ds \right.$$
$$\left. + \int_0^1 \int_0^{\frac{1}{s}} \|(P_{1j} - P_{2j})u - (P_{2i} - P_{1i})\|^{2k} du\, \log(s) s^{2k+1}\, ds \right) |S_i||S_j|$$

Again it is possible to integrate the inner integral analytically, interpreting the integrand as a polynomial, $au^2 + bu + c$. But this time the coefficients do not depend on the other variable s.

The outer integral then can be evaluated using quadrature rules. Unfortunately, when we put the boundaries of integration into the antiderivative of the inner integral, we are not able to cancel the expression $\frac{1}{s}$ in the integrand. This might cause numerical problems due to its singularity of degree one in zero. One could again substitute $\frac{1}{s} = v$ and integrate over an unbounded interval using Gauss-Laguerre quadrature, but it seems not to have that much promise.
However, we tested for $k = 0$, integrating the inner integral analytically and then directly using Gauss-Legendre quadrature (c.f. Figure 2.8). It converges quite good, but just using Gauss-Legendre quadrature for (2.13) without doing any transformations of the integrals seems to work better and with less effort, since for the analytic integration we would have to implement every antiderivative individually for k from 0 up to N_{series}.

II.c) Log-weighted Gauss-Legendre quadrature rule: Since we have to integrate over logarithmic weighted polynomials, it suggests itself to apply a logarithmic weighted quadrature. There are different approaches to do so. We base our ansatz on a paper by M. Carley (see [3]), taking an m-point Gauss-Legendre quadrature rule $(t_j, v_j)_{0 \le j \le m-1}$ and imposing the following constraints:

$$(\psi_i(x, t_j))_{0 \le i \le 2m-1,\, 0 \le j \le m-1} \, (w_j(x))_{0 \le j \le m-1} = (m_i(x))_{0 \le i \le 2m-1},$$

with

$$\psi_i(x, t) := \begin{cases} L_i(t), & i \in \{0, 1, ..., m-1\} \\ L_i(t) \log|x - t|, & i \in \{m, ..., 2m-1\}, \end{cases}$$

where L_i denotes the i^{th} Legendre polynomial, and

$$m_i(x) := \int_{-1}^{1} \psi_i(x,t)\, dt.$$

m_i can be determined analytically for a real valued translation value x, see [3, Section 2.2]. The overdetermined system of equations is solved in a least squares sense. The challenge is to find a good choice of the translation value x. It is clear that it would be best to use that

$$\log|at^2 + b(s)t + c(s)| = C + \log|x_1 - t| + \log|x_2 - t|,$$

where $x_1(s), x_2(s)$ are the roots of the polynomial $at^2 + b(s)t + c(s)$. Due to the dependency on s, we would have to solve the above system for every node s_i of the quadrature rule used for the outer integral. This involves clearly too much computational effort.

To get rid of the s-dependency, we use Duffy's trick before applying the quadrature. The roots are mostly complex valued. Since we have only formulas for real translation value x available, we take absolute values of the roots as translation value: $x = |x_1|, |x_2|$.
We test the achievement for the fix choice of the translation value $x = 0.9$. We use $x = 0.9$, because evaluation of the roots for several polynomials of the above form indicated, that their absolute value lies often near one.
We also test for the absolute values of the roots of the polynomial $at^2 + bt + c$, $x = |x_i|$, $i = 1, 2$. The results show that we do not gain accuracy using this ansatz (cf. Figure 2.8). The reason might be that it is not sufficient to take translation values in the same order of magnitude of the roots and we really need to take the complex roots themselves as translation values. This demands for antiderivatives of integrands with complex translations.

II.d) Geometric composite Gauss-Legendre quadrature rule: The last method we look at is using a geometric composite Gauss-Legendre quadrature rule, which promises to capture the singularity at zero better than taking an ordinary Gauss-Legendre quadrature because of the higher density of quadrature nodes around zero. It is suggested in the dissertation of P. Meury [10] resp. in [13]. The partition of the interval is made in such a way that there is a strong refinement towards zero.

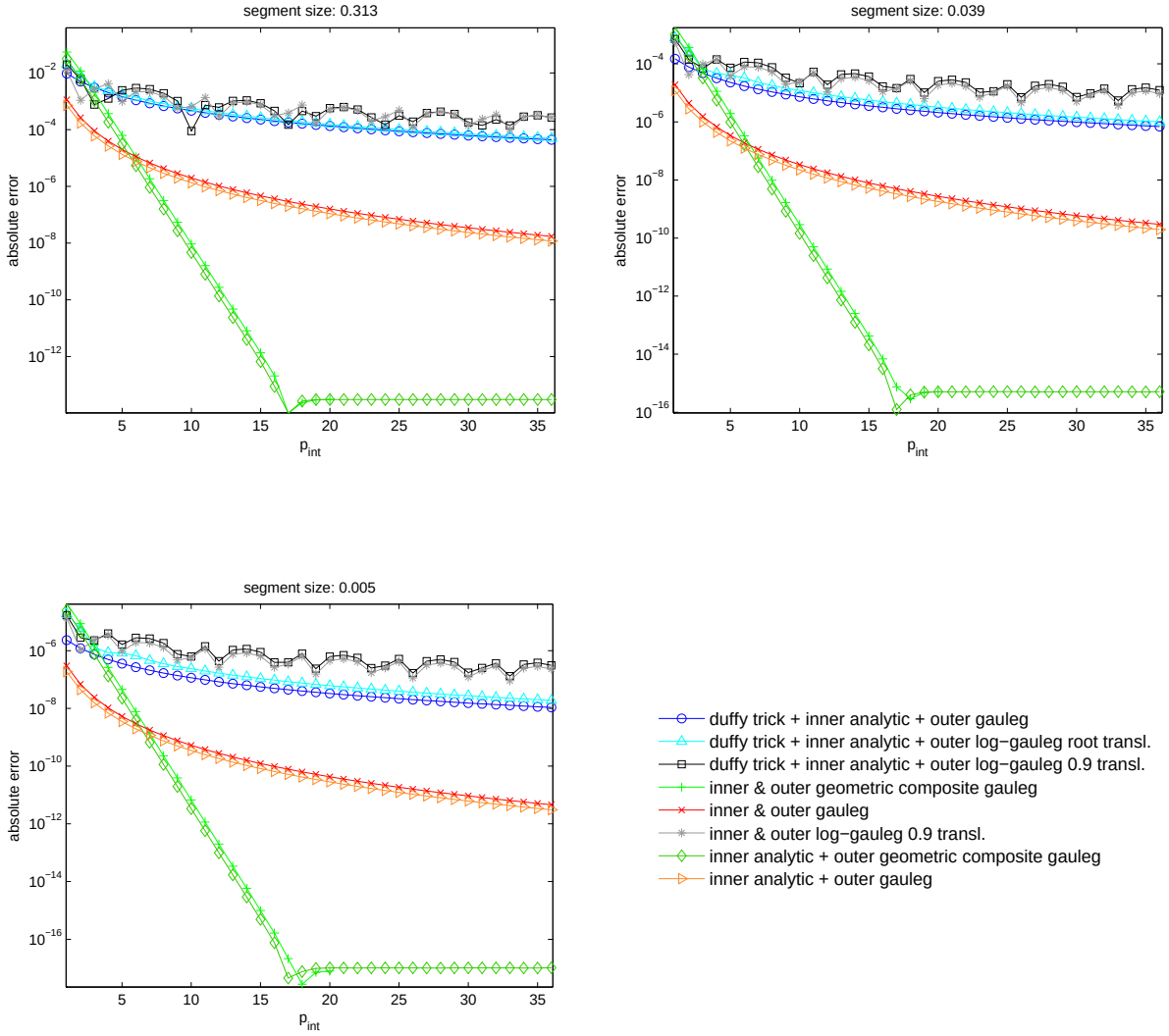

Figure 2.6: Convergence of different quadrature rules integrating $\int_0^1 \int_0^1 \log(\|\xi_1(s) - \xi_2(t)\|)\, ds\, dt$, where ξ_1 resp. ξ_2 parametrize the 1. and 2. segment of a grid Γ_{disc} approximating the unit disc using an equidistant mesh of different sizes.

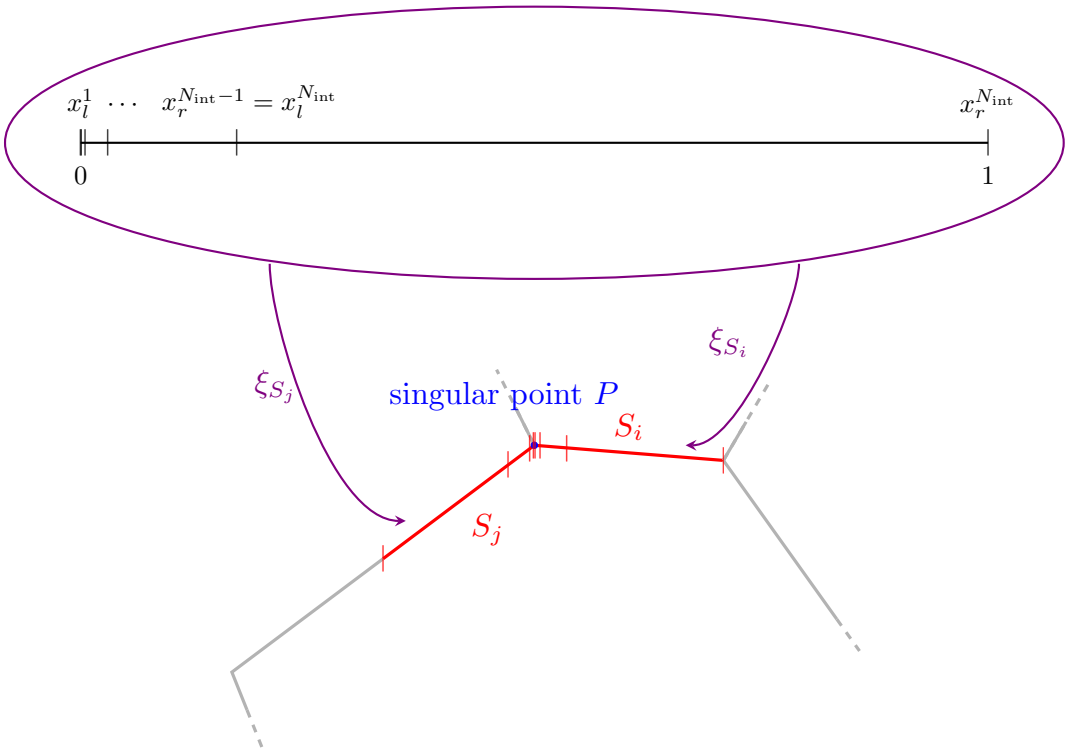

Figure 2.7: Visualization of the subintervals for geometric composite Gauss-Legendre quadrature rule, $\sigma = (\sqrt{2}-1)^2$.

On the unit interval $(0,1)$, the left and right interval bounds x_l^k, x_r^k of the k^{th} subinterval are chosen in such a way that

$$x_l^k = \begin{cases} 0, & k = 1, \\ \sigma^{N_{\text{int}}-k+1}, & k > 1, \end{cases}, \; x_r^k = \sigma^{N_{\text{int}}-k},$$

where N_{int} is the total number of subintervals, $k \in \{1, ..., N_{\text{int}}\}$ and $\sigma \in (0,1)$ (cf. Figure 2.7). In our case, we set $\sigma := (\sqrt{2}-1)^2 \approx 0.1716$, since numerical experiments in [13] show that a choice of σ between $0.1 < \sigma < 0.2$ is optimal. The partition is then mapped to our neighbouring segments in such a way that the singular point P is the image of zero. This can be done by the aid of the parametrizations of the segments S_i and S_j, ξ_i, ξ_j, namely. In Figure 2.7 one can find an example showing the transformed subintervals.
It remains to discuss what degree p_{int} of the interpolation polynomial for the Gauss-Legendre quadrature rule one should choose on each subinterval. We chose, as P. Meury did in [10], uniform degree p_{int} on all subintervals although in [13], they recommend to linearly increase the polynomial degree for optimal convergence. But this would highly increase the computational cost of the algorithm. Thus we abandon this fact and just use uniform degree p_{int} on all subintervals, which also leads to a good convergence result (see Figure 2.8). The total number of subintervals is chosen to be $N_{\text{int}} = p_{\text{int}}$.

For the test we use the already existing code of P. Meury in [10]. The main part of the code is given by ($q := p_{\text{int}} + 1$)

```
/* Initialize Gauss Legendre quadrature rule */
_x = (double *) malloc(q*sizeof(double));
mxAssert(_x != NULL,"Out of memory");
_w = (double *) malloc(q*sizeof(double));
mxAssert(_w != NULL,"Out of memory");

gauleg(_x,_w,q);

/* Compute composite Gauss-Legendre quadrature rule */
n = q*(q-1);
sigma = (sqrt(2.0)-1.0)*(sqrt(2.0)-1.0);

xl = sigma;
xr = 1.0;
ii = n-1;
for(i=1; i<q; i++){
  for(j=q-1; j>=0; j--){
    mxAssert(ii >= 0 && ii < n,"Index out of bounds");
    w[ii] = (xr-xl)*_w[j];
    x[ii] = (xr-xl)*_x[j]+xl;
    ii--;
  }
  xr = xl;
  xl = xl*sigma;
}
```

It turns out that measuring convergence of quadrature errors versus polynomial degree p_{int} of the interpolation used for the quadrature rule, we get the best result for it. Even though one should keep in mind that the number of quadrature points is much bigger ($p_{int}(p_{int}+1)$) compared to $p_{int}+1$, the number of quadrature points of the other quadratures. Therefore, one needs to do much more function evaluations, which can also be costly. It turns out that this additional computational effort to evaluate the integrals is bigger than increasing the polynomial degree p_{int} up to comparable accuracy for p_{int} not too big. Despite of its higher computational effort, we decided to take geometric composite Gauss-Legendre quadrature rule to be absolutely sure that everything converges well. Notice that to optimize computational cost, it seems promising to investigate more time here: Plotting the errors versus computational time one observes that evaluating the inner integral analytically and using geometric composite Gauss-Legendre quadrature for the outer integral is very time efficient. Further investigation could yield a compact expression for antiderivatives of the inner integral of (2.13) depending on k.

III. Segments which satisfy (2.11) but neither are identical nor direct neighbours: To close the first case of our discussion we have to handle segments which satisfy (2.11) but are neither identical nor direct neighbours. In this case, we apply the series expansion because we are still quite near to the singularity and want to avoid cancellation due to the possibly big values of the individual parts of the difference. We use simply Gauss-Legendre quadrature rule to evaluate the integrals: Since we do not have any singularity lying in our domain of integration, the integrand is analytic and the quadrature converges optimally.

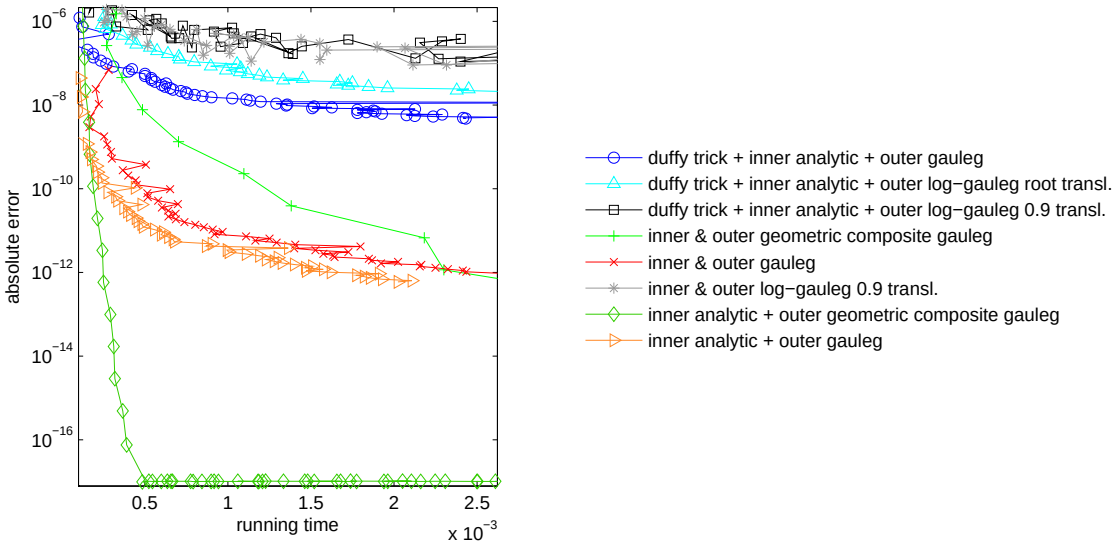

Figure 2.8: Convergence of different quadrature rules v.s. running time integrating $\int_0^1 \int_0^1 \log(\|\xi_1(s) - \xi_2(t)\|)\, ds\, dt$, where ξ_1 resp. ξ_2 parametrize the 1. and 2. segment of a grid Γ_{disc} approximating the unit disc using an equidistant mesh of size 0.005.

Second case:

If the segments S_i and S_j satisfy equation (2.12), we cannot guarantee that the series expansions from Section 2.2.1 converge. Fortunately, we are far enough away from the singularity at zero and thus do not need to expand the integrand into series. Again we use the Gauss-Legendre quadrature rule to approximate the integrals.

2.3 Assembly of Right Hand Side

Now we are coming back to the right hand side **RHS**. The most direct way to write it out would be

$$\mathbf{RHS} = \mathbf{V}^T \mathbf{P}_{\mathbb{Y}}^T \mathbf{B} \left(\widetilde{Id} - \widetilde{\mathcal{A}}_\kappa \right) \mathbf{P}_{\mathbb{X}} \mathbf{U}_{\text{inc}},$$

where

$$\mathbf{U}_{\text{inc}} = (\gamma_D^{\Omega_0} u_{\text{inc}},\, \gamma_N^{\Omega_0} u_{\text{inc}},\, 0,\, ...,\, 0)^T.$$

But the alert reader might remark that in this form, we are not allowed to take piecewise constants to approximate the Neumann data space, since $H^{\frac{1}{2}}(\partial\Omega_i)$ does not contain the discontinuous finite element space $\mathcal{S}^0_{\mathcal{T}}(\Gamma_{\text{disc}})$. Unfortunately, $\mathbf{U}_{\text{inc}}$ is in general not part of the space $\mathbb{X}(\Gamma)$ and so $\widetilde{\mathcal{A}}_{\kappa_0} \mathbf{U}_{\text{inc}}$ does not have to vanish (c.f. Corollary 1). Thus, we are not able to replace $\widetilde{\mathcal{A}}_\kappa$ by the

more regular operator $\widetilde{\mathcal{A}}_\kappa - \widetilde{\mathcal{A}}_{\kappa_0}$ on the right hand side.
To avoid this problem we decided to restrict ourselves to plane incident waves. This commonly used class of waves satisfies the interior Helmholtz scattering problem on $\overline{\Omega}_0^c$. We really need the boundedness of the domain, since u does not satisfy the Sommerfeld radiation condition.

The plane wave $u_{\text{inc}} = \exp(\mathrm{i}\kappa_0 \mathbf{d} \cdot \mathbf{x})$ fulfills

$$-\Delta u_{\text{inc}}(\mathbf{x}) - \kappa_0^2 u_{\text{inc}}(\mathbf{x}) = 0, \ \mathbf{x} \in \overline{\Omega}_0^c$$

and thus represents a valid Cauchy datum for the interior Helmholtz scattering problem, i.e.

$$(\gamma_D^{\Omega_0} u_{\text{inc}}, -\gamma_N^{\Omega_0} u_{\text{inc}}) \overset{\text{Thm. } 5}{=} (\gamma_D^{\overline{\Omega}_0^c} u_{\text{inc}}, \gamma_N^{\overline{\Omega}_0^c} u_{\text{inc}}) \in \mathcal{C}(\partial\overline{\Omega}_0^c).$$

Using Theorem 4, we have that

$$\left(-\frac{Id}{2} + \mathcal{C}^0_{\kappa_0,\,\text{ext0}}\right)(\gamma_D^{\Omega_0} u_{\text{inc}}, -\gamma_N^{\Omega_0} u_{\text{inc}}) = (0,0),$$

where ext0 stands for domain $\overline{\Omega}_0^c$. Using Theorem 6 we obtain therefore

$$\left(-\frac{Id}{2} - \mathcal{C}^0_{\kappa_0,\,0}\right)(\gamma_D^{\Omega_0} u_{\text{inc}}, \gamma_N^{\Omega_0} u_{\text{inc}}) = (0,0)$$

and furthermore, since $\partial\Omega_i \subset \Omega_0^c$, it additionally holds for $i \in \{1, ..., n\}$ that

$$\left(\frac{Id}{2}\chi_{\partial\Omega_0} - \mathcal{C}^i_{\kappa_0,\,0}\right)(\gamma_D^{\Omega_0} u_{\text{inc}}, \gamma_N^{\Omega_0} u_{\text{inc}}) = (\gamma_D^{\Omega_i} u_{\text{inc}}, \gamma_N^{\Omega_i} u_{\text{inc}}).$$

Finally, one obtains the identity

$$\begin{aligned}\mathcal{A}_\kappa U_{\text{inc}} &= \begin{pmatrix}\gamma_D^{\Omega_i}\Phi_\kappa(U_{\text{inc}}) \\ \gamma_N^{\Omega_i}\Phi_\kappa(U_{\text{inc}})\end{pmatrix}_{0\le i\le n} \\ &= (0, 0, -\gamma_D^{\Omega_1} u_{\text{inc}}, -\gamma_N^{\Omega_1} u_{\text{inc}}, ..., -\gamma_D^{\Omega_n} u_{\text{inc}}, -\gamma_N^{\Omega_n} u_{\text{inc}})^T,\end{aligned}$$

which directly leads to

$$(Id - \mathcal{A}_\kappa) U_{\text{inc}} = (\gamma_D^{\Omega_i} u_{\text{inc}}, \gamma_N^{\Omega_i} u_{\text{inc}})_{0\le i\le n}.$$

Rewriting this result in segmentwise notation we have that the right hand side has the form

$$\mathbf{RHS} = \mathbf{V}^T \mathbf{P}_{\mathbb{Y}}^T \mathbf{B} \mathbf{P}_{\mathbb{X}} \widetilde{\mathbf{U}},$$

where

$$\widetilde{\mathbf{U}} := \left(\int_{S_i} \gamma_D^{\Omega_i} u_{\text{inc}}(\mathbf{x})\, dS(\mathbf{x}), \int_{S_i} \gamma_N^{\Omega_i} u_{\text{inc}}(\mathbf{x})\, dS(\mathbf{x})\right)^T_{1\le i\le N_{\text{seg}}}.$$

We evaluate the integrals in $\widetilde{\mathbf{U}}$ using standard Gauss-Legendre quadrature to approximate

$$\int_0^1 u_{\text{inc}}(\xi_i(t))|S_i|\, dt$$

for the Dirichlet entries for the i^{th} segment resp.

$$\int_0^1 \mathbf{n}_{S_i} \cdot \nabla_{\xi_i(t)} u_{\text{inc}}(\xi_i(t))|S_i|\,dt = \int_0^1 \mathbf{n}_{S_i} \cdot \mathbf{d}\,\mathrm{i}\kappa_0 \exp(\mathrm{i}\kappa_0 \mathbf{d} \cdot \xi_i(t))|S_i|\,dt$$

for the Neumann entries.
The MATLAB function which calculates the right hand side is named `assem_RHS.m` and is found in the folder `BEM_2nd_kind`. It uses the function `RHS.m` out of `Library_2nd_kind`.

3 Numerical Experiments

In this chapter we discuss numerical results based on the implementation of the above derived boundary element methods. We look at the following geometrical obstacles:

- a unit disc
- a unit square
- two half discs
- two half squares
- four quart discs
- four quart squares.

The wave numbers κ_i for the different domains are chosen from the interval $[1, 10]$ and the incident plane waves u_{inc} have the directions of propagation $(1, 0)^T$ or $\frac{\sqrt{2}}{2}(1, 1)^T$.

We discuss the first test in detail and explain there what is plotted exactly in what figure. For the subsequent tests we require these basics to be known and just explain new remarkable details.

3.1 A Unit Disc

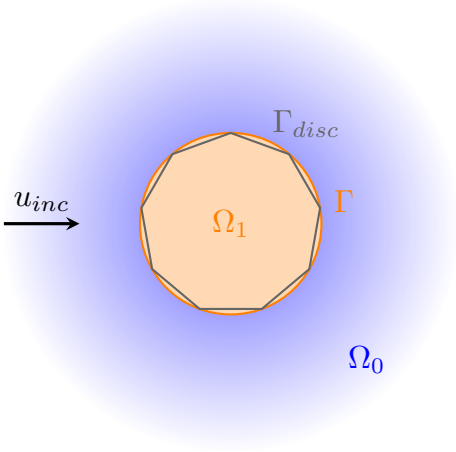

Figure 3.1: Geometry of the considered Helmholtz problem

We begin our discussion with a Helmholtz transmission problem on two domains. Ω_1, the bounded domain, is defined to be the unit disc while Ω_0 describes the

exterior domain, i.e. $\Omega_1 = \overline{\Omega}_1^c$. We make two test cases, where the first one takes small wave numbers on the two domains ($\kappa_0 = 1$, $\kappa_1 = 2$), while for the second problem we define the wave number of the domain Ω_1 to be quite big ($\kappa_0 = 1$, $\kappa_1 = 10$). We do this to test the numerical schemes for the dependency on the size of the wave number. The choices for the direction of propagation of the incident plane wave are $\mathbf{d} = \frac{\sqrt{2}}{2}(1,1)^T$ for the first resp. $\mathbf{d} = (1,0)^T$ for the second test.

Mie solution: The considered test case is important, since this is the only case for which we have given a well-known analytic solution, called *Mie solution*. It is obtained rewriting the problem using polar coordinates and then applying separation of variables to it. For detailed information about the Mie solution consult the paper [7], published by the authors Hsiao and Xu and references therein. Since we need a slightly more general representation for the Mie solution, we we give it explicitly in Appendix B. A representation for the Neumann trace of the Mie solution can also be found there.

$L^2(\Gamma_{\text{disc}})$ convergence results: First of all let us discuss the convergence results. The approximation error is measured in the $L^2(\Gamma_{\text{disc}})$-norm. Unfortunately, there is only an analytic solution available for the problem concerning the unit disc. Therefore, we have to use the most accurate approximation as a reference solution in general. This approximation is meant to be the one calculated on the finest grid we considered. In addition, there is an error contribution not only due to the approximation of the function values but also due to the approximation of the geometry of the mesh. But the latter mentioned contribution can be neglected, since using [12, Example 8.1.8 together with Section 8.3 (Table 8.3, k=0)] we have guaranteed that the overall convergence rates of the error are preserved for the system which is perturbed by the piecewise linear approximation of the boundary. To get an idea of the informative value of the calculated errors, we compare the convergence results using the analytic Mie solution as a reference solution with the errors obtained using the highest resolution as a reference solution (see Figure 3.2). It turns out that we have slightly smaller errors for the second finest approximation. This implies that the order of convergence improves slightly . But there seems to be no loss of quality of evidence.

We know the solution to be smooth. Thus, using Thm. 10 and Thm. 9, we expect the error of the Dirichlet data $\|\gamma_D^{\Gamma_{\text{disc}}} u_{\text{ref}} - \gamma_D^{\Gamma_{\text{disc}}} u_h\|_{L^2(\Gamma_{\text{disc}})}$ to converge in $\mathcal{O}(N_{\text{seg}}^{-2}) = \mathcal{O}(h_{\mathcal{T}}^2)$ for the classical formulation resp. in $\mathcal{O}(N_{\text{seg}}^{-1}) = \mathcal{O}(h_{\mathcal{T}})$ for the new second kind method. $\gamma_D^{\Gamma_{\text{disc}}}$ and $\gamma_N^{\Gamma_{\text{disc}}}$ are the trace operators taking the trace respectively to the fixed orientation on each segment. u_{ref} represents the reference solution and u_h stands for the numerical approximation.

For the Neumann error $\|\gamma_N^{\Gamma_{\text{disc}}} u_{\text{ref}} - \gamma_N^{\Gamma_{\text{disc}}} u_h\|_{L^2(\Gamma_{\text{disc}})}$, we expect a convergence in $\mathcal{O}(N_{\text{seg}}^{-1}) = \mathcal{O}(h_{\mathcal{T}})$ for both approaches using again the quasi optimality error estimate from Thm. 10 together with Thm. 8.

Indeed, looking at the first two images in Fig. 3.3 and Fig. 3.5, we obtain the theoretically expected orders of convergence. Notice that in Fig. 3.5, the

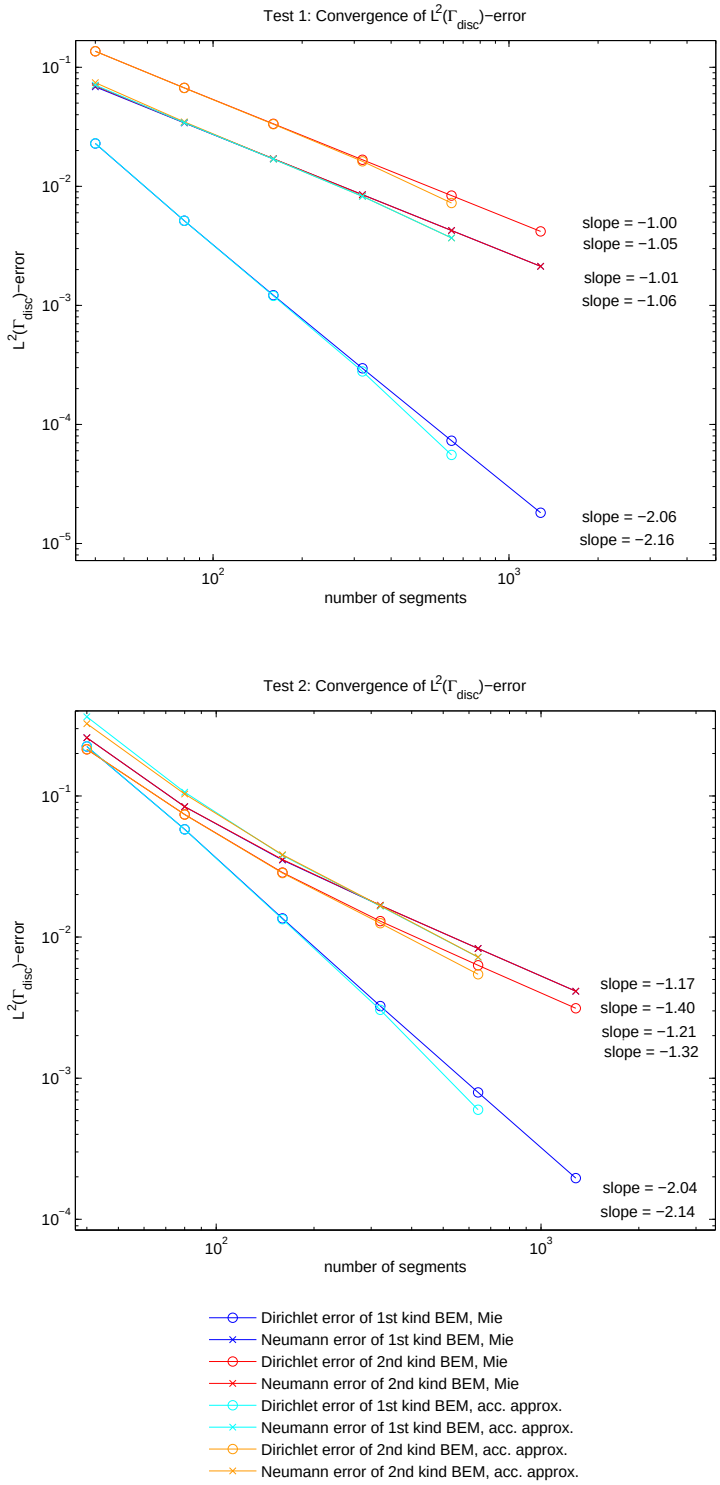

Figure 3.2: Comparison of convergence of approximation errors for the geometry of the unit disc: The upper plot shows the convergence errors for the wave numbers $\kappa_0 = 1$ and $\kappa_1 = 2$. On the lower plot we see the errors for the wave numbers $\kappa_0 = 1$, $\kappa_1 = 10$. The incident waves u_{inc} have the direction of propagation $\mathbf{d} = \frac{\sqrt{2}}{2}(1,1)^T$ respectively $\mathbf{d} = (1,0)^T$.

N_{seg}	$\|\gamma_D^{\Gamma_{\text{disc}}} u_{\text{ref}} - \gamma_D^{\Gamma_{\text{disc}}} u_h\|_{L^2(\Gamma_{\text{disc}})}$	eoc	$\|\gamma_N^{\Gamma_{\text{disc}}} u_{\text{ref}} - \gamma_N^{\Gamma_{\text{disc}}} u_h\|_{L^2(\Gamma_{\text{disc}})}$	eoc
40	$2.240 \cdot 10^{-1}$		$2.586 \cdot 10^{-1}$	
80	$5.797 \cdot 10^{-2}$	-1.95	$8.402 \cdot 10^{-2}$	-1.62
160	$1.355 \cdot 10^{-2}$	-2.10	$3.517 \cdot 10^{-2}$	-1.26
320	$3.242 \cdot 10^{-3}$	-2.06	$1.677 \cdot 10^{-2}$	-1.07
640	$7.921 \cdot 10^{-4}$	-2.03	$8.290 \cdot 10^{-3}$	-1.02
1280	$1.957 \cdot 10^{-4}$	-2.02	$4.133 \cdot 10^{-3}$	-1.00
Theory:		-2		-1

Table 3.1: Error and order of convergence for the classical first kind approach.

convergence rate is slightly higher for the first two refinement steps. Such a convergence behaviour is always seen in our tests for high wave numbers. See Table 3.1 and Table 3.2 for detailed information about the convergence rates of Test 2.

N_{seg}	$\|\gamma_D^{\Gamma_{\text{disc}}} u_{\text{ref}} - \gamma_D^{\Gamma_{\text{disc}}} u_h\|_{L^2(\Gamma_{\text{disc}})}$	eoc	$\|\gamma_N^{\Gamma_{\text{disc}}} u_{\text{ref}} - \gamma_N^{\Gamma_{\text{disc}}} u_h\|_{L^2(\Gamma_{\text{disc}})}$	eoc
40	$2.138 \cdot 10^{-1}$		$2.585 \cdot 10^{-1}$	
80	$7.398 \cdot 10^{-2}$	-1.53	$8.399 \cdot 10^{-2}$	-1.62
160	$2.866 \cdot 10^{-2}$	-1.37	$3.543 \cdot 10^{-2}$	-1.25
320	$1.298 \cdot 10^{-2}$	-1.14	$1.682 \cdot 10^{-2}$	-1.07
640	$6.307 \cdot 10^{-3}$	-1.04	$8.298 \cdot 10^{-3}$	-1.02
1280	$3.130 \cdot 10^{-3}$	-1.01	$4.135 \cdot 10^{-3}$	-1.00
Theory:		-1		-1

Table 3.2: Error and order of convergence for the new second kind approach.

Condition number of the Galerkin matrices: The condition number of the Galerkin matrices $\text{Cond}_2(\mathbf{G}) := \|G\|_2 \|G^{-1}\|_2$ of the two methods is evaluated in every refinement step and visualized in a logarithmic scaled plot found on the left middle of Fig. 3.3 and Fig. 3.5. We have that the condition number of the Galerkin matrix of the classical approach increases quadratically compared to the number of segments N_{seg} used for the discretization. This is what theoretical analysis proposes. For a more detailed explanation see [6, p. 58] and references therein.

The results for the new formulation show that the spectral condition number is uniformly bounded w.r.t. to the number of segments N_{seg}, which is direct proportional to $h_{\mathcal{T}}^{-1}$. This is exactly what we expect due to the results of X. Claeys. The general boundedness of the spectral condition number $\text{Cond}_2(\mathbf{G}) := \|G\|_2 \|G^{-1}\|_2$ remains open to show.

Our numerical results also indicate an increase of the condition number of the Galerkin matrix $\mathrm{Cond}_2(\mathbf{G})$ for choices of bigger wave numbers κ_i.

To obtain numerical solutions of high resolution, one often makes use of iterative or approximative methods to solve the Galerkin equations. Their convergence rate highly depends on the spectrum of the Galerkin matrix. The spectral condition number Cond_2 gives us information about the spectrum. Namely, for symmetric positive definite matrices $\mathbf{A}$ we have that

$$\mathrm{Cond}_2(\mathbf{A}) = \frac{\lambda_{\max}(\mathbf{A})}{\lambda_{\min}(\mathbf{A})},$$

where $\lambda_{\max}(\mathbf{A})$ resp. $\lambda_{\min}(\mathbf{A})$ are the maximal and minimal eigenvalue of the matrix $\mathbf{A}$. So, since in our case the spectral condition number is uniformly bounded in $h_{\mathcal{T}_l}$ for $l \to \infty$, we have the advantage that fast convergence of the iterative methods is guaranteed.

Convergence of the iterative solver GMRES: In our thesis we test the convergence of the iterative solver GMRES. A bound for the error depending on the number of iterations can be found in [11, Subsection 6.11.4]. Indeed, we have very fast convergence of GMRES for small values of κ_i. Also for bigger wave numbers the convergence remains quite good: We only need 60 iterations to achieve machine precision, which is quite a bit better than the result for the classical approach (see plots on the middle left of Fig. 3.3 resp. Fig 3.5). It is to emphasize that there is a broad spectrum of preconditioners one can use to obtain a better convergence results, but this also involves additional computational effort.

Global potential and traces on $\overline{\Omega}^c_{0\mathrm{disc}}$: The two plots on the bottom of Fig. 3.3 and Fig. 3.5 show the approximated potential $\Phi_\kappa + u_{\mathrm{inc}}$ on a section of $\mathbb{R}^2$, whereas the first four plots in Fig. 3.4 resp. Fig. 3.6 show the Dirichlet resp. Neumann data on the discretized boundary of the exterior domain $\overline{\Omega}^c_{0\mathrm{disc}}$. To get the right Neumann trace, taking the normal vectors pointing inside the domain $\Omega_{0\mathrm{disc}}$, we have to take formally the boundary of $\overline{\Omega}^c_{0\mathrm{disc}}$. The blue and green graphs show the values for the two different approaches calculated on a quite coarse mesh of 80 segments. They are plotted using the parametrization of the boundary

$$\xi : [0,1] \to \partial\Omega_{0\mathrm{disc}}.$$

Additionally, the Mie solution is plotted in red using the same parametrization. The figures should get a feeling how the approximations behave. One can nicely see the symmetry of the solution relatively to the direction of propagation of the incident plane wave.

Pointwise errors on the boundary of the exterior domain: The two plots on the bottom of Fig. 3.4 resp. Fig. 3.6 show the pointwise errors on the boundary of the exterior domain:

$$|\gamma_D^{\overline{\Omega}^c_{0\mathrm{disc}}} u_{\mathrm{ref}}(\xi(t)) - \gamma_D^{\overline{\Omega}^c_{0\mathrm{disc}}} u_h(\xi(t))|.$$

The plot on the left shows the error of the finest resolutions compared to the Mie solution, while the plot on the right shows the pointwise error between the finest resolutions of the two different approaches.
We have that the finest resolutions of the two methods lie near to each other. The scale of the error between the two finest resolutions is about one decimal power smaller than the one we get for the error relatively to the analytic Mie solution. Also the behaviour of pointwise error plotted on the left fits well together with the results for the $L^2(\Gamma_{\text{disc}})$-errors: The mean value of all the pointwise errors of the two Neumann traces is practically the same. Furthermore, the mean of the Dirichlet trace of the classical first kind approach is quite smaller than the one of the new second kind method.

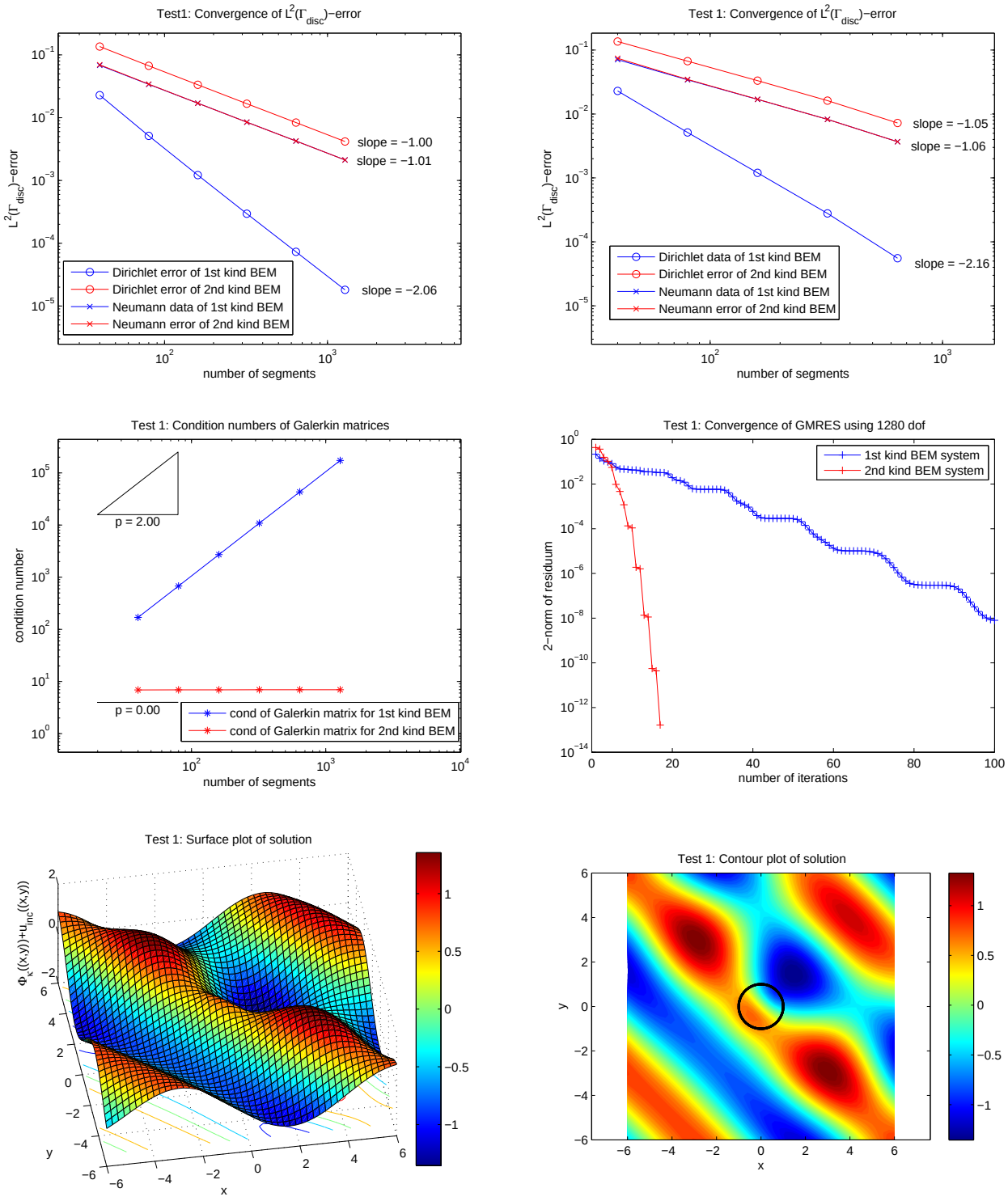

Figure 3.3: Test 1: Helmholtz transmission problem with two domains Ω_0, Ω_1 where Ω_1 is a disc of radius one, Ω_0 the exterior domain. The appropriate wave numbers are chosen as $\kappa_0 = 1, \kappa_1 = 2$. The incoming wave u_{inc} is a plane wave with direction of propagation $\mathbf{d} = \frac{\sqrt{2}}{2}(1,1)^T$.

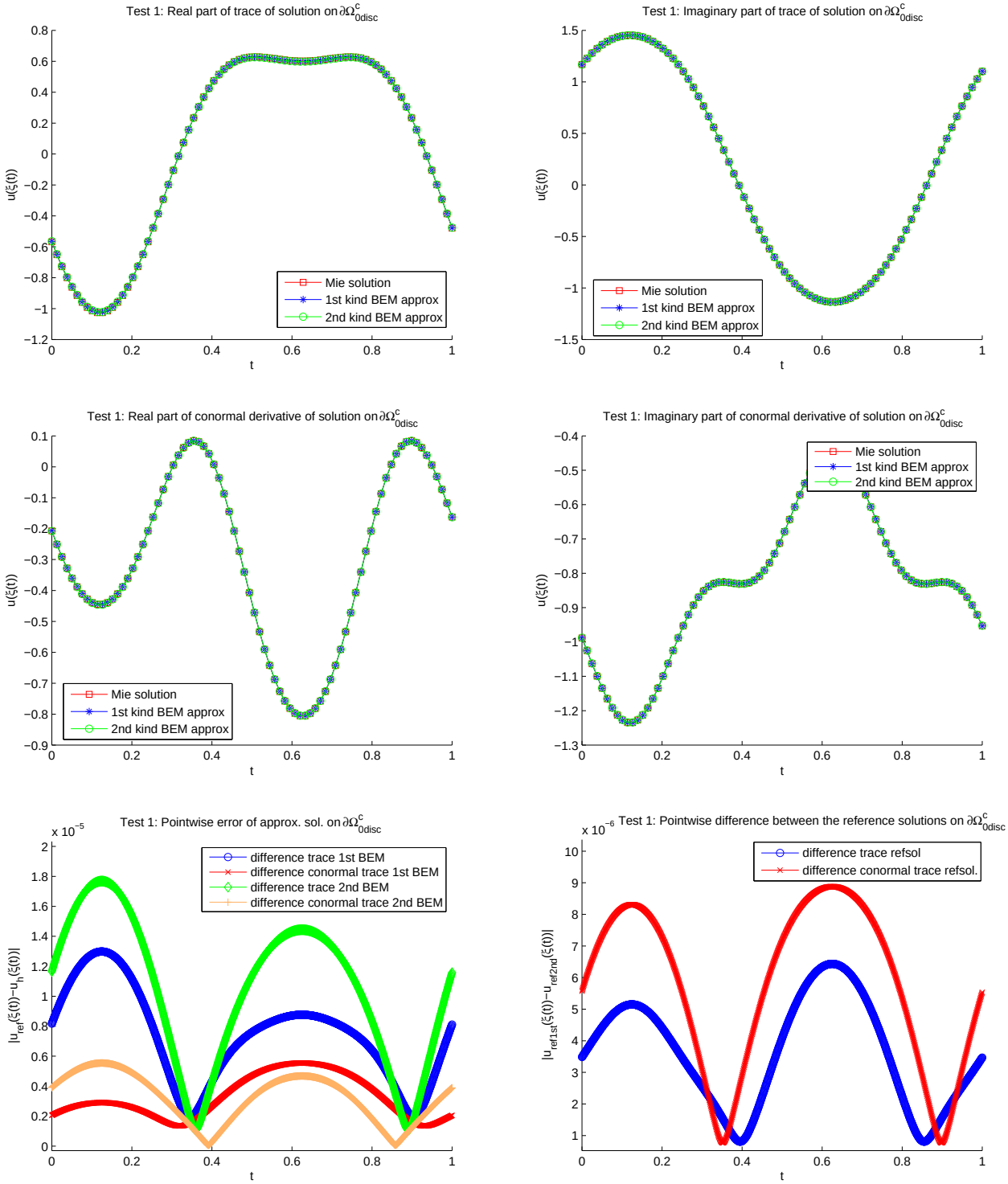

Figure 3.4: Test 1: Helmholtz transmission problem with two domains Ω_0, Ω_1 where Ω_1 is a disc of radius one, Ω_0 the exterior domain. The appropriate wave numbers are chosen as $\kappa_0 = 1, \kappa_1 = 2$. The incoming wave u_{inc} is a plane wave with direction of propagation $\mathbf{d} = \frac{\sqrt{2}}{2}(1,1)^T$.

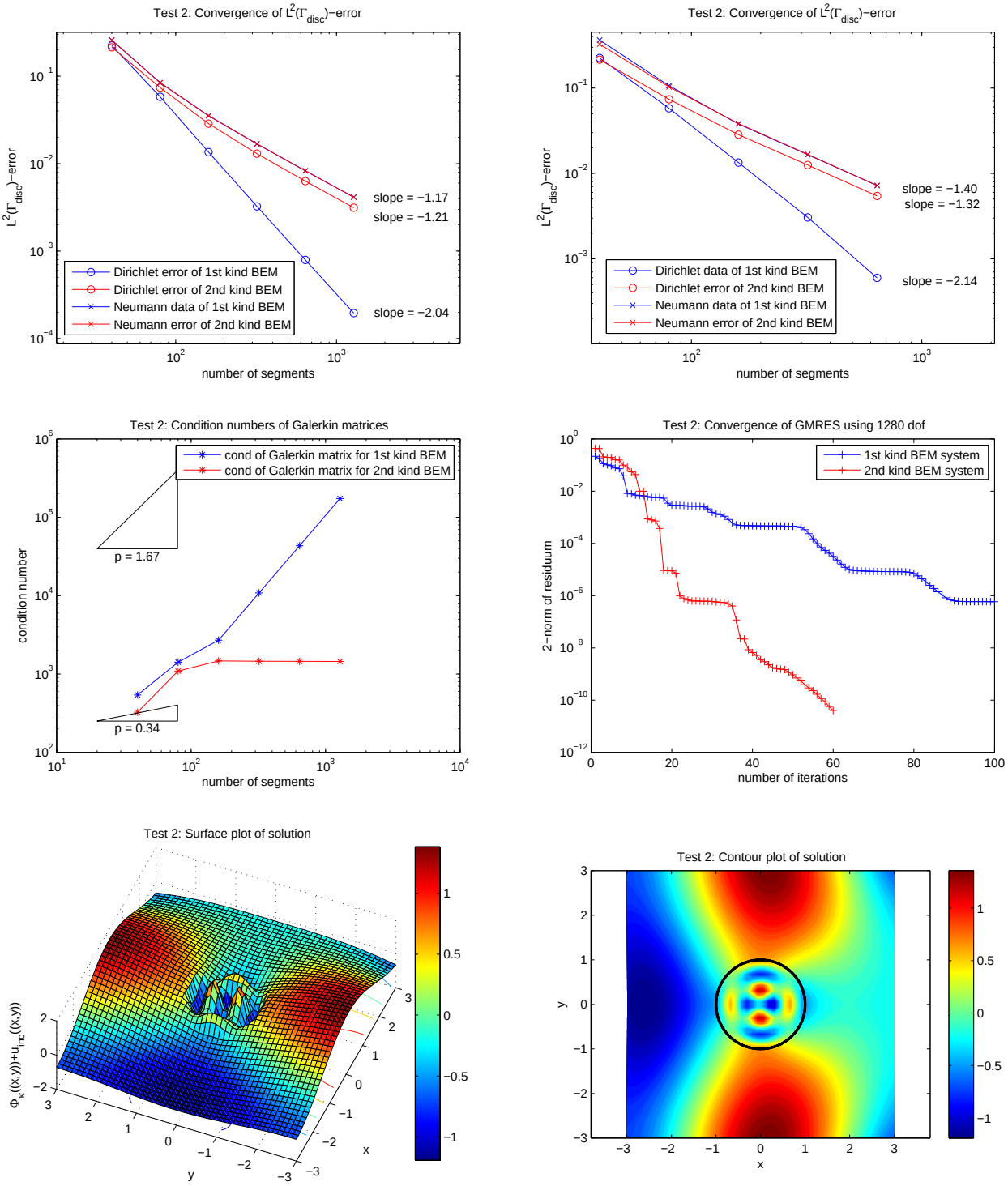

Figure 3.5: Test 2: Helmholtz transmission problem with two domains Ω_0, Ω_1 where Ω_1 is a disc of radius one, Ω_0 the exterior domain. The appropriate wave numbers are chosen as $\kappa_0 = 1, \kappa_1 = 10$. The incoming wave u_{inc} is a plane wave with direction of propagation $\mathbf{d} = (1, 0)^T$.

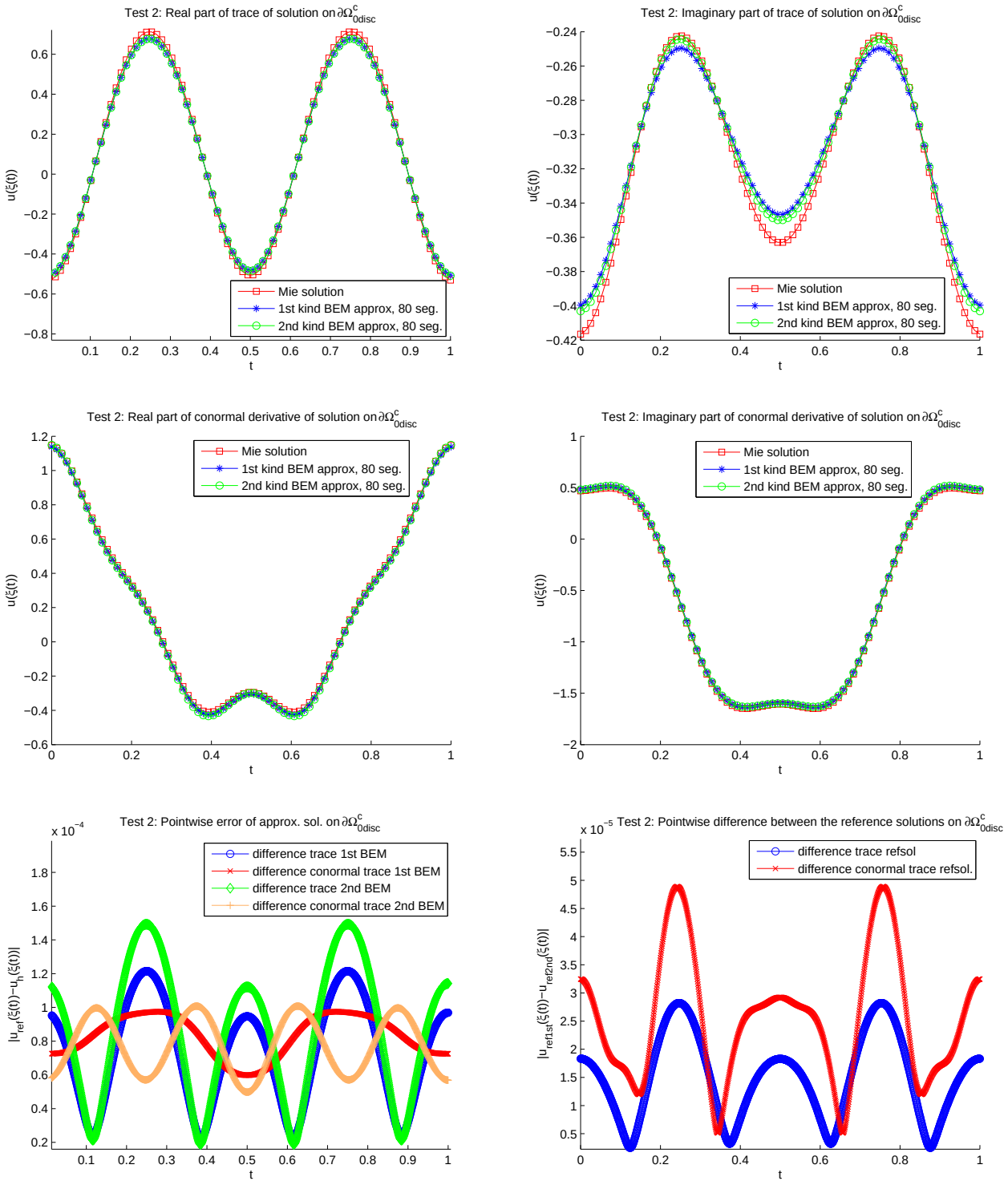

Figure 3.6: Test 2: Helmholtz transmission problem with two domains Ω_0, Ω_1 where Ω_1 is a disc of radius one, Ω_0 the exterior domain. The appropriate wave numbers are chosen as $\kappa_0 = 1, \kappa_1 = 10$. The incoming wave u_{inc} is a plane wave with direction of propagation $\mathbf{d} = (1, 0)^T$.

3.2 A Unit Square

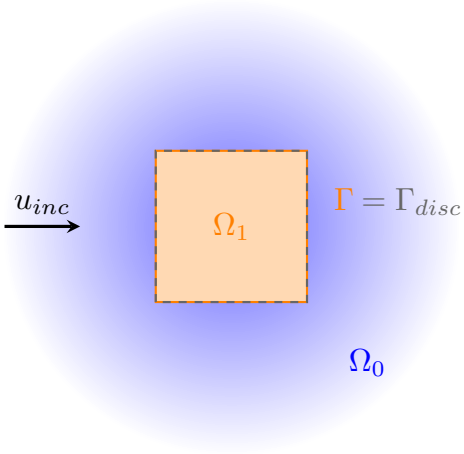

Figure 3.7: Geometry of the considered Helmholtz problem

The second geometry we consider is the unit square. More precisely, we define Ω_1 to be a square with side length one, while $\Omega_0 = \overline{\Omega}_1^c$ represents the exterior domain. As for the unit disc, we again look at two different Helmholtz transmission problems, one taking small wave numbers and the other one using bigger ones on the two domains. Which wave numbers and what direction of propagation of the incident wave we concretely choose can be found below the figures showing the results of the appropriate test.

$L^2(\Gamma_{\text{disc}})$ convergence results: For the case of the unit square we have to settle for the approximation of highest resolution as a reference solution. Additionally, it is obvious that there is no error due to the discretization of the geometry of the boundary, i.e. $\Gamma_{\text{disc}} \equiv \Gamma$.
The Dirichlet data of the solution should again be quite regular, such that together with Thm. 10 and Thm. 9 we expect a convergence of the $L^2(\Gamma_{\text{disc}})$-error in $\mathcal{O}(N_{\text{seg}}^{-2})$ for the classical first kind approach resp. $\mathcal{O}(N_{\text{seg}}^{-1})$ for the new second kind formulation.
Due to the jump of the outward normal vector on the edges of the domains, the Neumann data has to be discontinuous. Therefore we obtain using the definition of $H^s(\Gamma)$ in [9, p. 98] together with the Sobolev embedding theorem stated in [12, Thm. 2.5.4] that

$$\gamma_N^{\Gamma_{\text{disc}}} u \notin H^l(\Gamma) \text{ for all } l > \frac{1}{2}.$$

This fact gives us together with the quasi optimal error estimates (Thm. 10 and Thm. 8) a convergence behaviour of $\mathcal{O}(N_{\text{seg}}^{-\frac{1}{2}})$ in the best case.
Despite of this, we discretize the boundary Γ in such a way that the corners fall into edge points of the segments. Thus, the singularity due to the corner can be ignored because the jumps are automatically well approximated by our piecewise constant ansatz functions. Therefore, we expect the convergence to be not

affected by the singularities at the corners. This gives us that the convergence behaviour for the Neumann data could be in the best case $\mathcal{O}(N_{\text{seg}}^{-1})$. What we obtain is indeed a convergence in $\mathcal{O}(N_{\text{seg}}^{-1})$ for the new second kind ansatz while for the first kind formulation we only attain $\mathcal{O}(N_{\text{seg}}^{-0.5})$ (cf. plots on the top of Figures 3.8 and 3.10). The rate of -0.5 coincides with the results obtained from Meury in his PhD [10, Figure 3.4], using a FEM-BEM coupling method based on the same BEM library as we use for our classical first kind approach.

Again, for the choice of big wave numbers, linear convergence of the expected order is not attained from the beginning (cf. Table 3.3 and Table 3.4). We obtain even higher convergence in the first few steps. But the rates decrease in such a way that it seems realistic that they converge to the theoretical result. To ensure agreement with the theoretical result, we would have to calculate data for further refinement steps, but this is not realistic because of the long expected running time.

Global potential and traces on $\overline{\Omega}^c_{\mathbf{0disc}}$: The two plots showing the imaginary resp. real part of the Neumann trace situated in the middle of Figure 3.9 resp. Figure 3.11 give an idea why the new second kind approach converges better: The traces we obtain using the classical first kind formulation oscillate around the jumps, while the new second kind approach does not have problems to capture the discontinuity. In the two plots at the bottom of Figures 3.9, 3.11, the absolute error between the two different solutions of highest resolution again indicates that the error contribution due to the oscillations cannot be neglected and might be the reason for the worser rate of convergence of the classical approach.

Condition number of the Galerkin matrices and GMRES: The condition numbers of the Galerkin matrices and GMRES tests behave similar to the ones of Test 1 and Test 2 for the unit disc. Therefore we refer to the discussion there. The only thing we have to remark is that there is even a stronger contrast of the results for convergence of the GMRES method: For the second kind method it converges very fast, while for the first kind approach there is no remarkable reduction of the residuum visible.

N_{seg}	$\|\gamma_D^{\Gamma_{\text{disc}}} u_{\text{ref}} - \gamma_D^{\Gamma_{\text{disc}}} u_h\|_{L^2(\Gamma_{\text{disc}})}$	eoc	$\|\gamma_N^{\Gamma_{\text{disc}}} u_{\text{ref}} - \gamma_N^{\Gamma_{\text{disc}}} u_h\|_{L^2(\Gamma_{\text{disc}})}$	eoc
40	$8.431 \cdot 10^{-1}$		$3.880 \cdot 10^{0}$	
80	$1.267 \cdot 10^{-1}$	-2.73	$1.638 \cdot 10^{0}$	-1.24
160	$1.995 \cdot 10^{-2}$	-2.67	$8.339 \cdot 10^{-1}$	-0.97
320	$3.638 \cdot 10^{-3}$	-2.46	$4.400 \cdot 10^{-1}$	-0.92
640	$6.973 \cdot 10^{-4}$	-2.38	$2.335 \cdot 10^{-1}$	-0.91
Theory:		-2		-0.5

Table 3.3: Error and order of convergence for the classical first kind approach.

N_{seg}	$\|\gamma_D^{\Gamma_{\text{disc}}} u_{\text{ref}} - \gamma_D^{\Gamma_{\text{disc}}} u_h\|_{L^2(\Gamma_{\text{disc}})}$	eoc	$\|\gamma_N^{\Gamma_{\text{disc}}} u_{\text{ref}} - \gamma_N^{\Gamma_{\text{disc}}} u_h\|_{L^2(\Gamma_{\text{disc}})}$	eoc
40	$1.373 \cdot 10^{0}$		$4.932 \cdot 10^{0}$	
80	$4.382 \cdot 10^{-1}$	-1.65	$1.895 \cdot 10^{0}$	-1.38
160	$1.393 \cdot 10^{-1}$	-1.65	$7.938 \cdot 10^{-1}$	-1.26
320	$5.414 \cdot 10^{-2}$	-1.36	$3.671 \cdot 10^{-1}$	-1.11
640	$2.251 \cdot 10^{-2}$	$-1,27$	$1.621 \cdot 10^{-1}$	-1.18
Theory:		-1		-1

Table 3.4: Error and order of convergence for the new second kind approach.

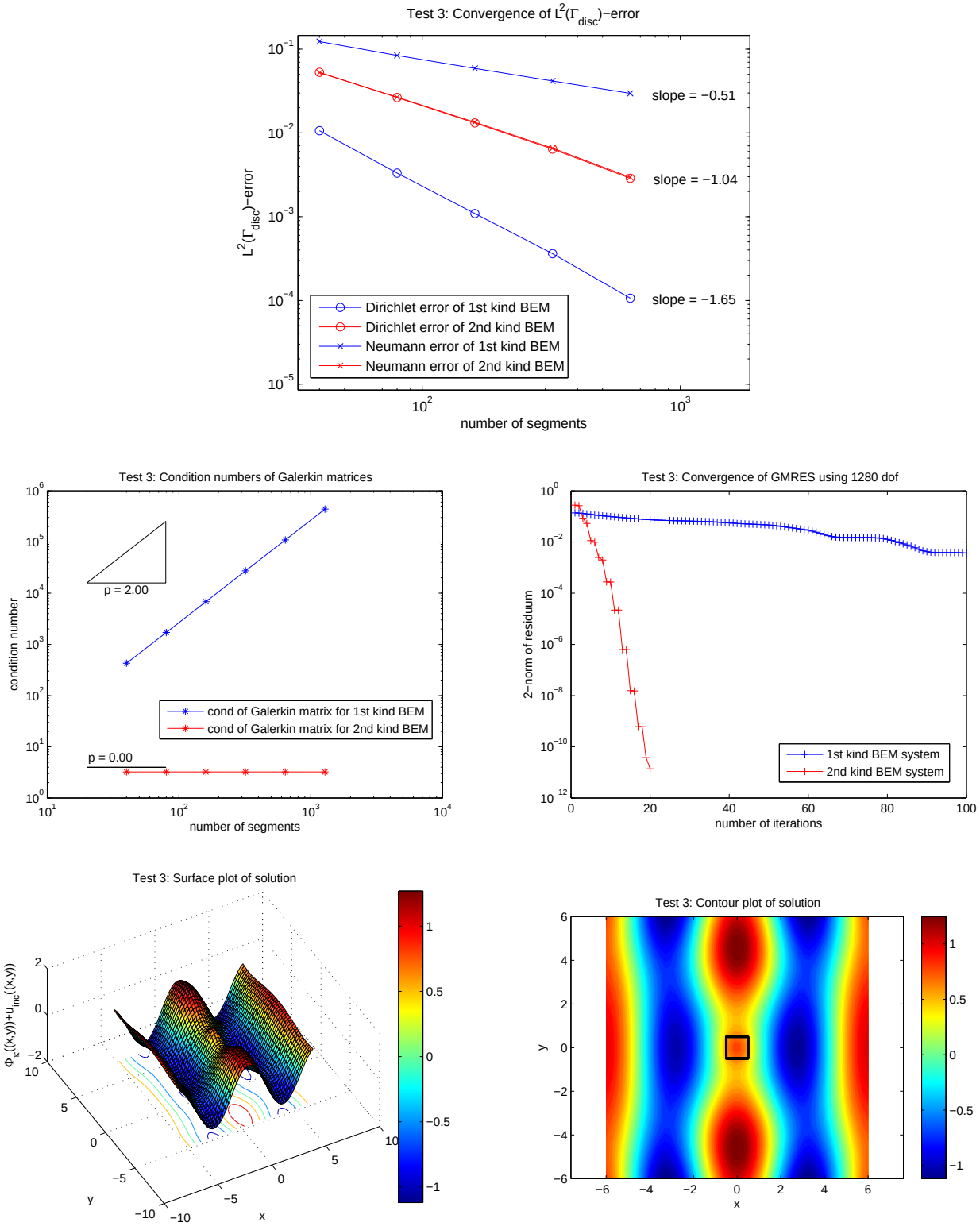

Figure 3.8: Test 3: Helmholtz transmission problem with two domains Ω_0, Ω_1 where Ω_1 is a square of side length one, Ω_0 the exterior domain. The appropriate wave numbers are chosen as $\kappa_0 = 1, \kappa_1 = 2$. The incoming wave u_{inc} is a plane wave with direction of propagation $\mathbf{d} = (1, 0)^T$.

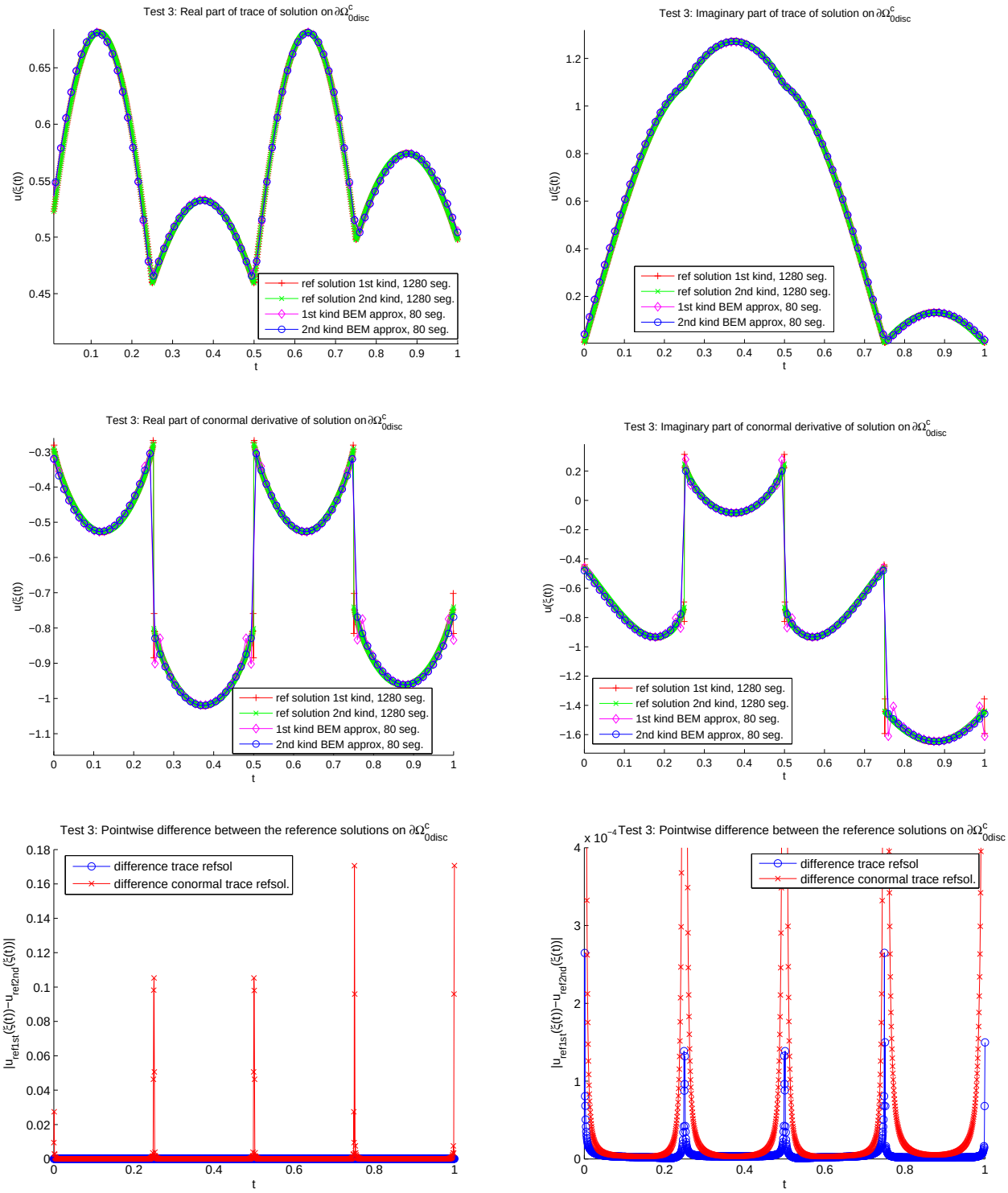

Figure 3.9: Test 3: Helmholtz transmission problem with two domains Ω_0, Ω_1 where Ω_1 is a square of side length one, Ω_0 the exterior domain. The appropriate wave numbers are chosen as $\kappa_0 = 1, \kappa_1 = 2$. The incoming wave u_{inc} is a plane wave with direction of propagation $\mathbf{d} = (1,0)^T$.

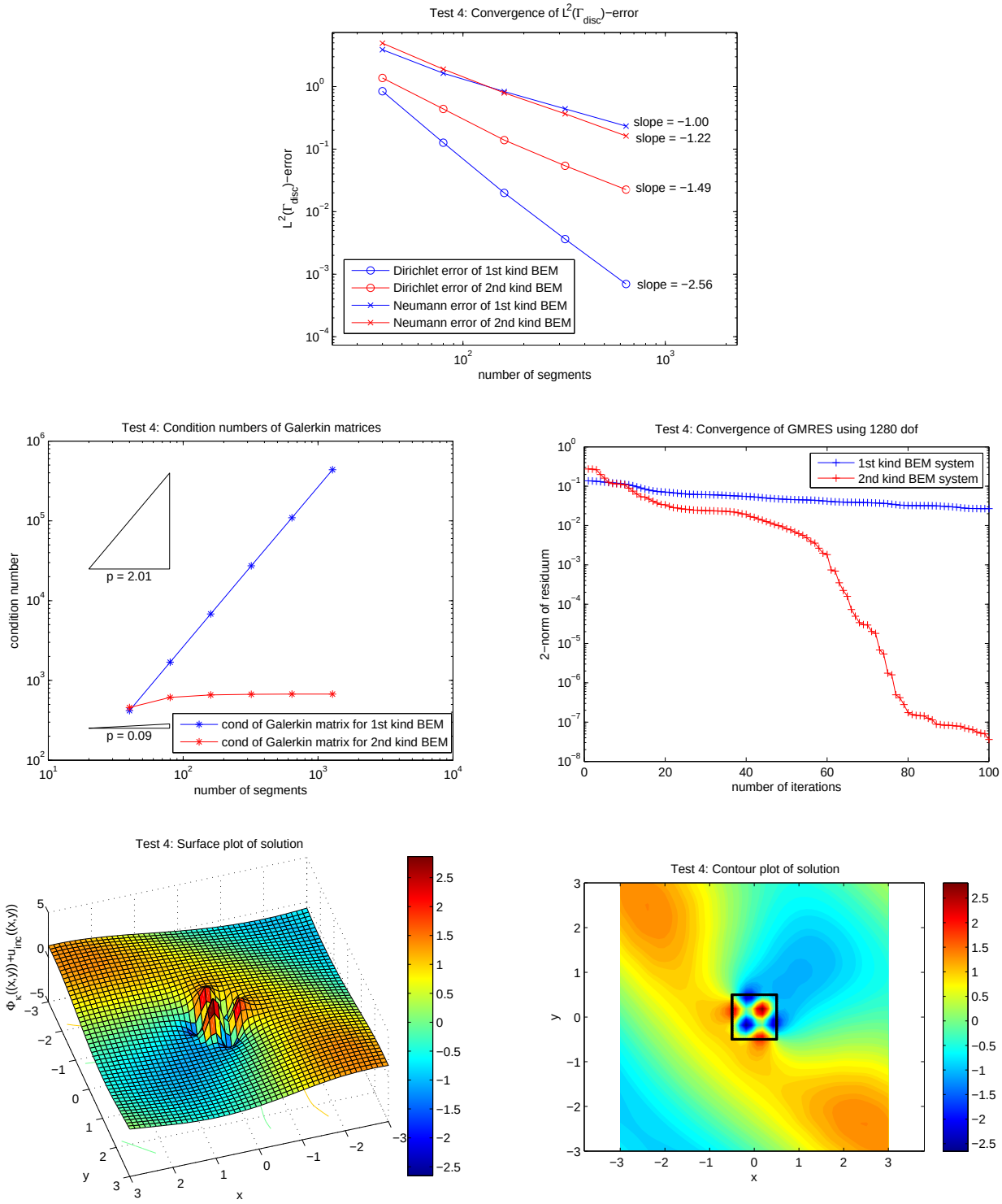

Figure 3.10: Test 4: Helmholtz transmission problem with two domains Ω_0, Ω_1 where Ω_1 is a square of side length one, Ω_0 the exterior domain. The appropriate wave numbers are chosen as $\kappa_0 = 1, \kappa_1 = 10$. The incoming wave u_{inc} is a plane wave with direction of propagation $\mathbf{d} = \frac{\sqrt{2}}{2}(1,1)^T$.

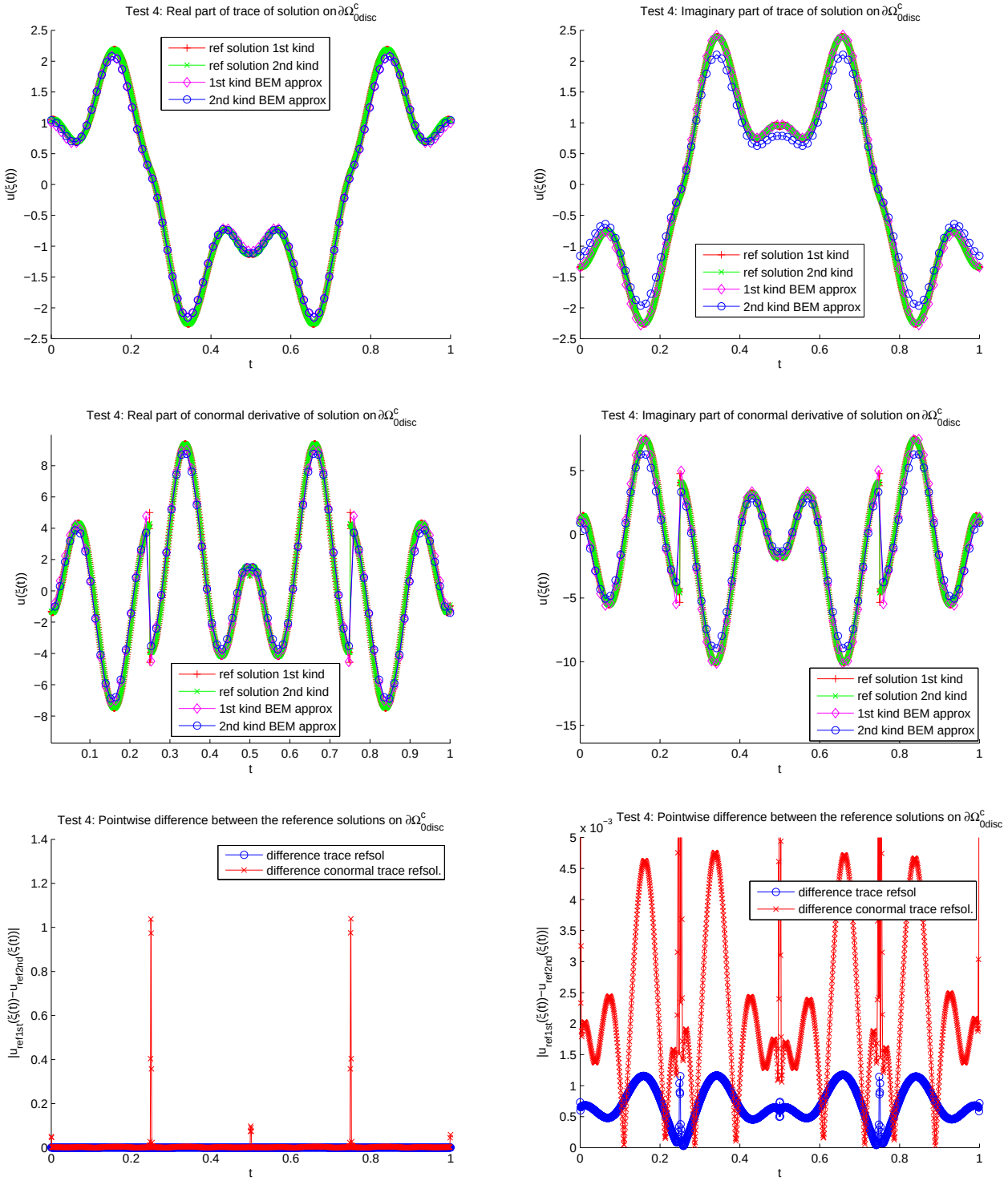

Figure 3.11: Test 4: Helmholtz transmission problem with two domains Ω_0, Ω_1 where Ω_1 is a square of side length one, Ω_0 the exterior domain. The appropriate wave numbers are chosen as $\kappa_0 = 1, \kappa_1 = 10$. The incoming wave u_{inc} is a plane wave with direction of propagation $\mathbf{d} = \frac{\sqrt{2}}{2}(1,1)^T$.

3.3 Two Half Discs

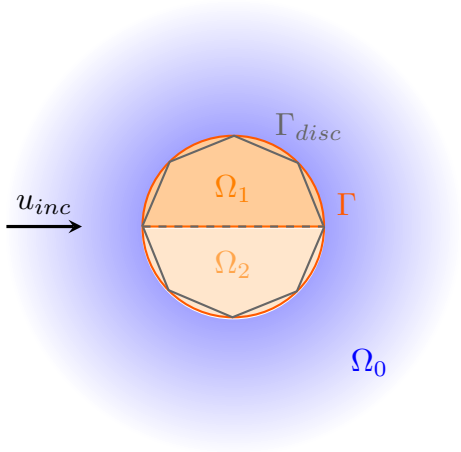

Figure 3.12: Geometry of the considered Helmholtz problem

Now we come to the first more complex example involving three domains. We bisect the unit disc into two parts by the aid of the x-axis. The upper half of the disc we name Ω_1, the lower half Ω_2. All the remaining part of $\mathbb{R}^2$, i.e. $\left(\overline{\Omega}_1 \cup \overline{\Omega}_2\right)^c$, we define to be the exterior domain Ω_0. We solve a Helmholtz transmission problem on this geometry with an incident plane wave having the direction of propagation $\mathbf{d} = (1,0)^T$ and wave numbers $\kappa_0 = 3$, $\kappa_1 = 1$, $\kappa_2 = 5$.

$L^2(\Gamma_{\text{disc}})$ convergence results: Table 3.5 and Table 3.6 show the detailed information about the evolution of the errors and convergence rates, while in the plot on the top of Figure 3.13 one can find an illustration for it. The Dirichlet data converges obviously as expected, since the solution should be quite regular. The rates for the Neumann error of the classical approach still decay remarkably in the last step. Therefore we reckon that it would decrease also for the next few steps.As for the previous cases, it was not possible to calculate further refinements due to the large computational effort.

Global potential and traces on $\overline{\Omega}^c_{0\text{disc}}$: Looking at Figure 3.14 one again finds oscillations in the first kind approximation of the Neumann data. They are situated at the discontinuities at the corners of the domains in $t = 0$, resp. $t = 1$ and $t = 0.5$. This leads, as in the discussion for the unit square to the conjecture that the first kind approach suffers the loss of convergence rate. The plots on the bottom of Figure 3.14 indicate that the oscillations have quite a big contribution to the error.

N_{seg}	$\|\gamma_D^{\Gamma_{\text{disc}}} u_{\text{ref}} - \gamma_D^{\Gamma_{\text{disc}}} u_h\|_{L^2(\Gamma_{\text{disc}})}$	eoc	$\|\gamma_N^{\Gamma_{\text{disc}}} u_{\text{ref}} - \gamma_N^{\Gamma_{\text{disc}}} u_h\|_{L^2(\Gamma_{\text{disc}})}$	eoc
60	$1.359 \cdot 10^{-1}$		$8.807 \cdot 10^{-1}$	
120	$2.437 \cdot 10^{-2}$	-2.48	$4.521 \cdot 10^{-1}$	-0.96
240	$5.309 \cdot 10^{-3}$	-2.20	$2.480 \cdot 10^{-1}$	-0.87
480	$1.346 \cdot 10^{-3}$	-1.98	$1.434 \cdot 10^{-1}$	-0.79
960	$3.322 \cdot 10^{-4}$	-2.02	$8.644 \cdot 10^{-2}$	-0.73
Theory:		-2		-0.5

Table 3.5: Error and order of convergence for the classical first kind approach.

N_{seg}	$\|\gamma_D^{\Gamma_{\text{disc}}} u_{\text{ref}} - \gamma_D^{\Gamma_{\text{disc}}} u_h\|_{L^2(\Gamma_{\text{disc}})}$	eoc	$\|\gamma_N^{\Gamma_{\text{disc}}} u_{\text{ref}} - \gamma_N^{\Gamma_{\text{disc}}} u_h\|_{L^2(\Gamma_{\text{disc}})}$	eoc
60	$3.451 \cdot 10^{-1}$		$9.992 \cdot 10^{-1}$	
120	$1.491 \cdot 10^{-1}$	-1.21	$4.354 \cdot 10^{-1}$	-1.20
240	$7.156 \cdot 10^{-2}$	-1.06	$2.106 \cdot 10^{-1}$	-1.05
480	$3.462 \cdot 10^{-2}$	-1.05	$1.023 \cdot 10^{-1}$	-1.04
960	$1.545 \cdot 10^{-2}$	$-1,16$	$4.572 \cdot 10^{-2}$	-1.16
Theory:		-1		-1

Table 3.6: Error and order of convergence for the new second kind approach.

Condition number of the Galerkin matrices and GMRES: As in the tests done before, the condition number of the Galerkin matrix obtained using the new second kind approach is bounded relatively to the number of segments, while for the first kind approach it diverges quadratically.
The convergence of the iterative solver GMRES is, similarly to the tests made before, very fast for the second kind formulation while for the first kind version comparably nothing happens.

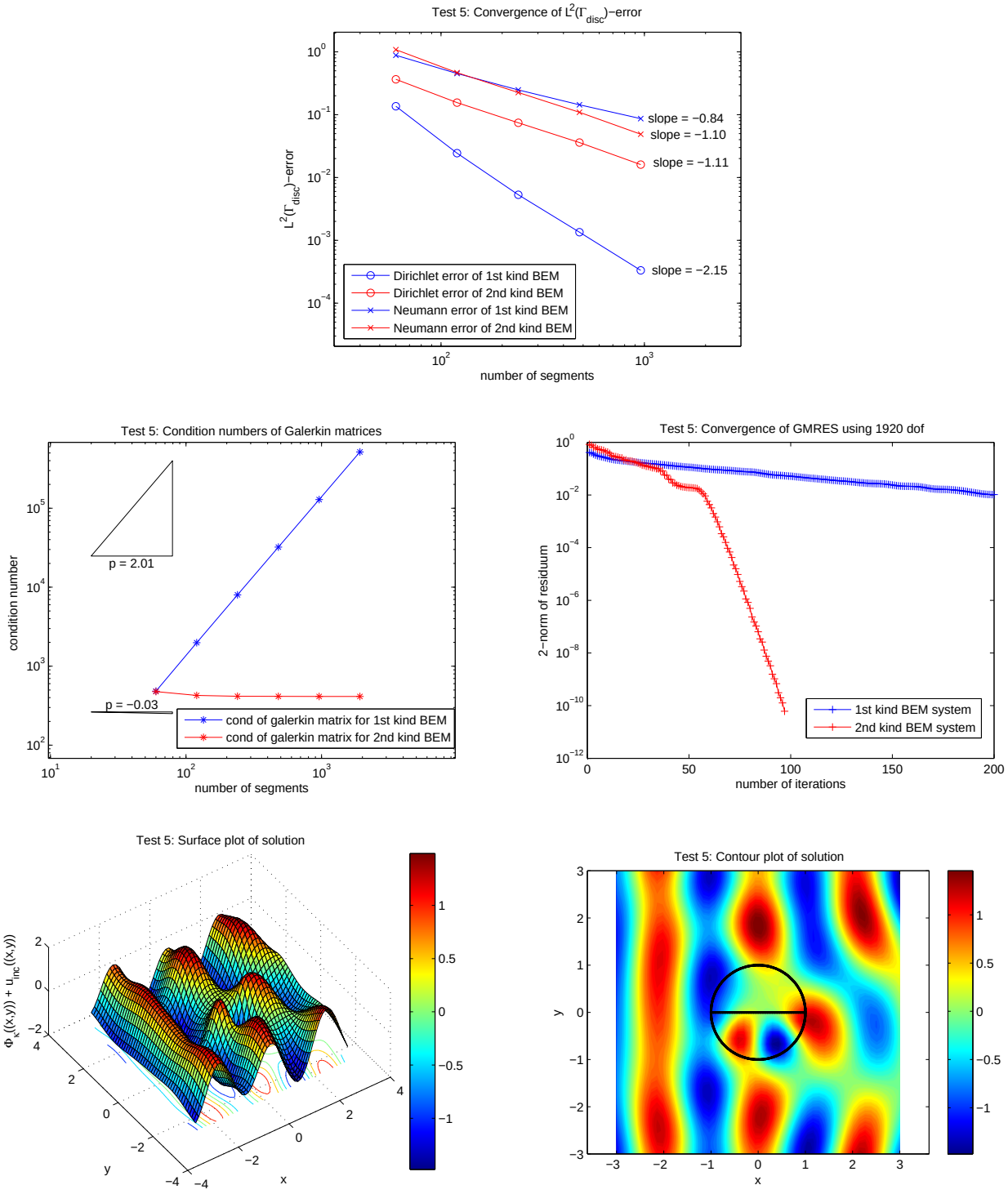

Figure 3.13: Test 5: Helmholtz transmission problem with tree domains $\Omega_0, \Omega_1, \Omega_2$ where Ω_1 is the upper half of a disc of radius one, Ω_2 is the lower half of the unit disc and Ω_0 the exterior domain. The appropriate wave numbers are chosen as $\kappa_0 = 3, \kappa_1 = 1, \kappa_2 = 5$. The incoming wave u_{inc} is a plane wave with direction of propagation $\mathbf{d} = (1, 0)^T$.

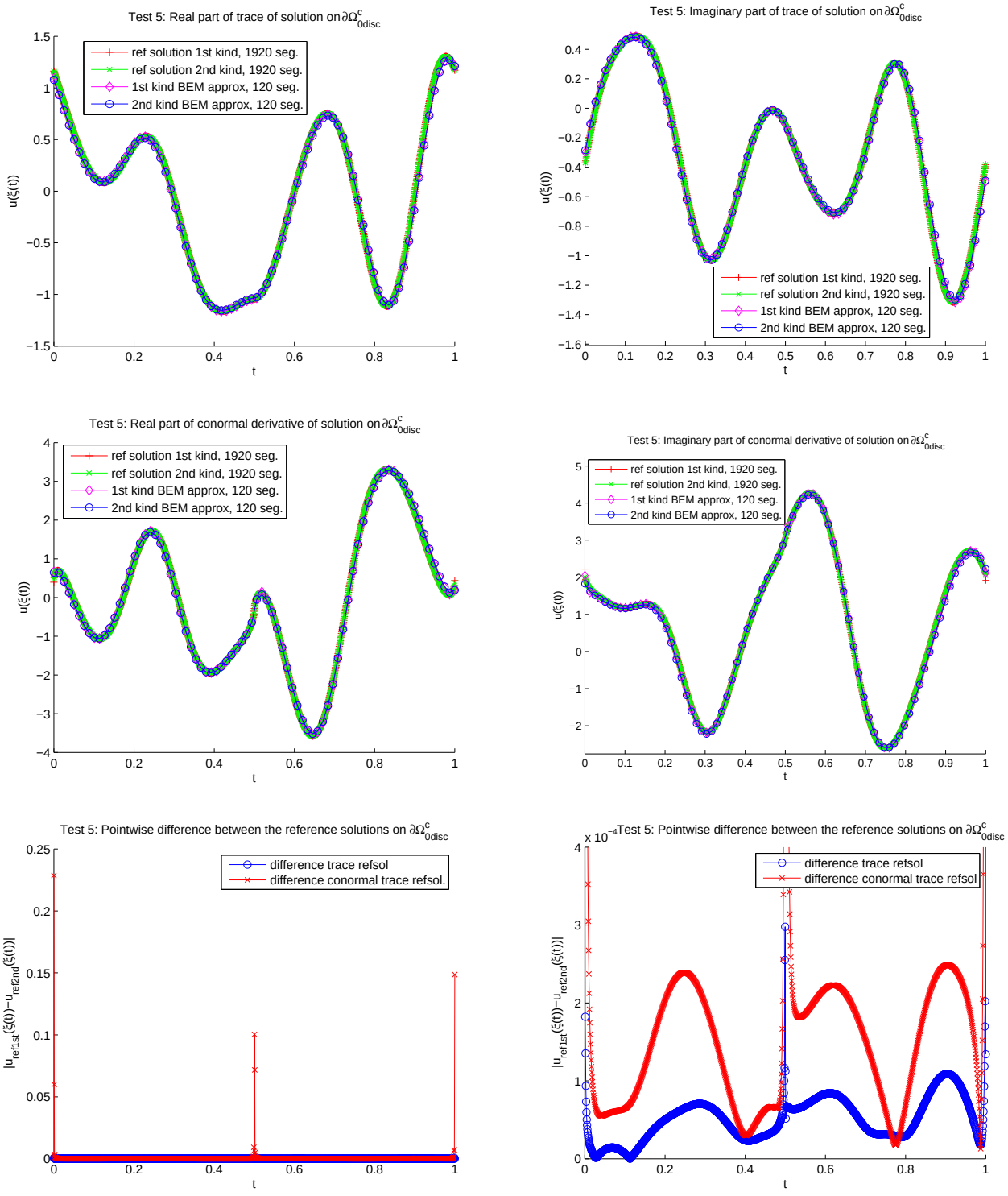

Figure 3.14: Test 5: Helmholtz transmission problem with tree domains $\Omega_0, \Omega_1, \Omega_2$ where Ω_1 is the upper half of a disc of radius one, Ω_2 is the lower half of the unit disc and Ω_0 the exterior domain. The appropriate wave numbers are chosen as $\kappa_0 = 3, \kappa_1 = 1, \kappa_2 = 5$. The incoming wave u_{inc} is a plane wave with direction of propagation $\mathbf{d} = (1, 0)^T$.

3.4 Two Half Squares

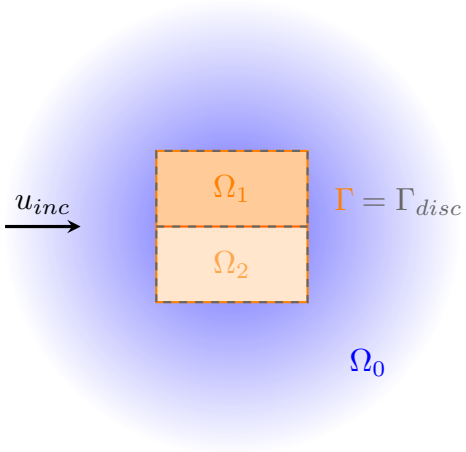

Figure 3.15: Geometry of the considered Helmholtz problem

The three domain problem we are going to study in this section is visualized above. The unit square is bisected by the x-axis. The upper rectangle is denoted to be Ω_1, the lower one is Ω_2 and outer space is named Ω_0. We take the incident wave having $\mathbf{d} = (1, 0)^T$ as direction of propagation and $\kappa_0 = 1$, $\kappa_1 = 10$ and $\kappa_2 = 5$ to be the wave numbers of the particular domains.

$L^2(\Gamma_{\mathbf{disc}})$ convergence results: The results we obtain solving the Helmholtz transmission problem based on this data are similar to the ones already discussed. We therefore refer to the discussions there. The expected convergence behaviour is $\mathcal{O}(N_{\text{seg}}^{-2})$ resp. $\mathcal{O}(N_{\text{seg}}^{-1})$ for the Dirichlet error of the first kind resp. second kind approach since the solution should be smooth enough.
We emphasize again the oscillations in the Neumann data of the first kind method at the discontinuities situated in the edges of the domains. Therefore we get a worser rate for the Neumann error of the first kind approach.

N_{seg}	$\|\gamma_D^{\Gamma_{\text{disc}}} u_{\text{ref}} - \gamma_D^{\Gamma_{\text{disc}}} u_h\|_{L^2(\Gamma_{\text{disc}})}$	eoc	$\|\gamma_N^{\Gamma_{\text{disc}}} u_{\text{ref}} - \gamma_N^{\Gamma_{\text{disc}}} u_h\|_{L^2(\Gamma_{\text{disc}})}$	eoc
60	$3.973 \cdot 10^{-2}$		$7.269 \cdot 10^{-1}$	
120	$8.949 \cdot 10^{-3}$	-2.15	$3.789 \cdot 10^{-1}$	-0.94
240	$2.221 \cdot 10^{-3}$	-2.01	$2.040 \cdot 10^{-1}$	-0.89
480	$6.316 \cdot 10^{-4}$	-1.81	$1.141 \cdot 10^{-1}$	-0.84
960	$1.722 \cdot 10^{-4}$	-1.87	$6.614 \cdot 10^{-2}$	-0.79
Theory:		-2		-0.5

Table 3.7: Error and order of convergence for the classical first kind approach.

N_{seg}	$\|\gamma_D^{\Gamma_{\text{disc}}} u_{\text{ref}} - \gamma_D^{\Gamma_{\text{disc}}} u_h\|_{L^2(\Gamma_{\text{disc}})}$	eoc	$\|\gamma_N^{\Gamma_{\text{disc}}} u_{\text{ref}} - \gamma_N^{\Gamma_{\text{disc}}} u_h\|_{L^2(\Gamma_{\text{disc}})}$	eoc
60	$1.263 \cdot 10^{-1}$		$7.724 \cdot 10^{-1}$	
120	$5.907 \cdot 10^{-2}$	-1.10	$3.830 \cdot 10^{-1}$	-1.01
240	$2.885 \cdot 10^{-2}$	-1.03	$1.916 \cdot 10^{-1}$	-1.00
480	$1.402 \cdot 10^{-2}$	-1.04	$9.402 \cdot 10^{-2}$	-1.03
960	$6.261 \cdot 10^{-3}$	$-1,16$	$4.219 \cdot 10^{-2}$	-1.16
Theory:		-1		-1

Table 3.8: Error and order of convergence for the new second kind approach.

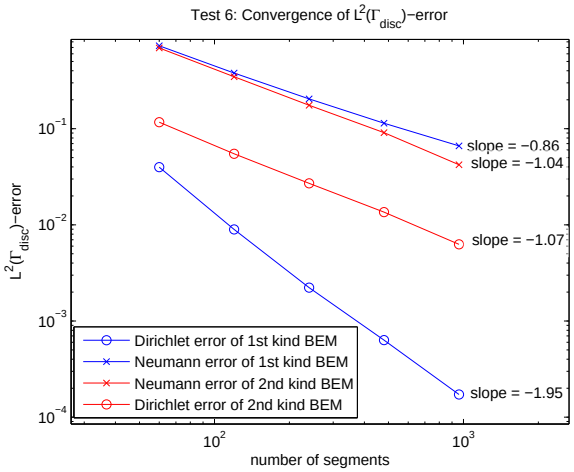

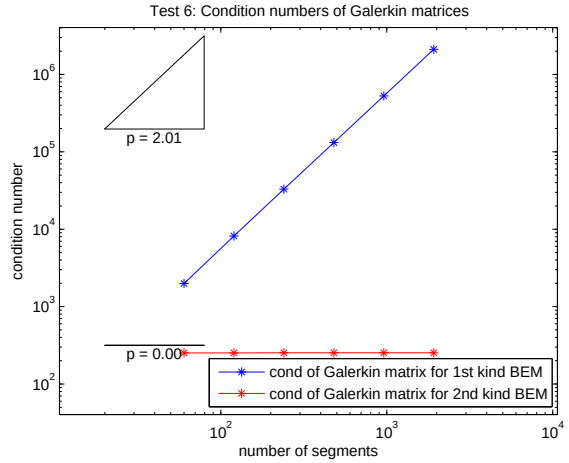

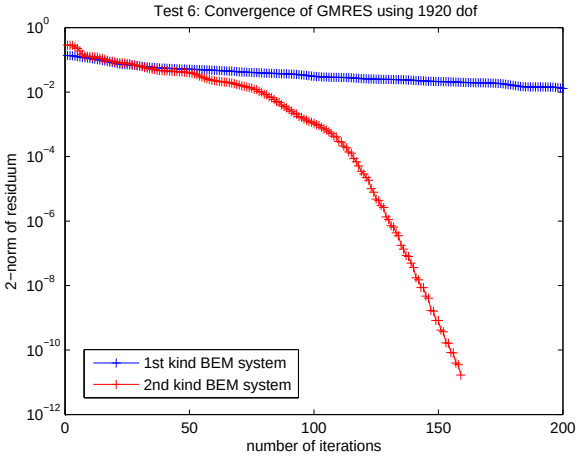

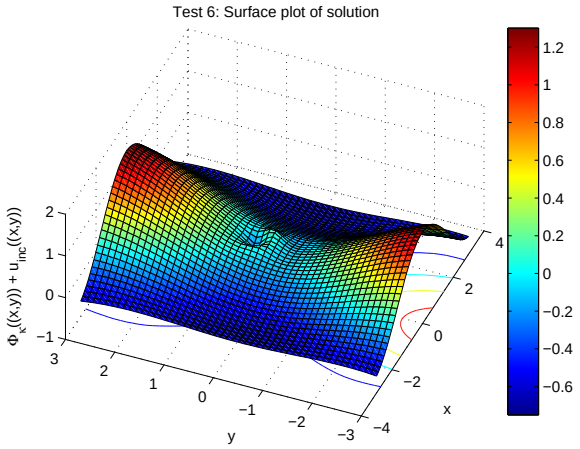

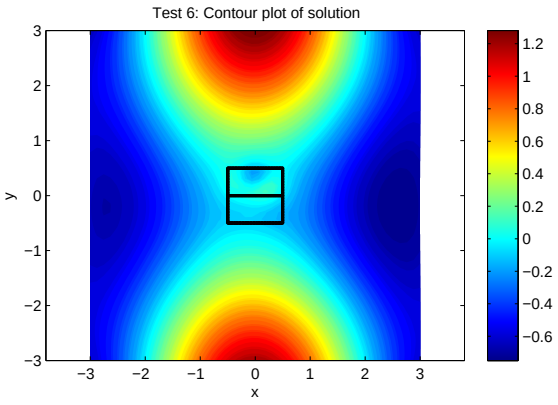

Test 6: Helmholtz transmission problem with tree domains $\Omega_0, \Omega_1, \Omega_2$ where Ω_1 is the upper half of a square of side length one, Ω_2 is the lower half of a square of side length one and Ω_0 the exterior domain. The appropriate wave numbers are chosen as $\kappa_0 = 1, \kappa_1 = 10, \kappa_2 = 5$. The incoming wave u_{inc} is a plane wave with direction of propagation $\mathbf{d} = (1, 0)^T$.

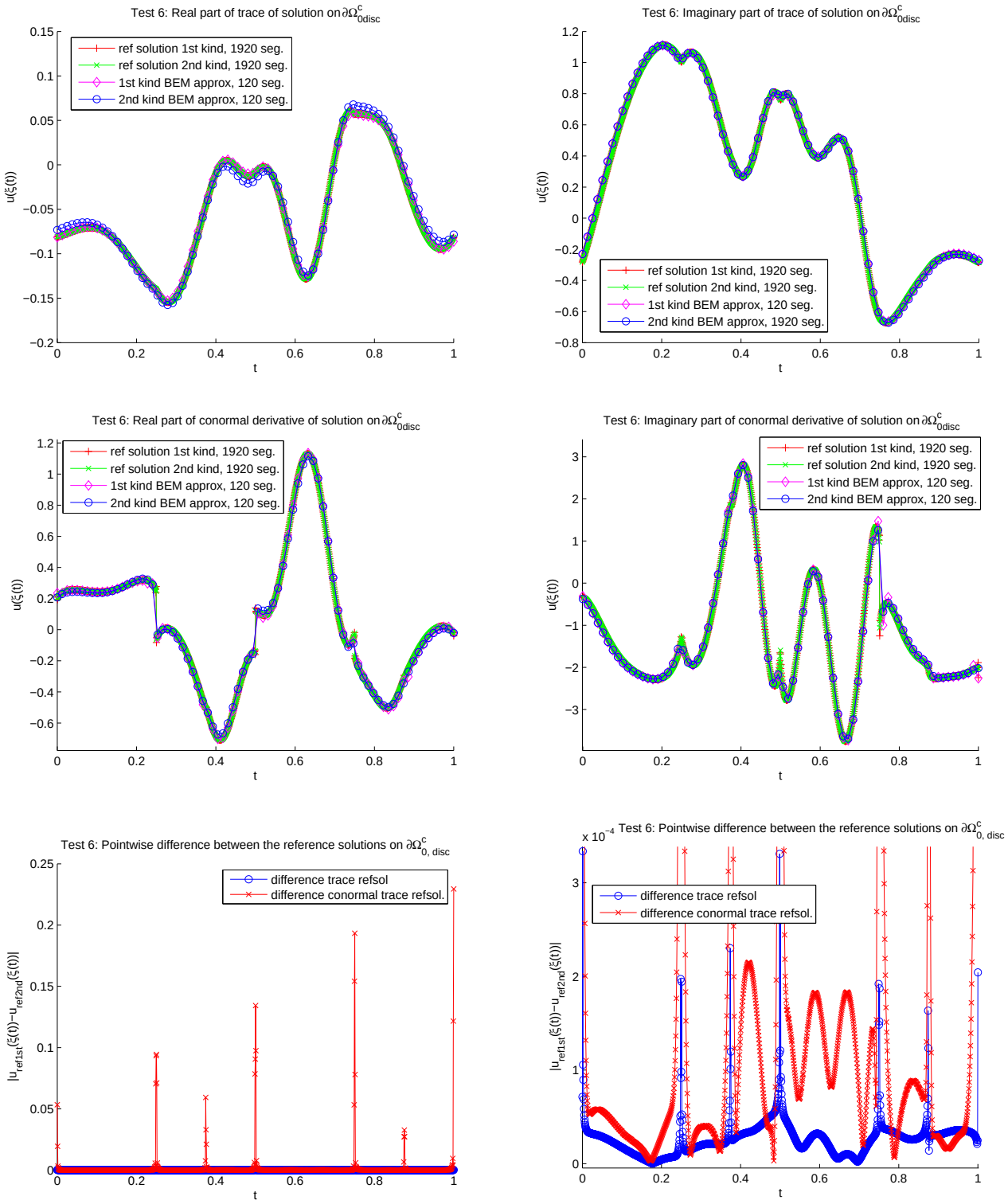

Test 6: Helmholtz transmission problem with tree domains $\Omega_0, \Omega_1, \Omega_2$ where Ω_1 is the upper half of a square of side length one, Ω_2 is the lower half of a square of side length one and Ω_0 the exterior domain. The appropriate wave numbers are chosen as $\kappa_0 = 1, \kappa_1 = 10, \kappa_2 = 5$. The incoming wave u_{inc} is a plane wave with direction of propagation $\mathbf{d} = (1, 0)^T$.

3.5 Four Quarter Discs

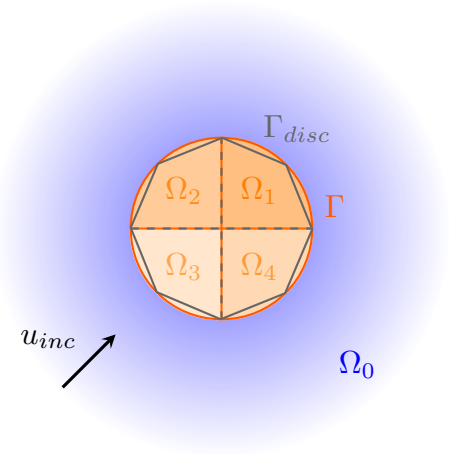

Figure 3.16: Geometry of the considered Helmholtz problem

We close the discussions with five domain problems. The unit disc is divided into four quarters. Ω_1 describes the right upper quarter of the unit disc, Ω_2 the left upper quarter, Ω_3 the left lower quarter and finally, Ω_4 is set to be the right lower part. As always, Ω_0 denotes the unbounded outer space. The wave numbers are chosen as follows: $\kappa_0 = 3$, $\kappa_1 = 1$, $\kappa_2 = 5$, $\kappa_3 = 2$ and κ_4=3. The incident wave has the direction of propagation $\mathbf{d} = \frac{\sqrt{2}}{2}(1,1)^T$.

$L^2(\Gamma_{\text{disc}})$ convergence results: The results for the error convergence are this time so nicely behaving that the convergence plot at the top of Figure 3.18 gives enough information: Linear convergence of the orders (-2) for the classical approach, resp. (-1) for the new method for the Dirichlet errors and (-0.5) resp. (-1) for the Neumann errors. This is exactly what we expect from the previous discussions (see Section 3.2).

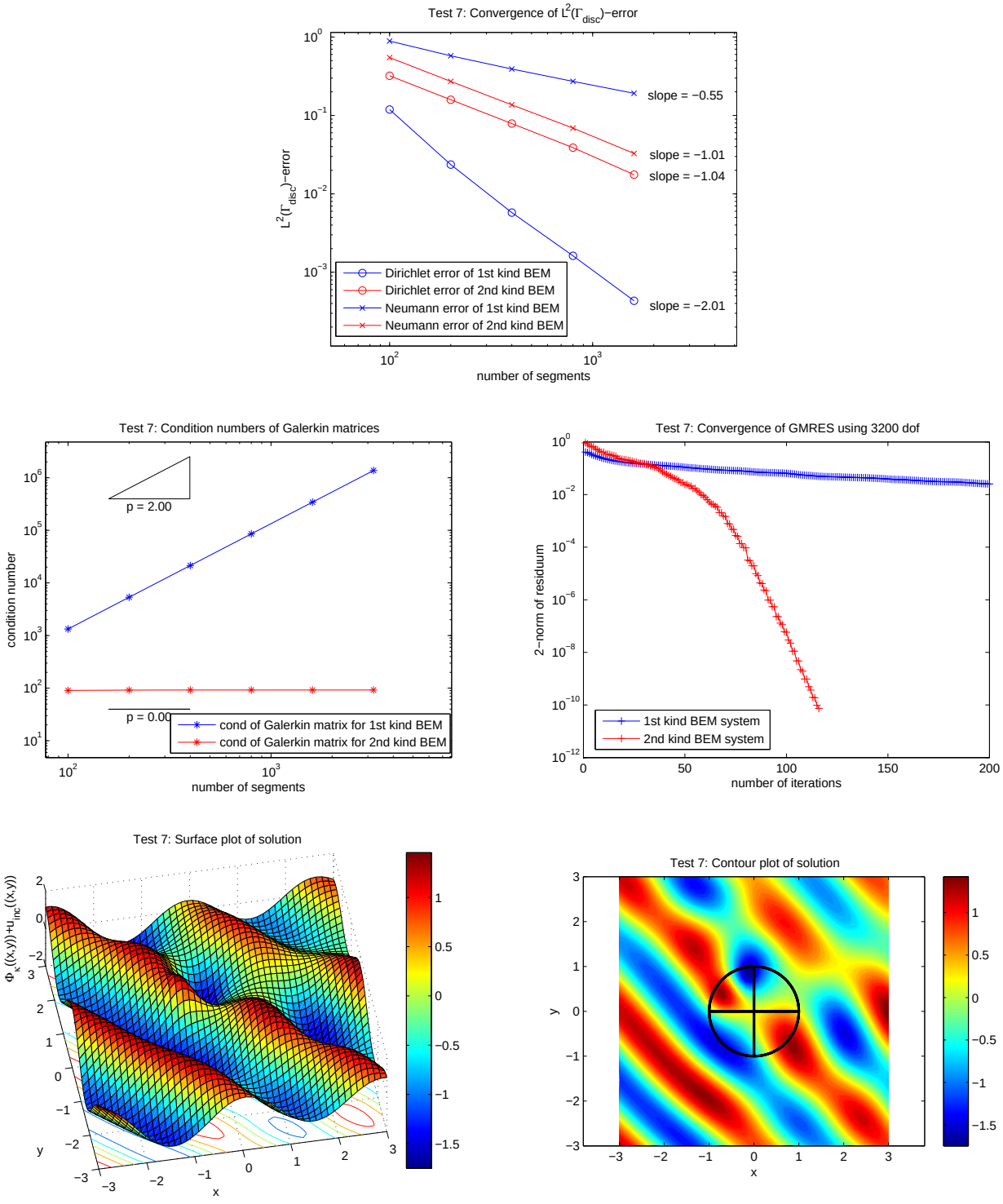

Figure 3.17: Test 7: Helmholtz transmission problem with five domains $\Omega_0, \Omega_1, \Omega_2, \Omega_3, \Omega_4$ where Ω_1 is the upper right quarter of a disc of radius one, Ω_2 is the upper left quarter of the disc and Ω_3 resp. Ω_4 are the lower left resp. lower right quarter of the unit disc. Ω_0 is the exterior domain. The appropriate wave numbers are chosen as $\kappa_0 = 3, \kappa_1 = 1, \kappa_2 = 5, \kappa_3 = 2, \kappa_4 = 3$. The incoming wave u_{inc} is a plane wave with direction of propagation $\mathbf{d} = \frac{\sqrt{2}}{2}(1,1)^T$.

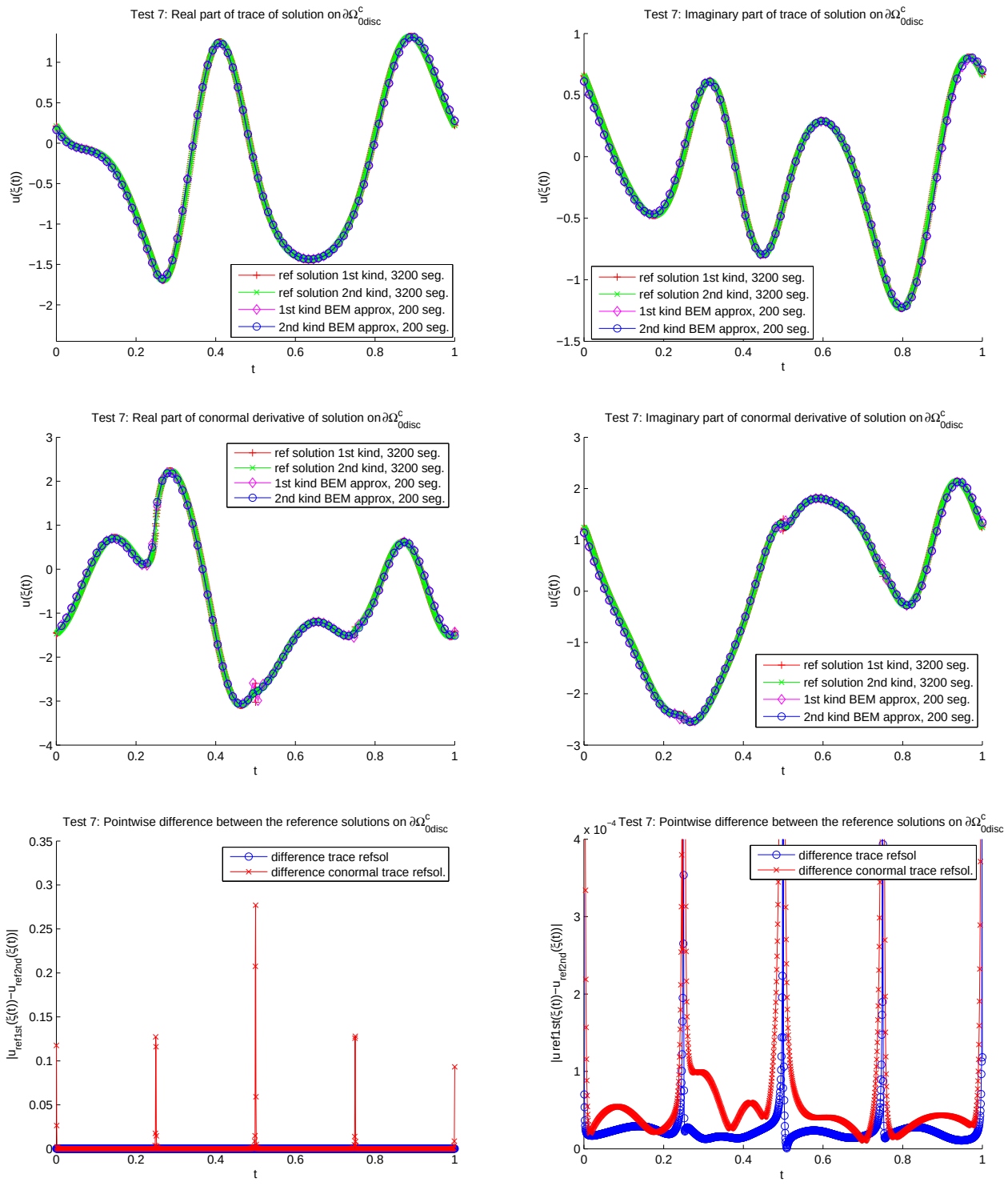

Figure 3.18: **Test 7:** Helmholtz transmission problem with five domains $\Omega_0, \Omega_1, \Omega_2, \Omega_3, \Omega_4$ where Ω_1 is the upper right quarter of a disc of radius one, Ω_2 is the upper left quarter of the disc and Ω_3 resp. Ω_4 are the lower left resp. lower right quarter of the unit disc. Ω_0 is the exterior domain. The appropriate wave numbers are chosen as $\kappa_0 = 3, \kappa_1 = 1, \kappa_2 = 5, \kappa_3 = 2, \kappa_4 = 3$. The incoming wave u_{inc} is a plane wave with direction of propagation $\mathbf{d} = \frac{\sqrt{2}}{2}(1,1)^T$.

3.6 Four Quarter Squares

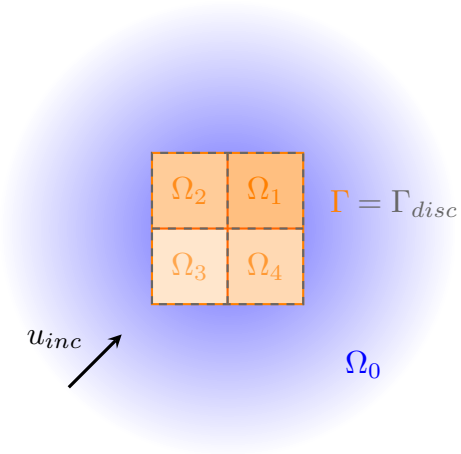

Figure 3.19: Geometry of the considered Helmholtz problem

In this section we consider the same constellation as in the section before. We substitute the unit disc for the unit square. But this is the only change. The results are as expected except for the convergence rate of the Dirichlet error for the classical method. It should have a behaviour like $\mathcal{O}(N_{\text{seg}}^{-2})$ instead of $\mathcal{O}(N_{\text{seg}}^{-1.75})$. But it is close enough to the expected order that we do not have to bother with it. Since the graphs in the convergence plot on the top of Figure 3.20 are straight lines, we omit a detailed table showing the detailed behaviour of the error.

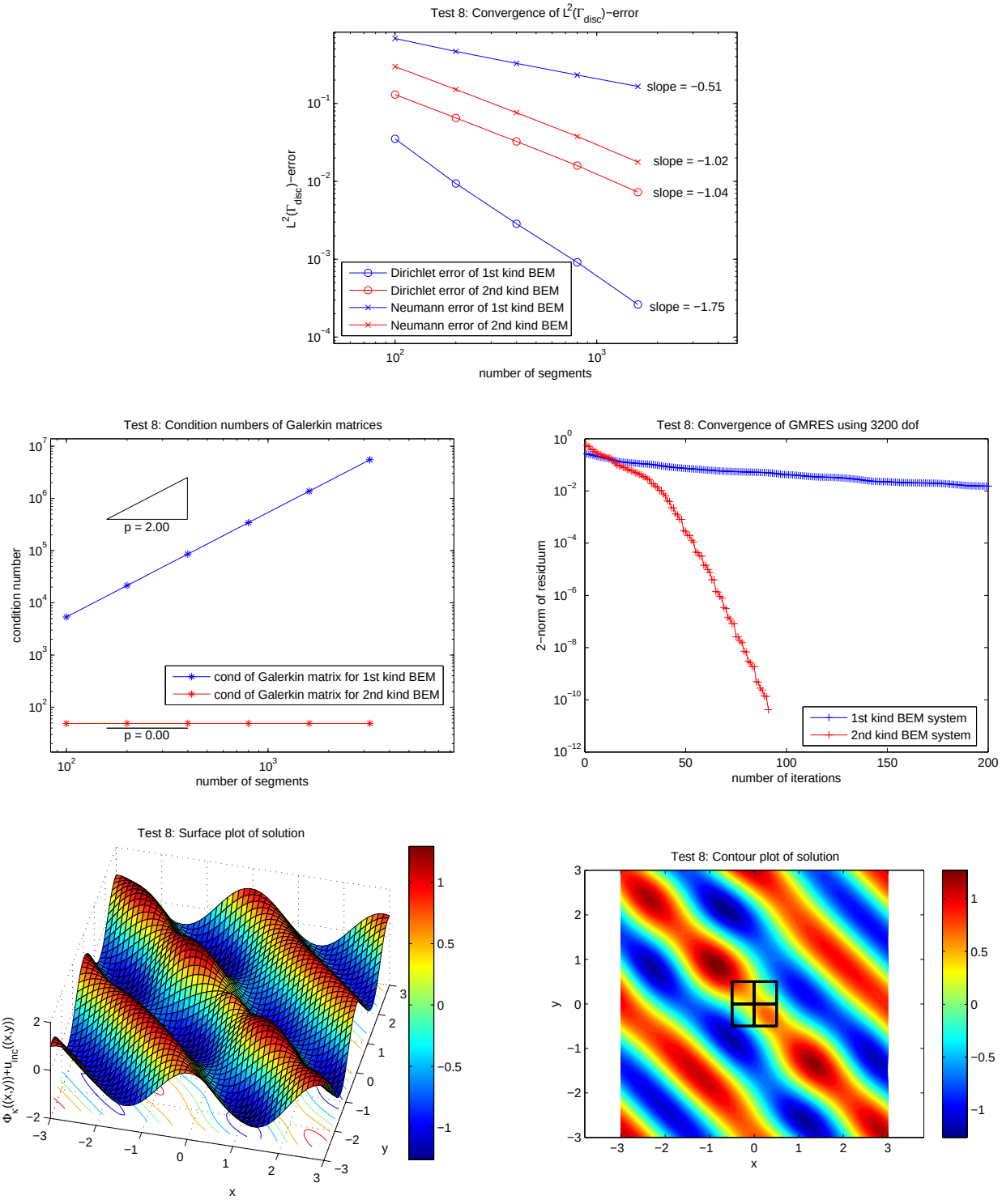

Figure 3.20: Test 8: Helmholtz transmission problem with five domains $\Omega_0, \Omega_1, \Omega_2, \Omega_3, \Omega_4$ where Ω_1 is the upper right quarter of a square of side length one, Ω_2 is the upper left quarter of the square and Ω_3 resp. Ω_4 are the lower left resp. lower right quarter of the unit square. Ω_0 is the exterior domain. The appropriate wave numbers are chosen as $\kappa_0 = 3, \kappa_1 = 1, \kappa_2 = 5, \kappa_3 = 2, \kappa_4 = 3$. The incoming wave u_{inc} is a plane wave with direction of propagation $\mathbf{d} = \frac{\sqrt{2}}{2}(1,1)^T$.

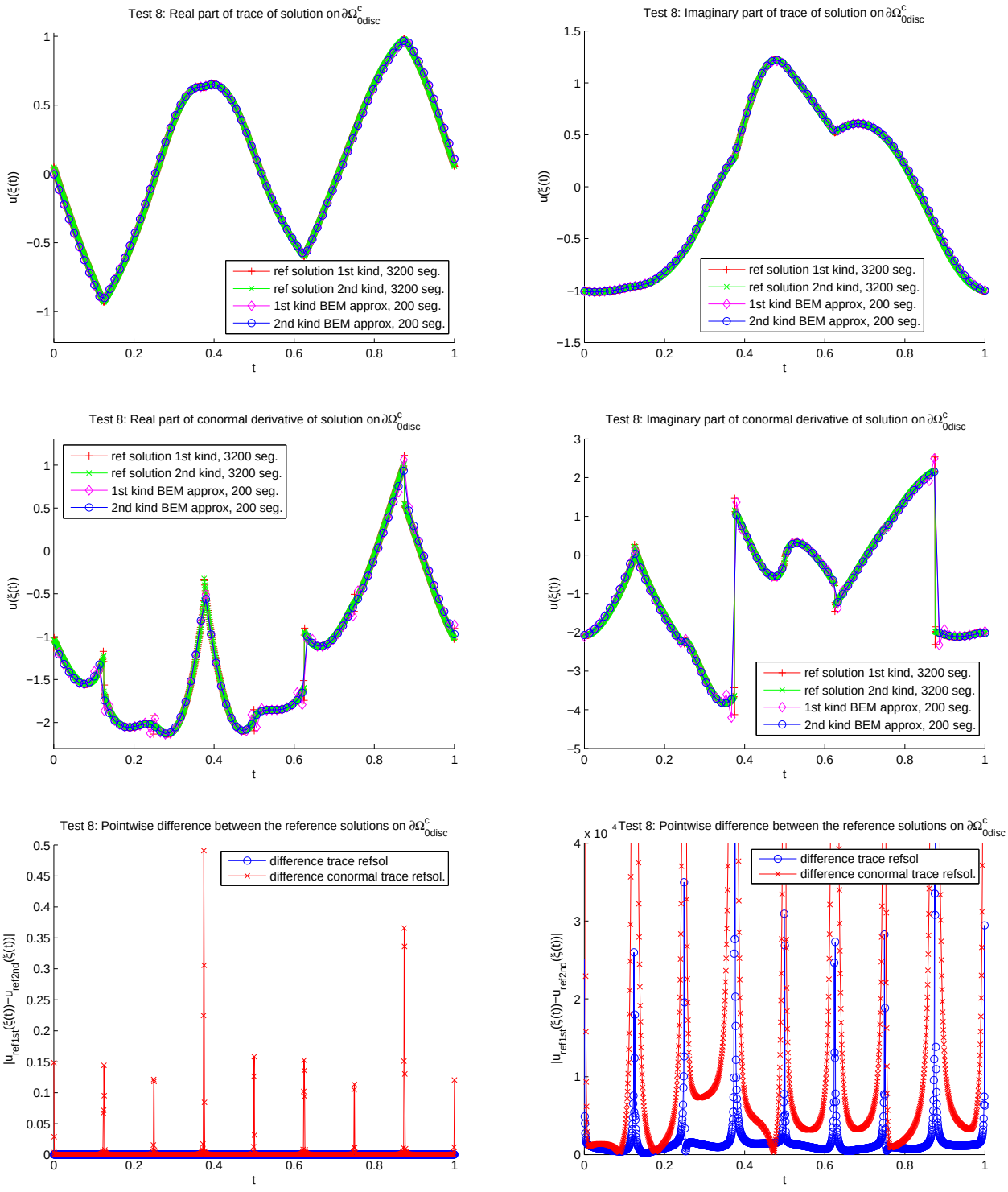

Figure 3.21: Test 8: Helmholtz transmission problem with five domains $\Omega_0, \Omega_1, \Omega_2, \Omega_3, \Omega_4$ where Ω_1 is the upper right quarter of a square of side length one, Ω_2 is the upper left quarter of the square and Ω_3 resp. Ω_4 are the lower left resp. lower right quarter of the unit square. Ω_0 is the exterior domain. The appropriate wave numbers are chosen as $\kappa_0 = 3, \kappa_1 = 1, \kappa_2 = 5, \kappa_3 = 2, \kappa_4 = 3$. The incoming wave u_{inc} is a plane wave with direction of propagation $\mathbf{d} = \frac{\sqrt{2}}{2}(1,1)^T$.

4 Conclusion and Outlook

We have shown in Section 1.8, that the new second kind formulation (1.47) is equivalent to the Helmholtz transmission problem defined in Section 1.2. This implies that our numerical method using piecewise constant boundary elements to approximate both Dirichlet and Neumann data is well defined. Together with Theorem 10 we have guaranteed quasi-optimal convergence for the approximation error of the method.

The tests in Section 3 show that the new second kind method is, like Claeys' second kind method, very well conditioned: The Galerkin matrices are uniformly bounded compared to the number of segments N_{seg}. So in contrast to the classical methods there is no more preconditioning necessary to use iterative solvers like GMRES efficiently.
It remains open to establish this property theoretically.

A further benefit of the new method is the better approximation of the Neumann data compared to the classical approach. The numerical solution does not show oscillations at the discontinuities and we get a better convergence rate of the error.

On the other hand, we have a deficit in the approximation for the Dirichlet trace: Since for homogeneous Helmholtz problems the solution is quite smooth, it usually makes sense to approximate with piecewise linear ansatz functions or even ansatz functions of higher polynomial degree, because we then get better convergence rates.

Definitely, our method using only piecewise constant ansatz functions is easier to implement, especially in higher dimensions than two, since we do not have to bother about neighbouring dependencies.

Further investigation can be done by making the existing code more time-efficient and investing more time to find an even better quadrature to evaluate the matrix entries (see Subsection 2.2.2).
Also an extension to three dimensions could be made or one could discuss the new second kind formulation for transmission problems based on other strongly elliptic partial differential operators.

Also it would be interesting to test the behaviour of the new second kind scheme using (at least for the Dirichlet part) other finite dimensional subspaces as ansatz spaces. For example one could take boundary element spaces of higher polynomial degree. One of the central questions then is: Do we still get the better convergence of the Neumann error?

A Bessel Functions and Identities

Here we list some useful identities involving Hankel and Bessel functions of first and second kind, i.e. $H_\alpha^{(1)}$, $H_\alpha^{(2)}$, respectively J_α, Y_α, for any $\alpha \in \mathbb{N}$. They can be found in most formularies, see for example [2] and [1]. First of all, we can express the Hankel functions by complex combinations of Bessel functions. For $z \in \mathbb{R}$, it holds:

$$H_\alpha^{(1)}(z) = J_\alpha(z) + \mathrm{i}Y_\alpha(z), \tag{A.1}$$

$$H_\alpha^{(2)}(z) = J_\alpha(z) - \mathrm{i}Y_\alpha(z), \tag{A.2}$$

where the series expansions of the Bessel functions are

$$J_\alpha(z) = \left(\frac{1}{2}z\right)^\alpha \sum_{k=0}^{\infty} \frac{(-4)^{-k}}{k!(\alpha+k)!} z^{2k}, \tag{A.3}$$

$$\begin{aligned} Y_\alpha(z) = \frac{2}{\pi}\log\left(\frac{1}{2}z\right) J_\alpha(z) - \frac{\left(\frac{1}{2}z\right)^{-\alpha}}{\pi} \sum_{k=0}^{\alpha-1} \frac{4^{-k}(\alpha-k-1)!}{k!} z^{2k} \\ - \frac{\left(\frac{1}{2}z\right)^{\alpha}}{\pi} \sum_{k=0}^{\infty} \frac{(-4)^{-k}\left(\psi(k+1)+\psi(\alpha+k+1)\right)}{k!(\alpha+k)!} z^{2k}. \end{aligned} \tag{A.4}$$

ψ is the *Digamma function*, the derivative of the Gamma function. Since we assume the input data to be a natural number we can use the following representation:

$$\psi(n) = -\gamma + \sum_{k=1}^{n-1} \frac{1}{k}, \quad n \in \mathbb{N}, \tag{A.5}$$

$$\gamma := \lim_{n\to\infty} \left(\sum_{k=1}^{n} \frac{1}{k} - \log(n) \right) = 0.577215664901532\ldots .$$

For the derivatives of the Bessel resp. Hankel functions there hold the recursions

$$\begin{aligned} \frac{d}{dz}F_\alpha(z) &= F_{\alpha-1}(z) - \frac{\alpha}{z}F_\alpha(z), \\ \frac{d}{dz}F_\alpha(z) &= -F_{\alpha+1}(z) + \frac{\alpha}{z}F_\alpha(z), \quad F \in \{J, Y, H\} \end{aligned} \tag{A.6}$$

B Mie Solution

In the case of the geometric obstacle being the disc with radius R and an incident plane wave with direction of propagation $\mathbf{d} = (d_1, d_2)^T = (\cos(\theta_0), \sin(\theta_0))$, $\theta_0 := \cos^{-1}(d_1)$, one can derive the exact solution of the Helmholtz transmission problem. It is called *Mie solution* and obtained by reformulating the Helmholtz transmission problem in polar coordinates and then applying separation of variables. First, let us rewrite the incident plane wave u_{inc} using polar coordinates:

$$\begin{aligned} u_{\text{inc}}(r,\theta) &= \exp\left(\mathrm{i}\kappa_0 \mathbf{d} \cdot (r\cos(\theta), r\sin(\theta))^T\right) \\ &= \exp\left(\mathrm{i}\kappa_0 r(\cos(\theta_0)\cos(\theta) + \sin(\theta_0)\sin(\theta))\right) \\ &= \exp\left(\mathrm{i}\kappa_0 r\cos(\theta - \theta_0)\right) \\ &= \sum_{n\in\mathbb{Z}} \mathrm{i}^n J_n(\kappa_0 r)\exp(\mathrm{i}n(\theta-\theta_0)). \end{aligned}$$

The Mie solution then can be expressed in the following way:

$$u(r,\theta) = \begin{cases} \sum_{n\in\mathbb{Z}} a_n J_n(\kappa_1 r)\exp(\mathrm{i}n(\theta-\theta_0)), & r \le R, \\ \sum_{n\in\mathbb{Z}} \left(b_n H_n^{(1)}(\kappa_0 r) + \mathrm{i}^n J_n(\kappa_0 r)\right)\exp(\mathrm{i}n(\theta-\theta_0)), & r > R, \end{cases}$$

with Fourier coefficients a_n, b_n, given by

$$\begin{aligned} a_n &= \frac{\kappa_0 \mathrm{i}^n \left(J_n'(\kappa_0 R)H_n^{(1)}(\kappa_0 R) - J_n(\kappa_0 R)H_n^{(1)'}(\kappa_0 R)\right)}{\kappa_1 J_n'(\kappa_1 R)H_n^{(1)}(\kappa_0 R) - \kappa_0 J_n(\kappa_1 R)H_n^{(1)'}(\kappa_0 R)}, \\ b_n &= \frac{\mathrm{i}^n\left(\kappa_0 J_n'(\kappa_0 R)J_n(\kappa_1 R) - \kappa_1 J_n'(\kappa_1 R)J_n(\kappa_0 R)\right)}{\kappa_1 J_n'(\kappa_1 R)H_n^{(1)}(\kappa_0 R) - \kappa_0 J_n(\kappa_1 R)H_n^{(1)'}(\kappa_0 R)}. \end{aligned} \tag{B.1}$$

The Neumann trace of the Mie solution on the disc of radius R we obtain by simply taking the derivative in r. So we have

$$\gamma_N^{\Omega_1} u(\theta) = \sum_{n\in\mathbb{Z}} \kappa_1 a_n J_n'(\kappa_1 R)\exp(\mathrm{i}n(\theta-\theta_0)), \quad \theta \in [0, 2\pi),$$

with a_n as defined above in (B.1). The facts stated in this Chapter are based on a paper of Hsiao and Xu [8].

Bibliography

[1] *Digital Library of Mathematical Functions*. http://dlmf.nist.gov/, 2011-08-29.

[2] M. Abramowitz and I.A. Stegun. *Handbook of mathematical functions with formulas, graphs, and mathematical tables*, volume 55. Dover publications, 1964.

[3] M. Carley. Numerical quadratures for singular and hypersingular integrals in boundary element methods. *SIAM Journal on Scientific Computing*, 29(3):1207, 2008.

[4] X. Claeys. A single trace integral formulation of the second kind for acoustic scattering. 2011.

[5] M.G. Duffy. Quadrature over a pyramid or cube of integrands with a singularity at a vertex. *SIAM journal on Numerical Analysis*, pages 1260–1262, 1982.

[6] N. Heuer. *Preconditioners for the p-version of the boundary element Galerkin method in IR3*. PhD thesis, Schr., 1998.

[7] G. C. Hsiao and L. Xu. A system of boundary integral equations for the transmission problem in acoustics. *Appl. Numer. Math.*, 61:1017–1029, 2011.

[8] G.C. Hsiao and W.L. Wendland. *Boundary integral equations*, volume 164. Springer Verlag, 2008.

[9] W.C.H. McLean. *Strongly elliptic systems and boundary integral equations*. Cambridge University Press, 2000.

[10] P. Meury. Stable finite element boundary element Galerkin schemes for acoustic and electromagnetic scattering. *ETH Dissertation*, (17320), 2007.

[11] Y. Saad. *Iterative methods for sparse linear systems*. Society for Industrial Mathematics, 2003.

[12] S.A. Sauter and C. Schwab. *Boundary element methods*. Springer, 2011.

[13] C. Schwab. Variable order composite quadrature of singular and nearly singular integrals. *Computing*, 53(2):173–194, 1994.

[14] O. Steinbach. *Numerical approximation methods for elliptic boundary value problems: finite and boundary elements*. Springer Verlag, 2008.

[15] T. Von Petersdorff and R. Leis. Boundary integral equations for mixed Dirichlet, Neumann and transmission problems. *Mathematical methods in the applied sciences*, 11(2):185–213, 1989.